DOI:10.14753/SE.2014.1845

New aspects of retinal photoreceptor morphology and development in normal and pathological conditions

Ph.D. Thesis

Dr. Ágnes Ida Berta

Doctoral School of Molecular Medicine
Semmelweis University

PhD Supervisor: Dr. Ágoston Szél, D.Sc.

Official reviewers: Dr. Róbert Gábriel, D.Sc.
Dr. Gábor Somfai, Ph.D.

Head of the examination board: Dr. András Csillag, D.Sc.

Members of the examination board: Dr. Gábor Gerber, Ph.D.
Dr. Zsuzsanna Szepessy, Ph.D.

Budapest, 2013

DOI:10.14753/SE.2014.1845

Contents

DOI:10.14753/SE.2014.1845

I. List of abbreviations

AGC protein kinases= protein kinase A, C and G families

AO= anti-opsin

BSA= bovine serum albumin

CD18 = integrin beta-2

cGMP= cyclic guanosine monophosphate

COS-1=monoclonal antibody labeling the red/green opsin

CRABP= cellular retinoic acid binding proteins

crd1 = gene locus of cone-rod dystrophy 1

crd2 = gene locus of cone-rod dystrophy 2

crd3 = gene locus of cone-rod dystrophy 3

crd4 = gene locus of cone-rod dystrophy 4

CRX= cone-rod homeobox

DABCO = 1,4 diazobizyklo-[2.2.2]oktan)

DAPI= 4',6'-diamino-2-phenylindole

DNA= deoxyribonucleic acid

DPM= disintegrations per minute

DRMs= detergent-resistant membranes

ECM= extracellular matrix

erd= gene locus of early retinal degeneration

ERG= electroretinography

GC= ganglion cell(s)

GCL= ganglion cell layer

GFAP= glial fibrillary acidic protein

GS = glutamine synthetase

hCAR= Human cone arrestin

IL= inner layer

ILM= inner limiting membrane

INL= inner nuclear layer

IPL= inner plexiform layer

IS= inner segment(s)

KI-67=Kiel-67

L opsin= green opsin

L/M opsin= green/red opsin

M opsin= red opsin

mAb= monoclonal antibody

mRNA= messenger ribonucleic acid

NR2E3 or PNR= photoreceptor-specific nuclear receptor

NRL= neural retina leucine zipper

OL= outer layer

OLM= outer limiting membrane

ONF= optic nerve fibers

ONL= outer nuclear layer

OPL= outer plexiform layer

OS= outer segment(s)

OS-2= monoclonal antibody labeling the blue opsin

P1, P5, P10 and P15= postnatal days 1, 5, 10, 15

PAX6= paired box protein 6

PBS= phosphate buffer saline

PCNA= proliferating cell nuclear antigen

PCNA= proliferating cell nuclear antigen

PE= pigment epithelium

PHH3= Phospho Histone H3

PKCα= Protein kinase C α

PRA= progressive retinal atrophy

prcd= gene locus of progressive rod-cone degeneration

qRT-PCR = quantitative real time-PCR

rcd = gene locus of rod-cone dysplasia 1

rcd2= gene locus of rod-cone dysplasia 2

rcd3= gene locus of rod-cone dysplasia 3

rd= gene locus of rod dysplasia

RDS peripherin= peripherin 2

RDS= retinal degeneration slow

RHO= gene locus of autosomal dominant progressive retinal atrophy

RIS= rod inner segment(s)

ROS= rod outer segment(s)

RPE= retinal pigment epithelium

S opsin= blue opsin

SDS= sodium dodecyl sulfate

SDS-PAGE= SDS-polyacrilamide gel electrophoresis

SINE element= short interspersed nuclear element

TUNEL= terminal deoxynucleotidyl transferase dUTP nick end labeling

Type A PRA= gene locus of photoreceptor dysplasia

VRD= vitreoretinal degeneration

wk= week

wks= weeks

XLPRA= gene locus of X-linked progressive retinal atrophy

DOI:10.14753/SE.2014.1845

II. Introduction

The major cause of blindness in industrialized countries are diseases caused by the progressive dysfunction and the loss of retinal photoreceptors, which also explains the importance of experimental and clinical studies on this topic. It is one of the most genetically heterogenous disorders in man, with well over 100 genes found so far related only to hereditary degeneration forms (Hartong et al., 2006). The number of loci identified predispositioning age-related macular degeneration is continously increasing. The inherited and multifactorial forms of photoreceptor degeneration are different in several ways, but the common and a key event is the progredient loss or dysfunction of photoreceptor cells, occuring primary or secondary. Although the genetic and mechanistic heterogenity of photoreceptor degeneration is a challenge for developing therapeutic strategies, but recently there have been several successful approaches (Wright et al., 2010).

The inherited forms of photoreceptor degeneration are a common cause of visual impairment and the majority of them is monogenic, with a prevalence of ~1 in 3,000 (Pacione et al., 2003; Rattner et al., 1999). The most common subtype is retinitis pigmentosa, which is one of the two main causes of blindness in the adult population (20–64 year olds, (Buch et al., 2004). Typically the first symptom of retinitis pigmentosa is reduced night vision in early or middle life, due to rod dysfunction starting in the peripheral retina. Later on it slowly progresses to the mid-peripheral field or further, often leaving the patients with a small central island of vision due to the survival only of macular cones (Hartong et al., 2006). Usually retinitis pigmentosa results from a primary defect in rods, but this also leads to secondary cone loss at later stages and this is why it is classified as a rod–cone degeneration. There are also some rare subtypes of retinitis pigmentosa that show a primary dysfunction of both rods and cones. At the moment 46 genetic subtypes of retinitis pigmentosa are identified based on clinical symptoms, although some subtypes are part of different syndromes that also include non-ocular features. Other inherited photoreceptor degenerations include macular, cone and cone-rod degenerations, which are clinically distinguishable from retinitis pigmentosa. These disorders can present at any stage of life, but predominantly -just like retinitis pigmentosa- also cause severe visual loss in early to middle age. Early

loss or distortion of central vision is the common and pathognomonic clinical finding by cone-, cone–rod degenerations and also by inherited macular degenerations. These can usually be distinguished from one another by electrophysiological and other tests, because the photoreceptor defect in the cone and cone–rod degenerations is more generalized compared to the inherited macular degenerations. Macular degenerations result from anatomically circumscribed primary defects in macular rods, cones or retinal pigment epithelium. The further differential diagnosis is based on the fact that in cone–rod degenerations cones are more severely affected, while in cone degeneration cones are the only cell type involved (Wright et al., 2010).

The vertebrate retina is made of six major cell types (rod and cone photoreceptors, and horizontal, bipolar, amacrine and ganglion cells) that exhibit laminar organization and form numerous parallel microcircuits for integration and processing of visual signals (Figure 1a). The process of vision begins at the photoreceptors, which are unique sensory neurons that are specialized to capture light quanta. The chemical output of photoreceptors is integrated and processed by interneurons (bipolar, horizontal and amacrine cells) and transmitted to visual centers in the brain by ganglion cells (Masland, 2001; Swaroop et al., 2010).

The photoreceptors cells themselves are highly compartmentalized for specialized functions and are strongly associated with the retinal pigment epithelium, structurally and functionally, which supports photoreception (Figure 1b). Cone photoreceptors respond to bright light, mediate colour vision and foveal cones make high resolution of visual images ("sharp vision") possible. Rod photoreceptors function only under dim light conditions. They are so sensible that they can respond to single light quanta (Luo et al., 2008). Across the retina, rods and various cone subtypes always have a well-defined arrangement, occuring with different patterns in different species. This pattern is generated with the right number of components at the right place, and also with appropriate connection to interneurons for further processing of visual information (Figure 1c). As already mentioned, the retinal photoreceptor pattern is different in various species. In mice and humans, photoreceptors represent over 70% of retinal cells, but rods outnumber cones by 30:1 in mice and 18–20:1 in humans (Carter-Dawson and LaVail, 1979; Roorda and Williams, 1999). A major difference between humans (and diurnal primates) and mice (and most other mammals) is the presence in

humans of a thin, pit-like, cone-only region in the centre of the retina, called the fovea, which is responsible for highest visual acuity. In humans, the density of rods increases from the fovea to the periphery of the retina, with the highest rod density in the parafoveal region (Curcio et al., 1990).

The mammalian retina has only one type of rod visual pigment called rhodopsin, which has a peak spectral sensitivity at ~500 nm. Most mammals, including the mouse, have two types of cone opsins defining dichromatic colour vision: S opsin (also known as blue sensitive opsin), which has peak sensitivity in the short wavelength (ultraviolet or blue) region of the spectrum; and M opsin (also known as green-sensitive opsin), which has peak sensitivity in the medium–long wavelength (green) region of the spectrum (Swaroop et al., 2010). In humans and diurnal primates an additional opsin, L opsin (also known as red-sensitive opsin) is also present, which is sensitive to longer wavelength (red) light. The three opsin types establish trichromatic colour vision. Each human cone expresses only one of the three opsins, arranged in a mosaic-like pattern over the retina (Deeb, 2006; Nathans et al., 1986). In mice M opsins and S opsins are expressed in opposing gradients across the retina (Figure 1c).

DOI:10.14753/SE.2014.1845

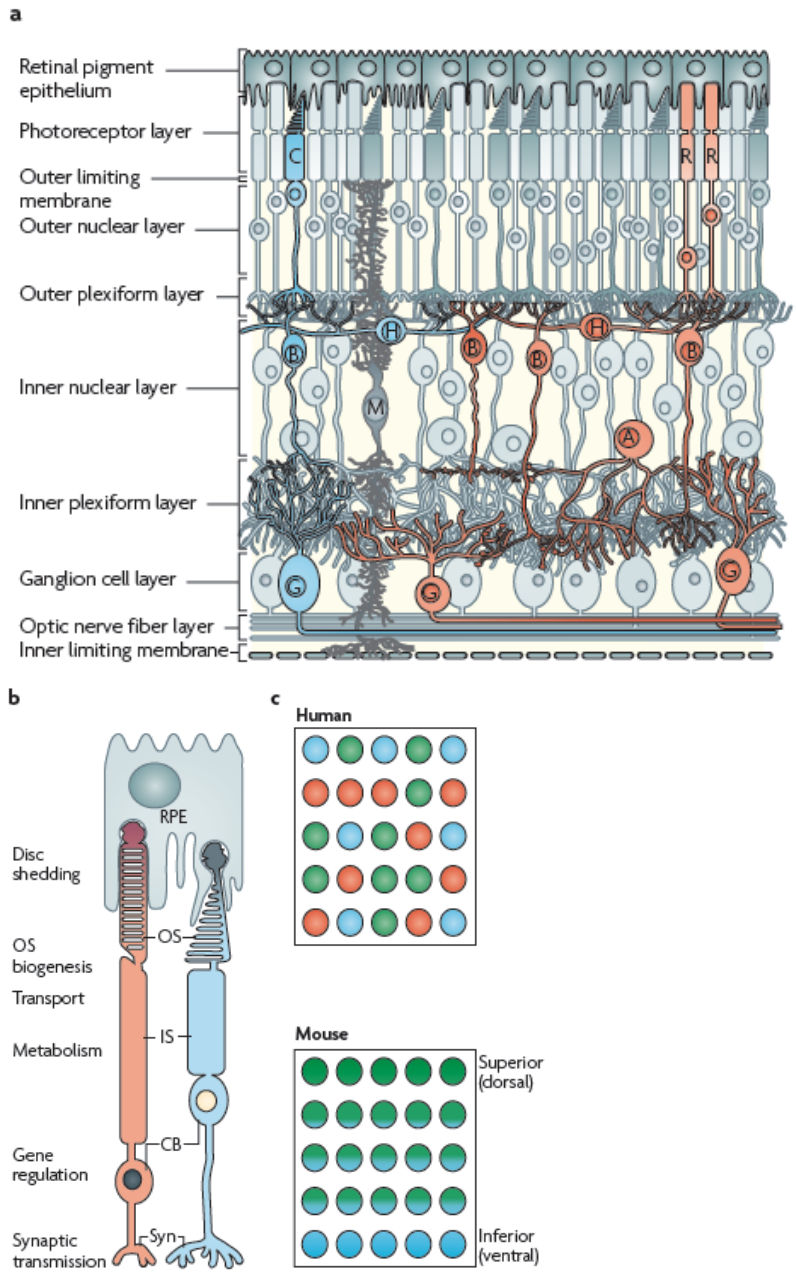

Figure 1. Structure of the retina, (Swaroop et al., 2010).

The outer segment, where the primary photoreceptive processes take place, is a specially transformed primary cilium (Davenport and Yoder, 2005). It is made of a dense stack of flattened membrane discs covered with the plasma membrane and contains more than 500 proteins species (Kwok et al., 2008). The phototransduction cascade is a series of biochemical reactions that convert a photon into a neural impulse in rod cells. This biochemical mechanism has been characterized in great detail (Deretic, 2006; Khorana, 1992; Maeda et al., 2003). The cascade is initiated by photon absorption in the chromphore 11-cis retinal which, by isomerization induces conformational change of the apoprotein opsin. The signal is then transferred to the phototransduction chain consisting of transducin-alpha, cGMP-phosphodiesterase, cGMP-gated cation channel which then leads to hyperpolarization of the plasma membrane. Important steps along the visual transduction are closely associated with the disc and plasma membranes (Khorana, 1992) of the outer segment.

The unique structural and functional organization of the vertebrate retina is finely adapted to the initial capture and processing of visual signals, but this organization also makes it unusually vulnerable to dysfunction (Masland, 2001). The genes known to influence photoreceptor degeneration are responsible for many, almost all, aspects of cellular structure and function (Figure 2, (Wright et al., 2010). Mutations affecting functions that are photoreceptor specific, such as phototransduction or the visual cycle, are only marginally more numerous than mutations affecting more general cell functions, such as protein folding, lipid metabolism or the extracellular matrix. Most of the mutations show widespread rather than photoreceptor specific expression patterns. There is no explanation why mutations in so many different genes cause photoreceptor degeneration (see review at (Wright et al., 2010).

DOI:10.14753/SE.2014.1845

On the basis of morphology and TUNEL staining in photoreceptor degenerations, early papers concluded, that apoptosis was the predominant way of cell death (Portera-Cailliau et al., 1994). However, it was later shown that TUNEL staining can detect both apoptotic and necrotic or autolytic cells (Colicos and Dash, 1996; Grasl-Kraupp et al., 1995). It was only recently (Lohr et al., 2006; Sancho-Pelluz et al., 2008) shown in mouse models that cell death can be caspase-independent or show features of autophagy. It is now accepted that caspase-independent and -dependent mechanisms are both involved, often cooperatively, in apoptotic cell death, including photoreceptor degeneration (Kroemer et al., 2009). Different cell-death mechanisms may be predominant during different stages of the disease or overlap at any one stage, however, apoptosis remains the predominant mode of cell death (Wright et al., 2010).

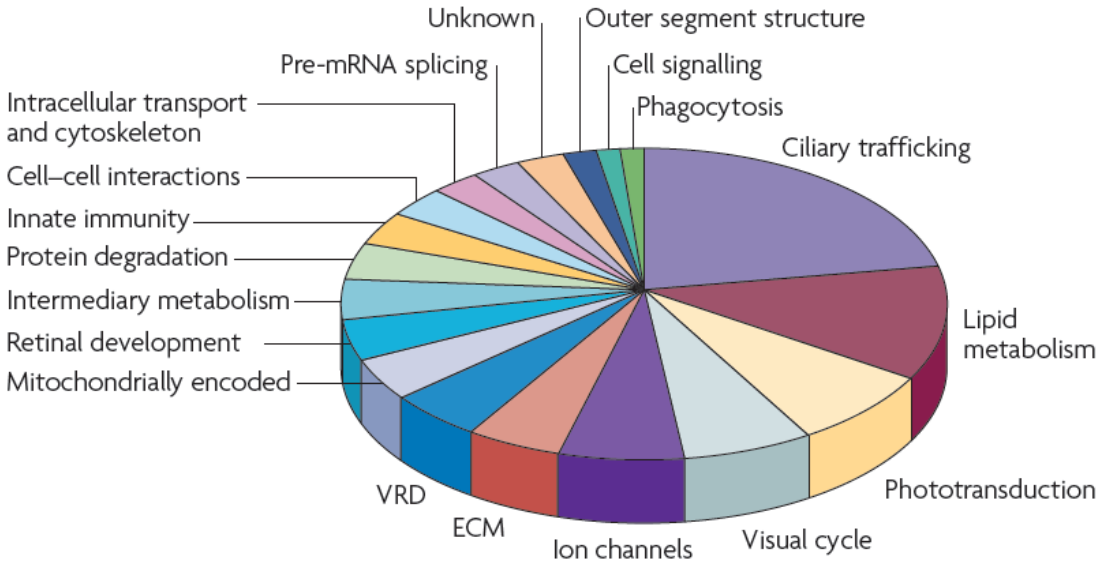

Figure 2. Functional categorization of genes influencing photoreceptor degeneration. In this pie chart it is shown, that the 146 genes implicated in photoreceptor degeneration play a role in numerous crucial cell functions (Wright et al., 2010).

DOI:10.14753/SE.2014.1845

The dog as a model for hereditary diseases has attracted the attention of basic research in the last 15 years, as numerous inherited canine retinal diseases show close homology to human diseases, however the retinal structure in the two species is in many ways different. The dog central retina is rod dominant, even within the highest cone density region of the area centralis. Both cone and rod densities are highest in the area centralis; cone and rod inner segments have a smaller cross-sectional area reflecting the higher density in this location compared with the peripheral retina. The majority of cones express L/M opsin, which enables better spatial and achromatic vision. S opsin may be expressed in a higher proportion of cones in the peripheral retina than in the area centralis (Mowat et al., 2008). The inferior peripheral retina typically has the lowest cone density of the whole retina. It is likely therefore that the visual acuity is lowest in this location and may reflect evolutionary pressures: since the canine has few airborne predators or prey, visual acuity in the superior field may be of low priority. Like many other nocturnal species, the dog eye contains an intraocular reflecting structure, the tapetum lucidum. The tapetum lucidum is a biologic reflector system that normally functions to provide the light-sensitive retinal cells with a second opportunity for stimulation of photoreceptors by photons, thereby enhancing visual sensitivity at low light levels. (Mowat et al., 2008; Ollivier et al., 2004). In dogs it is located in the choroid an contains layers of cells packed with organized, highly reflective material (Tapetum lucidum cellulosum, (Lesiuk and Braekevelt, 1983).

DOI:10.14753/SE.2014.1845

Dogs also suffer from various forms of inherited retinal blindness, the principal one of which is termed progressive retinal atrophy (Table 1). This group diseases can occur in different dog breeds, however all affected dogs show the same general, clinically recognizable ocular abnormalities (Aguirre, 2006). Diseases in the progressive retinal atrophy group are all progressive disorders, that affect the retinal photoreceptor cells primarily, or possibly secondary to the defects in the retinal pigment epthelial layer. In general, damages can be first recognized in the rod photoreceptors and subsequently in cones; hence the reason why night blindness is the predominant clinical finding prior to the severe visual dysfunction under both dim and bright light conditions. Associated with these defects, characteristic changes in the fundus can be observed clinically: retinal blood vessels become thin, there is an increased reflectivity of the tapetal layer (secondary to retinal thinning) and the optic nerve becomes pale. In the late stages of the diseases, most dogs develop secondary cataracts. Diseases in the progressive retinal atrophy group can be early-onset (age of manifestation < 6 weeks) or late onset (age of manifestation > 9 months, (Aguirre, 2006).

Disease Name	Breed	Gene locus
Rod-cone dysplasia 1	Irish setter	*rcd1*
Rod-cone dysplasia 2	collie	*rcd2*
Rod-cone dysplasia 3	Cardigan Welsch corgi	*rcd3*
Photoreceptor dysplasia	Miniature schnauzer	*Type A PRA*
Rod dysplasia	Norwegian elkhound	*rd*
Early retinal degeneration	Norwegian elkhound	*erd*
Progressive rod-cone degeneration	many breeds	*prcd*
X-linked PRA	Siberian husky, Samoyed	*XLPRA*
Autosomal dominant PRA	English mastiff, bullmastiff	*RHO*

Table 1: The progressive retinal atrophy group (Aguirre, 2006).

Another important clinical group of inherited retinal disorders in dogs are the cone-rod dystrophies (Table 2). Cone-rod dystrophies are disorders predominantly of cones, with rods being affected later and to a lesser extent, at least initially. In many cases the affected dogs show extensive impairment of visual function under both dim and light conditions. Of the four recognized cone-rod dystrophies (Table 2), three show extensive retinal disorder before one year of age (*crd1, crd2, crd 4*), whereas crd3 is a late-onset, slowly progressive disease (Aguirre, 2006).

Disease Name	Breed	Gene locus
Cone-rod dystrophy 1	pit bull terrier	*crd1*
Cone-rod dystrophy 2	pit bull terrier	*crd2*
Cone-rod dystrophy 3	pit bull terrier	*crd3*
Cone-rod dystrophy 4	miniature longhaired dachshound	*crd4*

Table 2: The cone-rod dystrophy group (Aguirre, 2006).

Early retinal degeneration (*erd*) is an autosomal recessive, early onset form of canine retinal degeneration characterized by aberrant functional and structural development of rod inner and outer segments, and rod and cone synapses. Rod and cone inner and outer segments show variable length, apparently the result of uncoordinated growth during development (Figure 3.). Abnormal development is followed by rapid degeneration of rods and cones. Affected dogs are initially night blind, and become totally blind between 48 and 72 weeks of age. The development of electroretinogram a- and b-waves was compared in normal and *erd* animals. In young normal dogs the response is a-wave dominated (between 2 and 4 wks), thereafter the b-wave becomes dominant. The *erd*-affected electroretinogram is a-wave dominated, until it disappears in older age (Acland and Aguirre, 1987). Genetical features of the disease have already been identified. The *erd* locus maps to *CFA 27* (homologous to *HSA12*p), and the disease results from a SINE element insertion in the serine/threonine kinase 38-like protein gene (*STK 38L*) that causes exon 4 to be skipped during transcription. This predicts the removal of 41 amino acids from the translated protein and elimination of critical conserved functional domains (Goldstein et al., 2010).

DOI:10.14753/SE.2014.1845

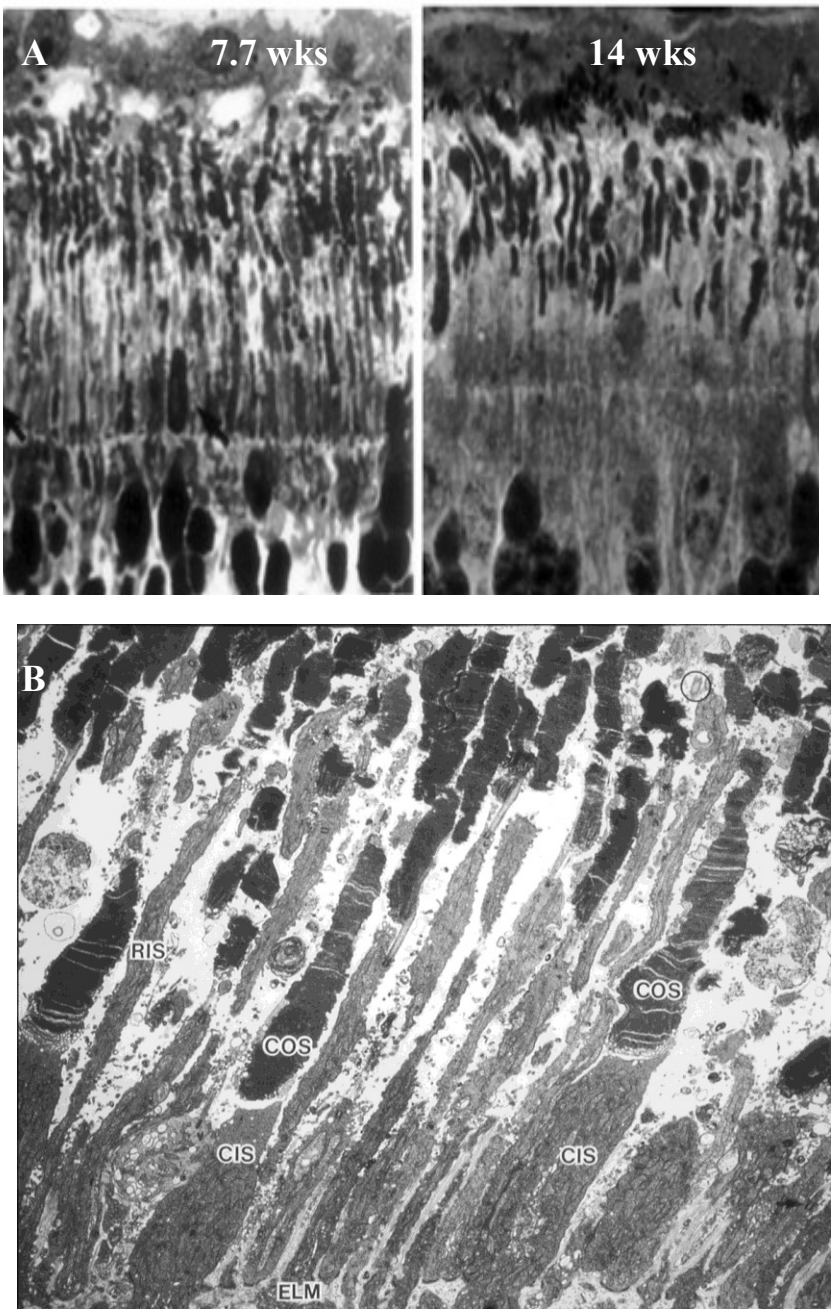

Figure 3. **A**: Photoreceptor layer from *erd*-affected dogs, by high resolution optical microscopy. At 7.7 wks the outer- and inner segments show variable length and are irregular in shape, at 14 wks photoreceptors are decreased severely in size and number. **B**: Photoreceptor layer, 54-day-old *erd* retina, electron micrograph. Cone inner- and outer segments are normal. Rod outer- and inner segments are extremely variable in length (Acland and Aguirre, 1987).

DOI:10.14753/SE.2014.1845

In mammals, the genesis of photoreceptors takes relatively long, weeks to months depending on the species, occuring pre- and postnatally (Carter-Dawson and LaVail, 1979; Morrow et al., 1998; Rapaport et al., 2004; Young, 1985). After the final mitosis step, the photoreceptor precursor is committed either to the rod or to cone maturation pathway (Figure 4). In humans, all photoreceptors are formed prenatally. The first cones and rods are born around foetal week 8 and 10, respectively. The mRNA of S opsin is detectable at foetal week 12, followed by rhodopsin, M opsin and L opsin at foetal week 15 (Cornish et al., 2004; Hendrickson et al., 2008). In the mouse, photoreceptor development is less advanced than in humans at birth, rods are born both pre-and postnatally. The eyes of the newborn animals remain closed for almost 2 weeks. Cone genesis starts at embryonic day 11 and is essentially complete at birth, while peak of rod genesis occurs in the first few postnatal days. S opsin is already expressed at late embryonic stages, but rhodopsin only subsequently after birth. Expression of M opsin begins later around postnatal day 6 (Carter-Dawson and LaVail, 1979; Young, 1985).

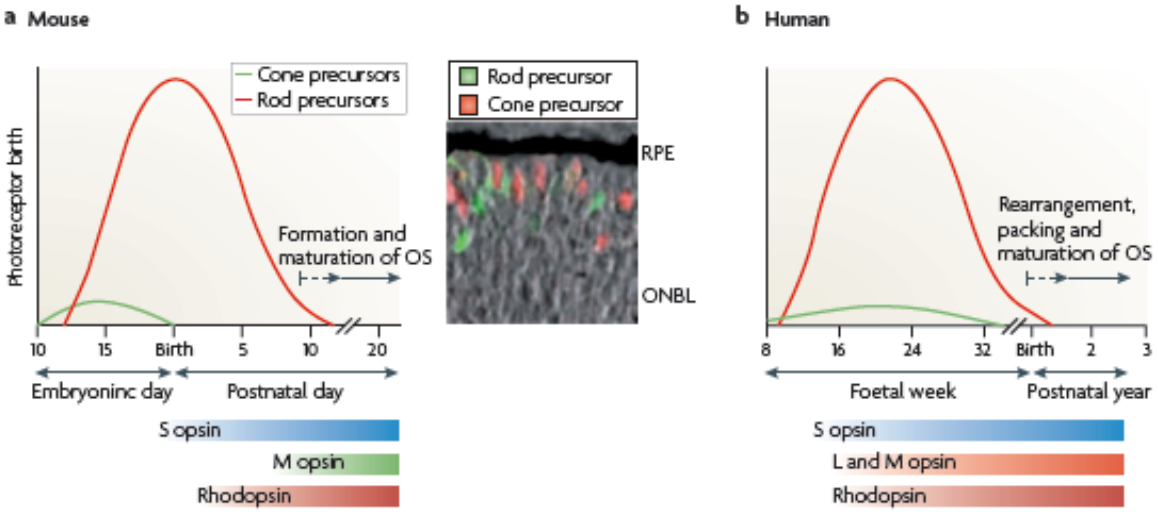

Figure 4. Comparison of photoreceptor generation and maturation in mice and humans. The main difference is that while in humans retinal development is almost completed by the time of birth, in mice the retina of newborn animals is immature and develops its structure in the first two weeks after birth (Swaroop et al., 2010).

DOI:10.14753/SE.2014.1845

The generation of functionally mature neurons from multipotent retinal progenitor cells proceeds through a series of steps and choices, committing cells to a particular fate. This process can be divided into five major steps: first, formation and proliferation of multipotent retinal progenitor cells; second, restriction of the competence of multipotent retinal progenitor cells; third, cell fate specification and commitment to photoreceptor precursors during or after final mitosis; fourth, expression of photoreceptor genes, such as those for phototransduction and morphogenesis; and fifth, axonal growth, synapse formation and outer segment biogenesis (Figure 5, (Swaroop et al., 2010).

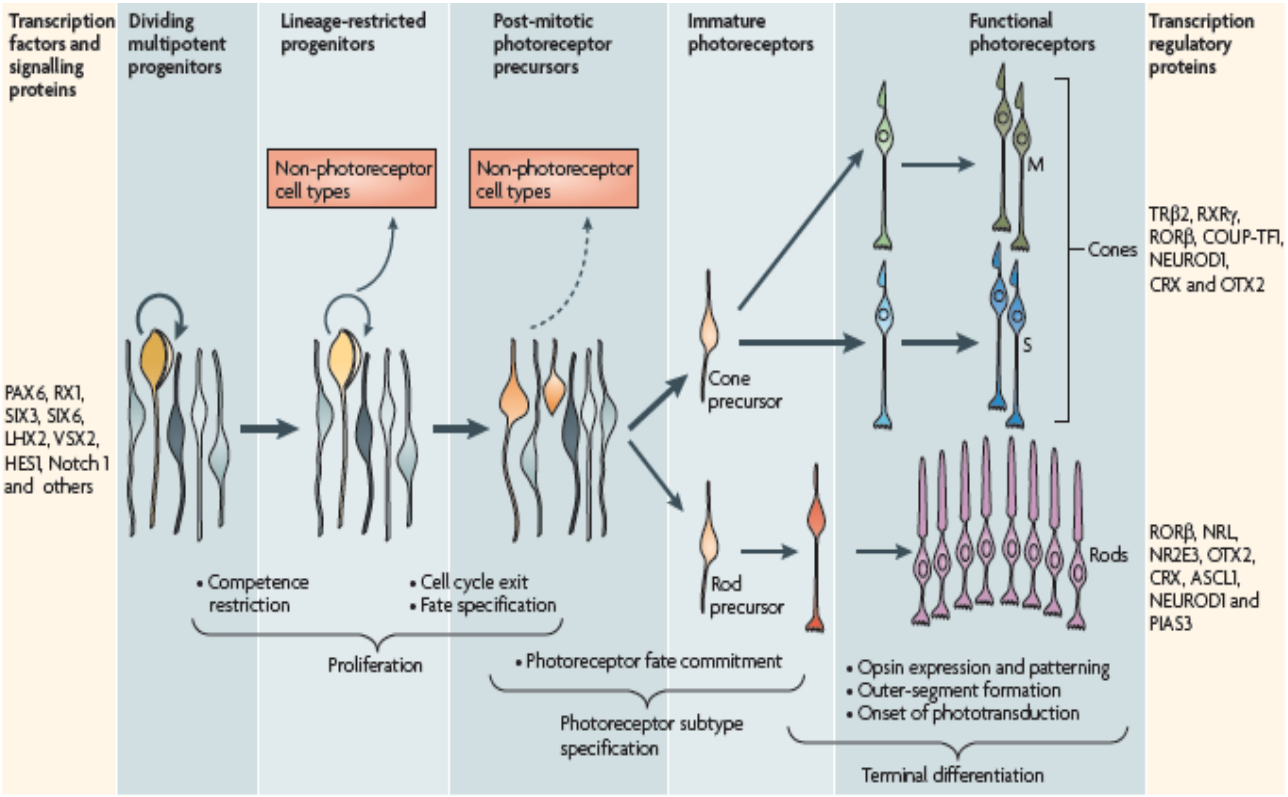

Figure 5. Stages of photoreceptor development from progenitors to mature photoreceptors. During cell type specification of photoreceptors, precursors are directed to become rods or cones by numerous transcription factors, signaling and regulatory proteins (Swaroop et al., 2010).

Lately it was demonstrated that a group of integral membrane proteins, the caveolins play a critical role in early vertebrate development. They are especially important in notochord and neuromast formation (Fang et al., 2006; Nixon et al., 2007). Caveolins are integral membrane proteins that are principal components of the special, Ω-shaped plasma membrane invaginations called caveolae. For formation of caveolae cholesterol is essential, as cholesterol binds caveolins and also influences caveolin transcription (Fielding et al., 1997; Murata et al., 1995). The caveolin–cholesterol interaction has also other aspects: caveolin binds to liposomes but only if they contain cholesterol, and this induces protein oligomerization (Murata et al., 1995), suggesting that caveolin oligomerization and membrane insertion is cholesterol-dependent. Caveolae were first identified in endothelial cells about 50 years ago and they were only later recognized, as a type of lipid rafts on the basis of their lipid composition. Although lipid rafts and caveolae are similar biochemically, they are morphologically different. Because of their unique, Ω-shaped appearance caveolae can be detected by electron microscopy, whereas lipid rafts are not visible. The different structure also suggest different functions (Head and Insel, 2007).

It is now known, that the lateral organization of the lipids in photoreceptor outer segment membranes is not uniform, since the membrane contains microdomains, that are resistant to nonionic detergents (Martin et al., 2005). Based on fatty acid analysis, detergent-resistant membranes (DRMs, also known as lipid rafts) represent 8% of the rod outer segment disc membranes and 12% of the rod outer segment plasma membrane (Elliott et al., 2008). In general, detergent-resistant membranes are plasma membrane subdomains that contain high concentrations of cholesterol and glycosphingolipids and are usually associated with certain proteins, however the lipid and protein components of such membrane domains may show variations. A general feature in various cell types is the presence of caveolin-1 and c-src in detergent-resistant membranes (Pike, 2003). Similarly to detergent-resistant membranes in other cell types, photoreceptor DRMs also contain caveolin-1 and c-src as shown by biochemical studies (Ghalayini et al., 2002; Martin et al., 2005). Until now immunocytochemical studies showed no or minimal amount of caveolin-1 at the rod outer segment level (Kim et al., 2006).

Caveolin was originally identified in transformed chick fibroblasts as a tyrosine-phosphorylated substrate of src (Glenney, 1989; Murata et al., 1995). Multiple isoforms

of caveolin have been identified: caveolin-1-α, caveolin-1-β, caveolin-2, and caveolin-3. While their structure is similar, their specific properties and tissue distribution are different in many ways. Caveolins have a similar molecular structure in vertebrate and non-vertebrate species (Caenorhabditis elegans), which indicates that caveolins are structurally and functionally conserved across species from worms to human (Scherer et al., 1997) and suggests that caveolins might have an important evolutionary role. The short cytoplasmic domain of the N-terminal region of caveolin-1 forms multivalent homo- and hetero-oligomers (Okamoto et al., 1998). In contrast to caveolin-1, caveolin-2 was not found to form homo-oligomers and exists mainly as a monomer (Scherer et al., 1995), or it forms stable hetero-oligomeric complexes with caveolin-1 (Scherer et al., 1997). Thus, caveolin-2 may function as an accessory protein in conjunction with caveolin-1 (Okamoto et al., 1998). Caveolin-1 and caveolin-2 are thought to originate from a common ancestor and are most abundantly expressed in adipocytes, endothelial cells, fibroblasts and smooth muscle cells (Okamoto et al., 1998; Scherer et al., 1997; Scherer et al., 1995). The expression of caveolin-3 is described to be dominantly to be muscle specific (Song et al., 1996; Tang et al., 1994; Way and Parton, 1996), although it has been shown that they are present in other cell types, such as astroglial cells (Nishiyama et al., 1999) and neurons of vegetative ganglia as well (Kiss et al., 2002). It has been proposed that members of the caveolin family members function as scaffolding proteins to organize and concentrate specific lipids (cholesterol and glycosphingolipids), lipid-modified signaling molecules and G proteins within caveolae, as binding may suppress or inhibit enzyme activity through the caveolin scaffolding domain, which is a common caveolin domain (Schlegel et al., 1998; Swaney et al., 2006).

There are only a few reports available about the presence and distribution of caveolins in the retina. In the mouse retina, caveolin-1 was found to be present in the outer plexiform layer in the synaptic ribbon of photoreceptor terminals (Kachi et al., 2001). In the rat retina caveolin-1 was detected in various retinal layers, between the inner plexiform layer and the outer limiting membrane, suggesting that caveolin-1 is expressed in Müller cells, this was also confirmed using Müller cell specific markers (Ueda, 2002). It was also shown with laser scanning confocal microscopical analysis that caveolin-1 is located in apical and basal surfaces of pigment epithelial cells.

(Bridges et al., 2001). Few years later a more detailed histological study was published showing caveolin-1 to be present in the majority of retinal layers of the rat (Kim et al., 2006). In contrast, caveolin-2 immunostaining was much weaker throughout the retina, with a more intense staining around the blood vessels. Caveolin-2 stained the processes of glial cells and Muller cells, but immunoreactivity was very limited in retinal neuronal cells including the ganglion cells, amacrine cells, bipolar cells, horizontal cells, and photoreceptor cells. This study group made no examinations about caveolin-3 and only central retinal regions were analysed (Kim et al., 2006). These first studies did not offer a comprehensive and accurate picture about the expression of caveolin isoforms in the mammalian retina.

DOI:10.14753/SE.2014.1845

III. Objectives

1. **Localization and expression pattern of caveolin-1 and c-src during retinal development** in order to understand their potential function in photoreceptor development. We wanted to compare the expression of these molecules to two highly abundant, well characterized proteins, rhodopsin and rhodopsin kinase. In addition, we also aimed at investigating the distribution profile of a kinase responsible for caveolin-1 phosphorylation, c-src, as well as the phosphorylated product, phospho-caveolin-1. To study potential colocalization and coexpression, double immunolabeling and co-immunoprecititation were used.

2. **Expression and distribution of caveolin isoforms in the retina of different species and in different retinal diseases, especially focusing on the human retina,** where relevant data on the topic were until now completely missing. We also wanted to compare degenerating and normal retina of the dog to reveal a possible role of caveolin and caveolin-related proteins in these retinal disorders. The dog retina and inherited canine retinal degenerations are especially interesting, because they show close homology to similar diseases in human.

3. **Detailed morphological and biochemical description of early retinal degeneration (*erd*), a canine retinal degeneration** characterized by abnormal photoreceptor development, followed by rapid photoreceptor degeneration. Although many other canine degenerations are now well characterized, in this disease the mechanism of photoreceptor degeneration was until now not described. Since in *erd* a special, elongated cell death period was observed, which is not followed by an appropriate change in the number of photoreceptors, our aim was to investigate the possibility if a cell proliferation compensates for the loss of photoreceptors. Various cell proliferation and cell-specific markers were planned to assess cell proliferation and to identify which cell types are proliferating.

4. **Comparison of *erd* with other canine retinal degenerations.** As in *erd* proliferating cells were found it the photoreceptor layer, we also wanted to investigate if the cell proliferation period is a unique characteristic of early retinal degeneration or not. We aimed at evaluating the cell proliferation rate in other canine retinal degenerations and comparing it to that of *erd*.

DOI:10.14753/SE.2014.1845

IV. Material and methods

1. Syrian hamster

Animals

In this study Syrian (golden) hamsters were used in different stages of postnatal development. The size and thickness of its retina makes it a suitable model animal for morphological and developmental studies. Samples were collected on postnatal days 1, 5, 10, 15 (P1, P5, P10 and P15) and in adulthood. More than 18-days-old hamsters were considered as adults. The animals were kept in standard conditions; food and water were added ad libitum. Retinal samples from a *Xenopus laevis* were also used in this study. All eyes were light adapted (animals were kept in light at least for 30 minutes) prior to sample collection. The experiments were approved by Animal Ethical Committee of Semmelweis University, Budapest (Leg. No. 1963-003-2004) and were in accordance with the Association of Research in Vision and Ophthalmology Resolution on Care and Use of Laboratory Animals.

Toluidine blue staining and electron microscopy

Retinas of hamsters (P1, P5, P10, P15, and P18) were fixed in 1% glutaraldehyde in Millonig's phosphate buffer (pH 7.4) overnight at 4ºC. After washes in Millonig's phosphate buffer and subsequently in cacodylate buffer, the samples were postfixed in 1% OsO_4 (in cacodylate buffer) for 1h at 4ºC. This was followed by a wash in cacodylate buffer and dehydration with ethanol during which samples were stained with 1% uranyl acetate in 70% ethanol for 1h at 4ºC. The samples were then embedded in araldite. Semithin and ultrathin sections were made on a Reichert-Jung Ultracut E (Leica, Austria). Semithin sections were stained with toluidine blue and viewed with a Zeiss Axiophot Microscope (Zeiss, Germany); the micrographs were obtained using an Olympus DP50 camera (Olympus, Japan). Ultrathin sections were contrast-stained with uranyl acetate and lead citrate and viewed in a Hitachi H 7500 electron microscope (Hitachi High-Technologies, Japan).

Immunocytochemistry

Hamster retinas were prepared as follows. Right after enucleation, the cornea, lens and vitreous body were removed and the posterior eyecup was subsequently fixed in 4% paraformaldehyde in 0.1 M phosphate buffer (pH 7.4) for 24 hours at 4°C. The solution was then replaced with 0.1 M phosphate buffered saline (PBS, pH 7.4), and rinsed for at least 24 hours before further processing. For cryoprotection the eyecups were incubated in 30% sucrose in 0.1 M phosphate buffer overnight which was followed by embedding in Tissue Tek. Cryo sections of 10 μm thickness were cut on a cryostat and dried onto poly-L-lysine coated glass microscope slides at 37°C. The *Xenopus laevis* retinas were fixed in 1% glutaraldehyde in Millonig's phosphate buffer (pH 7.4) overnight at 4ºC and semithin araldite sections were prepared as described above, followed by araldite extraction. Both section types were then soaked in PBS for 20 minutes and were treated subsequently with a blocking solution of 1% bovine serum albumin (BSA) and 0.1% Triton X-100 in PBS for 1 hour. The primary antibody was applied at 4°C overnight. For single immunolabeling the following primary antibodies were used: anti-caveolin-1 (polyclonal rabbit IgG, Transduction Laboratories, CA), anti-phospho(Tyr14)-caveolin-1 (polyclonal goat IgG, Santa Cruz Biotechnology, CA), anti-c-src (polyclonal rabbit IgG, Santa Cruz Biotechnology, CA), anti rhodopsin kinase (mouse monoclonal IgG-1, against GRK-1 C-terminal, a generous gift of Krzysztof Palczewski) and anti-opsin [AO rat polyclonal IgG to bovine rhodopsin, (Rohlich and Szel, 1993)]. All antibodies were diluted 1:100 in 1% BSA/PBS. Anti-rabbit and anti-mouse Alexa 488 (Molecular Probes, CA, 1:200) were used as secondary antibodies for 1h at room temperature. For the visualization of the cytoskeleton, F-actin was stained with Alexa fluor 594-labeled phalloidin (Molecular Probes, CA; 1:100). Vectashield HardSet Mounting Medium (Vector Laboratories, CA) with DAPI (4′,6-diamidino-2-phenylindole) was used to cover the slides. For double immunolabeling various combinations of the above antibodies were used as indicated in the figure legends. Control reactions were performed with rabbit, mouse and rat normal sera and non-specific primary antibodies, as well as omitting the primary antibodies to preclude the possibility of non-specific binding. The retinas were examined on a Nikon Eclipse E800 microscope using a Bio-Rad Radiance confocal imaging system (Bio-Rad Life Science Research, CA). Confocal Assistant (Todd Clark Brelje, University of Minnesota) and

Adobe Photoshop 7.0 (Adobe, Mountain View, CA) software was used for the image processing.

Immunoblot analysis of retinal lysates and isolation of ROS

After enucleation the cornea, lens and vitreous body were removed and the retina was detached from the posterior eyecup in various ages (P1, P5, P10, P15 and adult). All eyes were light adapted. For whole retinal lysates, 400 mg of each sample was lysed for 1 h at 0ºC in a lysis buffer containing 150 mM Tris/HCl, 1% Triton X-100 and Complete Mini Protease Inhibitor Coctail (Roche, Switzerland), according to the recommendation of the producer. Thereafter, the samples were centrifuged at 21,000x g for 10 minutes at 4ºC and the supernatants were used for further investigation. For ROS preparation 30 fresh hamster retinas were collected and outer segments were isolated using the modification (Martin et al., 2005) of a previously described method (Seno et al., 2001). Protein concentrations were determined by Bio-Rad Bradford assay. Equal amounts of total protein of each lysate were separated by 10% SDS-polyacrilamide gel electrophoresis (SDS-PAGE). SDS-PAGE was performed according to the method of Laemmli (Laemmli, 1970). Proteins were transferred on a Hybond-ECL nitrocellulose membrane (Amersham Biosciences, UK). Non-specific binding was blocked with skim milk. Immunoblot analysis was carried out with the following antibodies: anti-caveolin-1 (polyclonal rabbit IgG, Transduction Laboratories, CA), anti-phospho(Tyr14)-caveolin-1 (polyclonal goat IgG, Santa Cruz Biotechnology, CA), anti-c-src (polyclonal rabbit IgG, Santa Cruz Biotechnology, CA), anti rhodopsin kinase (mouse monoclonal IgG-1, against GRK-1 C-terminal, a generous gift of Dr. Krzysztof Palczewski) and anti-opsin [AO rat polyclonal IgG to bovine rhodopsin, (Rohlich and Szel, 1993)]. All antibodies were diluted 1:1000 in 1% BSA/PBS, except for caveolin-1, which was diluted 1:100. Biotinylated secondary antibodies were used in a dilution of 1:500. The immunoreactive bands were visualized using Vecastatin Elite ABC kit (Vector Laboratories, CA) and DAB staining. Tubulin-1 was used as loading control.

Immunoprecipitation and Western Blot

For immunoprecipitation, tissue preparation was the same as for immunoblot analysis. The samples were taken from Syrian hamster eyes of different ages: postnatal

day (P) P1 (50 retinas), P5 (30 retinas), P10 (30 retinas), P15 (30 retinas) and adult (10 retinas). The retinal tissue samples were collected and stored at -80 ºC until use. Then the samples were dissolved in a lysis buffer containing 50 mM Tris–HCl, 150 mM NaCl, 1 mM EDTA, 1 mM Na3PO4, 1 mM NaF, 10% glycerol, 0.5% Nonidet P40, 0.1 mM PMSF and 10g/ml aprotinin (pH 7.4).The lysate (0,5 mg from each sample) was incubated with anti-opsin antibody (Rohlich and Szel, 1993), for 5 h at 4ºC. The immune complex was bound to Protein A immobilized on Sepharose 4B for 1 hour and sedimented with centrifugation at 12,000x g, followed by five washes in lysis buffer (1 ml each). Bound protein was dissolved in SDS sample buffer (100 µl) and analyzed on SDS-PAGE, followed by transfer to nitrocellulose filter. Equal amounts of protein (as determined by BCA Protein Assay Kit, Thermo Fisher Scientific, Rockford, IL) were separated by 10% SDS-PAGE under reducing conditions, immunoblotted and probed with one of the following antibodies, anti-caveolin-1 and anti-c-src. Due to the small amount of sample, blots were stripped and subsequently probed with 1:1000 dilution of mouse anti-RDS mAb 3B6 or anti-Rom-1 mAb 1C6 (a generous gifts from Dr. Robert Molday). Appropriate HRP-conjugated secondary antibodies were subsequently used. 1:1000 dilution of mouse monoclonal to β-actin (Abcam, Cambridge, MA) was used as a loading control antibody. Control reactions without retinal samples were made to preclude non-specific interaction of antibodies.

2. Lemur

(black-and-white ruffed lemur*, Varecia variegata*)

The male lemur utilized in this study lived in captivity and died naturally at the age of 11 (normally these animals live for 19 years), without any eye diseases. Within a few hours of the death of the lemur, the bulb was removed and subsequently placed in a fixative (4% paraformaldehyde), then incubated for 24 h at 4°C. The retinas were then incubated overnight in 30% sucrose. Three samples were obtained from the lemur retina from the radial plane, and included the macular region, periphery, and ciliary body. 10 µm sections were prepared on a ThermoShandon cryotome. The distribution of the caveolins was determined via immunocytochemistry using isoform-specific antibodies.

The primary antibodies anti-caveolin-1 (1:100, polyclonal rabbit IgG; BD Biosciences, USA), anti-caveolin-2 (1:200, monoclonal mouse IgG; BD Biosciences, USA), and anti-caveolin-3 (1:100, monoclonal mouse IgG; BD Biosciences, USA) were diluted in 1% BSA and incubated overnight at 4°C. In order to detect caveolin-1 and -3, anti-rabbit and anti-mouse Alexa 488 (Invitrogen, USA), respectively, were employed as secondary antibodies. As caveolin-2 yielded a weak signal that was difficult to detect, we utilized biotinylated anti-mouse, then Streptavidin Alexa 488 (Invitrogen, USA), 1:100, in an effort to amplify the signal. Even when this extra method was used, caveolin-2 yielded the weakest signal among the variants. In order to visualize the cytoskeleton, Alexa fluor 594-labeled phalloidin (Invitrogen, USA) diluted to 1:100 was utilized to stain the F-actin. The slide was covered with a mounting medium containing 4 ,6-diamidino-2-phenylindole (Vectashield HardSet Mounting Medium;Vector Laboratories, USA). Control reactions were conducted using rabbit and mouse normal serum with non-specific primary antibodies, and the primary antibodies were omitted in order to prevent non-specific binding. Fluorescent triple-labeled specimens were inspected on a 2100 Multi Photon Imaging System (Radiance, USA) coupled to an Eclipse E800 microscope using a LaserSharp 2000 (Nikon, USA). Adobe Photoshop 7.0 and Confocal Assistant were used for primary image processing.

3. Human

Material

Three patients were involved in the study. Two males (ages: 50, 57) and one female (age: 50). They were operated for posterior uveal melanoma (melanoma malignum choroideae) in 2005 at the Department of Ophthalmology, University of Debrecen. All eyes were enucleated because of the tumor without prior treatment (they were disqualified for brachytherapy). The histological types of the tumors according to Callendar's classification were: spindle A, dominantly spindle B, and dominantly epitheloid tumor, respectively. The experiments involving human subjects were carried

out according to the Helsinki Declaration and with the approval of the Human Studies Ethical Committee, University of Debrecen.

Preparation of the retina

Right after enucleation a dorsal stitch was made for orientation, then a non-infiltrated part of the bulb was removed, and subsequently placed in the fixative (4% paraformaldehyde, in 0.1 M phosphate buffer, pH 7.4), and incubated for 24 hours at 4°C. Thereafter the solution was replaced with 0.1 M phosphate buffered saline (PBS, pH 7.4), and rinsed for at least 24 hours before further processing. Various parts of the retina have been collected this way, covering the whole retinal field. The retina was carefully detached from the posterior eyecup. Extreme care was taken to obtain samples from the peripheral part of the retina, even from behind the ora serrata. These ciliary and iridic regions cannot be separated from the ciliary body and the iris, so they were handled together. For frozen sections the retinas were incubated overnight in 30% sucrose (diluted in 0.1 M phosphate buffer), embedded in cryomatrix (ThermoShandon). 10 μm thick radial sections were prepared on a ThermoShandon cryotome. For radial semithin sectioning three samples were taken from the human retina following a radial plane including the macular region (M), periphery (P), ciliary body (CB).

Immunocytochemistry

Sections of 10 μm thickness were cut on a cryostat and dried onto poly-L-lysine coated glass microscope slides at 37°C. Sections were then soaked in phosphate buffered saline for 20 minutes. Subsequently, a blocking solution, 1% bovine serum albumin (BSA) with 0.1% Triton X-100 was applied for 2 hours. The primary antibody was applied at 4°C overnight. Primary antibodies anti-caveolin-1 (polyclonal rabbit IgG, Transduction Laboratories, www.translab.com), 1:100, anti-caveolin-2 (monoclonal mouse IgG, Transduction Laboratories), 1:200, and anti-caveolin-3 (monoclonal mouse IgG, Transduction Laboratories) 1:100, were diluted in 1% BSA at 4°C overnight. In the case of caveolin-1 and -3 anti-rabbit and anti-mouse Alexa 488

(Molecular Probes, www.invitrogen.com) were used as secondary antibodies. Since caveolin-2 gave a weak, hardly detectable signal with the previous method, we used biotinylated anti-mouse IgG, then Streptavidin Alexa 488 (Molecular Probes), 1:100, to intensify the signal. Even using this extra method caveolin-2 gave the weakest signal. For the visualization of the cytoskeleton, Alexa fluor 594-labeled phalloidin (Molecular Probes) was used to stain F-actin (1:100 in PBS). Vectashield HardSet Mounting Medium (Vector Laboratories, www.vectorlabs.com) with DAPI (4′,6-diamidino-2-phenylindole) was used to label the nuclei (blue) and to cover the slides. Control reactions were made using rabbit and mouse normal serum, non-specific primary antibodies and omitting the primary antibodies to preclude non-specific binding. The retinas were inspected on a Zeiss Axiophot microscope, using the appropriate filter set for the fluorescent antibodies. Fluorescent double or triple labeled specimens were also inspected on Radiance 2100 Multi Photon Imaging System coupled to a Nikon Eclipse E800 microscope using LaserSharp 2000. Adobe Photoshop 7.0 and Confocal Assistant softwares were used for the primary image processing.

4. Dogs

Animals

Dogs were maintained at the Retinal Disease Studies (RDS) facility in Kennett Square, PA, and supported by NEI/NIH (EY-06855) and Foundation Fighting Blindness Center grants; procedures were in adherence to the ARVO Resolution for the Use of Animals in Ophthalmic and Vision Research. The dogs represent an out bred population with a common genetic background segregating *erd* and other retinal disease alleles. 70 dogs were used in the study, including 44 crossbred *erd* affected dogs (age range, 4.3-165 weeks), and 26 non-affected dogs that were used as normal control subjects (age range, 4.7–25.7 weeks). All affected dogs were bred at the Retinal Disease Studies Facility (RDSF; University of Pennsylvania, New Bolton Center, Kennett Square, PA), and their genotype was determined either from the known status of their progenitors or from genetic testing for the disease-causing mutation. All normal control dogs came from the Baker Institute colony of specific pathogen-free dogs. After an ocular examination to identify abnormalities not associated with the primary retinal disease, all

animals were anesthetized by intravenous injection of pentobarbital sodium, the eyes enucleated, and the dogs euthanatized (Table 3).

Animal ID	*erd* status	Age(weeks)	Fixation
fetus	+/+	preterm	PF
E1038	-/-	4.3	PF
E1033	+/-	4.7	PF
E768	-/-	6.4	-
SPF#4	+/+	7	PF
E884	-/-	7.1	B
E886	-/-	7.1	B
E887	-/-	7.1	B
E1770	-/-	7.3	B
E936	-/-	7.7	PF
E942	-/-	7.7	PF
D129	+/+	8.2	-
E1039	-/-	8.3	PF
E1020	-/-	8.4	PF
E1034	+/+	8.7	PF
SPF#4	+/+	9	PF
E1029	-/-	9.1	PF
E1030	-/-	9.1	PF
E879	-/-	9.1	B
E880	-/-	9.1	B
E1022	-/-	9.3	PF
E658	-/-	9.6	-
E1024	-/-	10.4	PF
E937	-/-	11.6	PF
E943	-/-	11.6	PF
E783	-/-	11.9	-
SPF#4	+/+	12	PF
E1026	-/-	12.3	PF
#1887	+/+	12.3	PF
E1032	-/-	14.1	PF
GS54	+/+	25.7	PF
E585	-/-	48.1	B
E612	-/-	62	B
E918	-/-	68	B
E817	-/-	101	B
E857	-/-	165	B

Table 3. List of normal and diseased dogs used in the study

Disease status: +/+, wild type; +/-, *erd* carrier; -/- *erd* affected

Fixation: PF= 4% paraformaldehyde fixation and OCT embedding; B= Bouin's fixation and paraffin embedding, note that 34 dogs are not shown in the list: 21 used for rod

outer segment renewal and opsin biosynthesis and 10 for qRT-PCR and 3 control dogs used for Western blotting.

Immunocytochemistry

Retinas of 24 affected dogs in the age range of 4.3-165 weeks were examined morphologically. The retinas of 8 normal or carrier dogs (age range: one fetus, the others 4.7-25.7wks) were used as control specimens. Immediately after enucleation, the posterior segments were isolated and fixed, using 4% paraformaldehyde in 0.1 M phosphate-buffered saline at 4°C. The posterior segments were then cut into pieces that extended from the optic nerve to the ora serrata along the superior and inferior meridians, dehydrated, and embedded in either paraffin or OCT (Tissue Tek Optimal Cutting Temperature, Sakura Fientek, Torrance, CA). OCT sections of 7µm were cut on a Microm HM550 cryostat. Paraffin sections of 7µm were prepared on an American Optical 820 microtome by Excalibur Pathology Incorporation (Oklahoma City, OK). Sections from both the superior and inferior meridians were examined in a light microscope (Axioplan; Carl Zeiss Meditec GmbH Oberkochen, Germany) in contiguous fields ranging from the optic disc to the ora serrata. This included evaluation of the rod and cone OS and IS, and the thickness of the outer (ONL) and inner (INL) nuclear layers. For each dog, a single section from both quadrants (superior and inferior, respectively) was used for quantitative evaluation of the ONL and INL cells at two specific locations: A1, 2000 ± 500 µm from the optic nerve and A2, middle point of the retina ±500 µm. At each of these sites, the number of rows of nuclei in the ONL and INL were counted in three areas and averaged. For the same areas, the thickness (in micrometers) of the ONL and INL were measured. For illustration of retinal topography and retina development digital images were captured (Spot 4.0 camera, Diagnostic Instruments, Inc., Sterling Heights, MI) and imported into a graphics program (Photoshop and Illustrator; Adobe, Mountain View, CA) for display.

Ten *erd* (age range, 4.3–14.1 weeks) and 7 normal (age range, 4.7–25.7 weeks) retinas were used for immunocytochemistry. After enucleation, a slit was made through the globe at the level of the ora serrata, and the entire globe was fixed for 24 hours in 4% paraformaldehyde in 0.1 M phosphate-buffered saline at 4°C. The tissue was then trimmed, cryoprotected sequentially for 24 hours in a solution of 15% and 30% sucrose

in 0.1 M sodium phosphate buffer and 0.15 M sodium chloride (pH 7.2, phosphate-buffered saline; Pierce, Rockford, IL; referred to in the text as PBS) at 4°C, and embedded in OCT medium. Sections along the superior and inferior retinal meridian of the thirteen *erd* dogs and six normal dogs that were processed as described earlier were used for fluorescent immunohistochemistry, using cell-specific primary antibodies.

Retinal cell markers and antibodies	**Antibody type**	**Normal retinal localization or target protein**
Human cone arrestin (hCAR)	rabbit polyclonal	cones
PNA-rhodamine lectin	lectin	cone insoluble matrix
CNGA3	rabbit polyclonal	cone OS
Red/green opsin (COS-1)	mouse monoclonal IgG3	L/M-cone OS
Red/green opsin	goat polyclonal	L/M-cone OS
Red/green opsin	rabbit polyclonal	L/M-cone OS
Blue opsin (OS-2)	mouse monoclonal IgG3	S-cone OS
Blue opsin	goat polyclonal	S-cone OS
Blue opsin	rabbit polyclonal	S-cone OS
Rhodopsin	mouse monoclonal IgG1	rod OS
Rhodopsin	rabbit polyclonal	rod OS
Glutamine Synthetase	mouse monoclonal IgG2b	Müller cells
CD18 (CA16:3C10)	mouse monoclonal IgG1	canine monocytes, granulocytes, microglia
CRABP	rabbit polyclonal	Müller cells
PCNA	mouse monoclonal IgG2a	proliferating cell nuclear antigen
KI67	monoclonal mouse IgG1	nuclear cell proliferation antigen
Phospho Histone H3 (Ser 10)	rabbit polyclonal	mitosis
Phospho Histone H3 (Ser 10)(6G3)	mouse monoclonal	mitosis
TUNEL In Situ Cell Death Detection Kit, Fluorescein		apoptotic cell nuclei
Nestin, clone 10C2	mouse monoclonal IgG1	neuronal stem cells
NR2E3	rabbit polyclonal	Nr2e3
NRL	rabbit polyclonal	Nrl
PAX6	rabbit polyclonal	amacrine and ganglion cells, neuronal progenitors
Protein kinase C (PKCα)	mouse monoclonal IgG2b	Rod bipolar cells
Goα	mouse monoclonal IgG1	ON (rod and cone) bipolar cells
Calretinin	rabbit polyclonal	Horizontal cell and amacrine cells
Calbindin D-28K	rabbit polyclonal	Horizontal cells
Neurofilament 200 kDa	mouse monoclonal IgG1	Horizontal dendrites, ganglion cells, neurofilaments
Vimentin	mouse monoclonal IgG2bκ	Müller cells
GFAP	rabbit polyclonal	Müller cells, astrocytes
RDS/peripherin 3B6	mouse monoclonal IgG	rod and cone OS
CRX	rabbit polyclonal	Crx
Actin	rabbit polyclonal	loading control

Table 4. A list of antibodies and other retinal cell markers used on dog retinas for immunocytochemistry.

Cryosections (7µm thick) were incubated with the primary antibodies overnight at either 4°C or 1h on room temperature after a blocking step with 1.5% BSA/PBS, 0.25% Triton X-100 (Sigma-Aldrich, St. Louis, MO). The antigen–antibody complexes were visualized with fluorochrome-labeled secondary antibodies (Alexa Fluor, 1:200; Invitrogen, Carlsbad, CA). DAPI stain was used to detect cell nuclei. Slides were mounted with a medium composed of polyvinyl alcohol and DABCO (1,4 diazobizyklo-[2.2.2]oktan) (Gelvatol; Sigma-Aldrich, St. Louis, MO), and examined with an epifluorescence microscope (Axioplan; Carl Zeiss Meditec). Images were digitally captured (Spot 4.0 camera; Diagnostic Instruments, Inc.) and imported into a graphics program (Photoshop; Adobe, Mountain View, CA) for display.

Primary antibodies and other cell markers used to detect various retinal cell types or target proteins are detailed in Table 4. The latters include: *cones*: human cone arrestin, CNGA3 (cyclic nucleotide gated channel alpha 3), red/green cone opsin, blue cone opsin; r*ods*: rod opsin; *Müller cells, microglia and macrophages*: GS (glutamine synthetase), CD18 (integrin beta-2); *cell proliferation, retinal stem cells*: PCNA (proliferating cell nuclear antigen), KI-67 (Kiel-67), PHH3 (phospho-Histone H3), Nestin; *transcription factors*: PAX6 (paired box protein 6), NR2E3 (or PNR, photoreceptor-specific nuclear receptor), NRL (neural retina leucine zipper). Apoptotic nuclei were visualized by TUNEL (terminal deoxynucleotidyl transferase-mediated biotinylated UTP nick end labeling) with the *In Situ* Cell Death Detection kit (Roche Applied Science, Indianapolis, IN). Antigen retrieval was performed prior to PCNA and PHH3 labeling by heating in the presence of Antigen Unmasking Solution, High pH (Vector Laboratories, Burlingame, CA) using a microwave oven at 10% power.

Both single and double immunolabelings were used. The primary antibody pairs used for double immunolabeling were combinations of rabbit or goat polyclonal and mouse monoclonal antibodies. The antigen–antibody complexes were visualized with fluorochrome-labeled secondary antibodies (Alexa Fluor, 1:200; Invitrogen, Carlsbad, CA), and 4',6'-diamino-2-phenylindole (DAPI) stain was used to label cell nuclei. Slides were mounted with a medium composed of polyvinyl alcohol and DABCO (1,4 diazobicyklo-[2.2.2]oktan, Gelvatol; Sigma-Aldrich), and examined with an

epifluorescence microscope (Axioplan; Carl Zeiss Meditec, Thornwood, NY). Epifluorescence or transmitted light images were captured with a Spot 4.0 camera (Diagnostic Instruments, Inc., Sterling Heights, MI) and imported into a graphics program (Photoshop and Illustrator; Adobe, San Jose, CA) for display. When precise localization of markers was needed, sections were also imaged by confocal microscopy using a Nikon A1R Laser Scanning Confocal Microscope with DUS 32 Spectral detector (Nikon Instruments, Melville, NY) through a 63 X Plan objective lens. The specimens were excited at 488 and 561 nm, respectively, with multi line Argon and DPSS lasers.

For cell death and cell proliferation studies the following number of dog retinas were prepared: TUNEL assay 11 *erd* (age range, 4.3-14.1 weeks), 5 normal (age range, 4.7-12wks); PCNA 7 *erd* (age range, 4.3-14.1 weeks), 3 normal (age range, 7-12 weeks); PHH3 labeling 2 *erd* (ages 7.7 wks and 11.6 wks) and 1 normal (7 wks of age). PHH3 labeling was used to differentiate mitotic cells from those undergoing DNA repair labeled with PCNA. The tissues were prepared the same way as described before for immunocytochemistry. Sections were counterstained with 4',6'-diamino-2-phenylindole (DAPI). Positive control specimens included sections pretreated with DNase I (3 U/mL in 50 mM Tris-HCl [pH 7.5]) and 1 mg/mL BSA for 10 minutes at room temperature). For negative control subjects, the terminal transferase enzyme was omitted from the TUNEL reaction mixture. Histone H3 was used as a control to confirm the specificity of TUNEL labeling. Before PCNA and PHH3 labeling, antigen retrieval was performed: by heating and irradiating the sections for 10’ in Antigen Unmasking Solution, High pH (Vector Laboratories Inc., Burlingame, CA) using a microwave oven at 10% power. For PCNA labeling a dog fetus was used as a positive control. The specificity of PCNA labeling was also confirmed by KI 67 labeling, which was described earlier as a good cell proliferation marker in dogs (Beltran et al 2006). Sections were examined from the optic disc to the ora serrata by epifluorescence microscopy with the 40x objective. Images were digitally captured (Spot 4.0 camera; Diagnostic Instruments, Inc.) and imported into a graphics program (Photoshop, Mountain View, CA) for display. TUNEL-. PCNA- and PHH3-labeled cells in the ONL were counted throughout the entire length of the section (i.e., from disc to ora serrata). In determining the proportion of photoreceptor cells that undergo cell death as a function

of time, we express our results as the number of TUNEL-, PCNA and PHH3 labeled photoreceptor cells per 1 million μm^2 of ONL. The area of the ONL of each section was obtained by measuring the entire length of the ONL from optic disc to ora serrata, and multiplying it by the average thickness of the ONL throughout the section (mean value of the thickness measured in the ten locations, evenly distributed along the retina). For each dog, this procedure was performed at least in triplicate with sequential sections from both the superior and inferior meridian. The values were averaged and reported as the mean 1 ± SD.

Immunoblotting and densitometric analysis

Dogs of different ages were used for these studies including 2 *erd* affected dogs (6.4 wks and 9.9 wks) and 3 controls (16 wks). Equal amounts of total protein as determined by BCA Protein Assay Kit (former Pierce Biotechnology, now Thermo Fisher Scientific**,** Rockford, IL) were separated by 10% SDS-PAGE under reducing conditions, immunoblotted and probed with antibodies. These are detailed in Table 5 and include antibodies against red/green opsin, blue opsin, CNGA3, NRL, NR2E3, RDS/peripherin, and CRX. Appropriate HRP-conjugated secondary antibodies were used subsequently, and an antibody against β-actin was used as a loading control. Densitometric analysis of the blots was performed on Kodak Image Station 4000MM (Molecular Imaging Systems, Carestream Health, Rochester, NY). The net intensity was corrected for background intensity observed. Values in figure are expressed as corrected net intensity of the sample normalized to corrected net intensity of actin loading controls. Densitometry data were analyzed using Sigma Stat Version 3.1, and intensities from four independent measurements on two westerns were analyzed by Student t test using 95% or 99% confidence intervals.

DOI:10.14753/SE.2014.1845

Markers	Host	Normal retinal localization or target protein
Red/green opsin	rabbit polyclonal	L/M-cone OS
Blue opsin	rabbit polyclonal	S-cone OS
CNGA3	rabbit polyclonal	cone OS
NRL (H-120)	rabbit polyclonal	Nrl
NR2E3 (N-13)	goat polyclonal	Nr2e3
RDS/peripherin 3B6	mouse monoclonal IgG	rod and cone OS
CRX	rabbit polyclonal	Crx
Actin	rabbit polyclonal	loading control

Table 5. List of antibodies used for immunoblotting of dog retinas.

Rod outer segment renewal and opsin biosynthesis

Rod OS renewal and opsin biosynthesis were examined at specific time points following the injection of ^{3}H-fucose or ^{3}H-leucine (OS renewal) or a combination of ^{3}H-fucose/^{14}C-leucine (opsin biosynthesis) into the vitreous of anesthetized dogs using previously described methods.(Aguirre and O'Brien, 1986) Post-injection time points were 1, 2, 3 and 4 days for OS renewal, and 1, 2 and 4 days for opsin biosynthesis. In the 4 day interval following injection, the rods have renewed ~50% of their OS due to continuous addition of new discs at the base (Aguirre and O'Brien, 1986) For the renewal studies, the eyes were fixed in mixed-aldehyde/osmium solution, embedded in plastic resin, and 1 μm thick sections coated with a photographic emulsion and maintained at 4^{0} C in the dark until developed.(Aguirre and O'Brien, 1986). Two series of experiments were conducted to examine opsin biosynthesis, and loss of opsin labeling over time after injection. For these studies, eyes received a combination of ^{3}H-fucose and ^{14}C-leucine intravitreally. Eyes from dark adapted dogs were enucleated under dim red light, and crude rod outer segment preparations were made by vortexing and centrifugation in 40% (w/v) sucrose. After sonication, detergent solubilized rod OS proteins were separated in a 10% polyacrylamide gel, stained with Coomassie blue, and gel slices digested and counted in a scintillation counter (Aguirre and O'Brien, 1986). Disintegrations per minute (DPM) in the opsin peaks were normalized to the highest protein value for each set of gels, and to the DPM count for the post injection day 1 control eye of the same series.

Gene expression studies

Quantitative real time-PCR (qRT-PCR) was used to assess expression of selected genes at different time points of normal development (3 (n=3) and 7 (n=3) wks) and disease (6.4 (n=2), 8.3/9.9 (n=3) and 11.9/14.1 (n=2) wks). Retinas from 16 wk (n=3) normal dogs served as reference control. Total RNA was isolated by Trizol extraction (Invitrogen-Life Technologies, Carlsbad, CA), and concentration measured with a Nanodrop 1000 spectrophotometer (Thermo Fisher Scientific**,** Wilmington, DE). RNA samples were treated with RNase-free DNase (Ambion, Austin, Tx), and two µg total RNA from each sample was used for cDNA synthesis using the High Capacity cDNA reverse transcriptase Kit (Applied Biosystems (ABI), Foster City, CA). Quantitative RT-PCR was performed on a 7500 Real Time PCR System and software v2.0 (ABI) using 30 ng cDNA from each sample, and amplified using Taqman assays with canine-specific ABI inventoried probes for *STK38L/NRD2*, *LATS1* (Cf02626754_m1) and *CCNA1* (Cf02633425_m1); SYBR green analysis was used for *CCND1* (Forward: CATCTACACTGACAACTCCATCC; Reverse: CAGGTTCCACTTCAGTTTGTTC). For analysis of *STK38L/NRD2* one probe was located within the exonic deletion (Cf02709228_m1), and the second in exon 6, 3' to the exon 4 splicing defect, and used to exclude alterations in splicing resulting from the SINE element insertion (Cf02634613_m1). CT values of each gene were normalized to *GAPDH*, and comparisons between groups were done with the ΔΔCT method(Livak and Schmittgen, 2001). Statistical significance between different groups in comparisons to the 16 wks old normal control retinas was assessed with an unpaired *t*-test, and expressed as statistically significant ($p \leq 0.05$) or towards statistical significant ($0.05 \leq p \leq 0.1$).

DOI:10.14753/SE.2014.1845

V. Results

1. Expression of lipid raft-associated proteins during photoreceptor development

Similarly to other rodents, the hamster retina is undeveloped at birth (Greiner and Weidman, 1978). Syrian hamsters are born blind, the eyes open only at the end of the second postnatal week. On the first postnatal day (P1) the retina consists of three cell layers: retinal pigment epithelium (RPE), neuroblastic layer (NBL) and the ganglion cell layer (GCL). The immature inner plexiform layer (IPL) and optic nerve layer are also present. The neuroblastic layer is predominantly made of neuroblasts; however, a few nuclei reminiscent of cone nuclei located adjacent to the outer limiting membrane (OLM) can also be discerned. Outer- and inner segments (OS/IS) are not yet formed, but a slight protrusion of the apical portion of prospective photoreceptor cells above the level of the OLM can be clearly observed at a few places with electron microscopy (EM). Here, apically located centrioles are also present (Figure 6, A and B). At P5 the structure of the retina is similar to P1, but electron microscopy reveals that the distal regions of photoreceptors start to enlarge (prospective inner segments, Figure 6, C and D). At P10 the NBL has already been separated, by a thin, immature outer plexiform layer (OPL), into outer- and inner nuclear layer, and the IPL has widened. Photoreceptor OS and IS are not clearly defined with light microscopy, but using electron microscopy immature IS and OS are already recognizable at P10. The IS are small and in the OS the stacks of primitive discs show a random orientation. At P15 the retina of the hamster is similar to that of the adult (see Figure 11, Panel B). The OPL is still very thin, but is more straight and organized than it was at P10, while the IPL is morphologically mature. The OS and IS are distinguishable, but their size is smaller, than in the adult. With electron microscopy, OS and IS are relatively small, but structurally differentiated. In the OS discs are packed parallel to each other and are arranged horizontally (Figure 6, E and F).

DOI:10.14753/SE.2014.1845

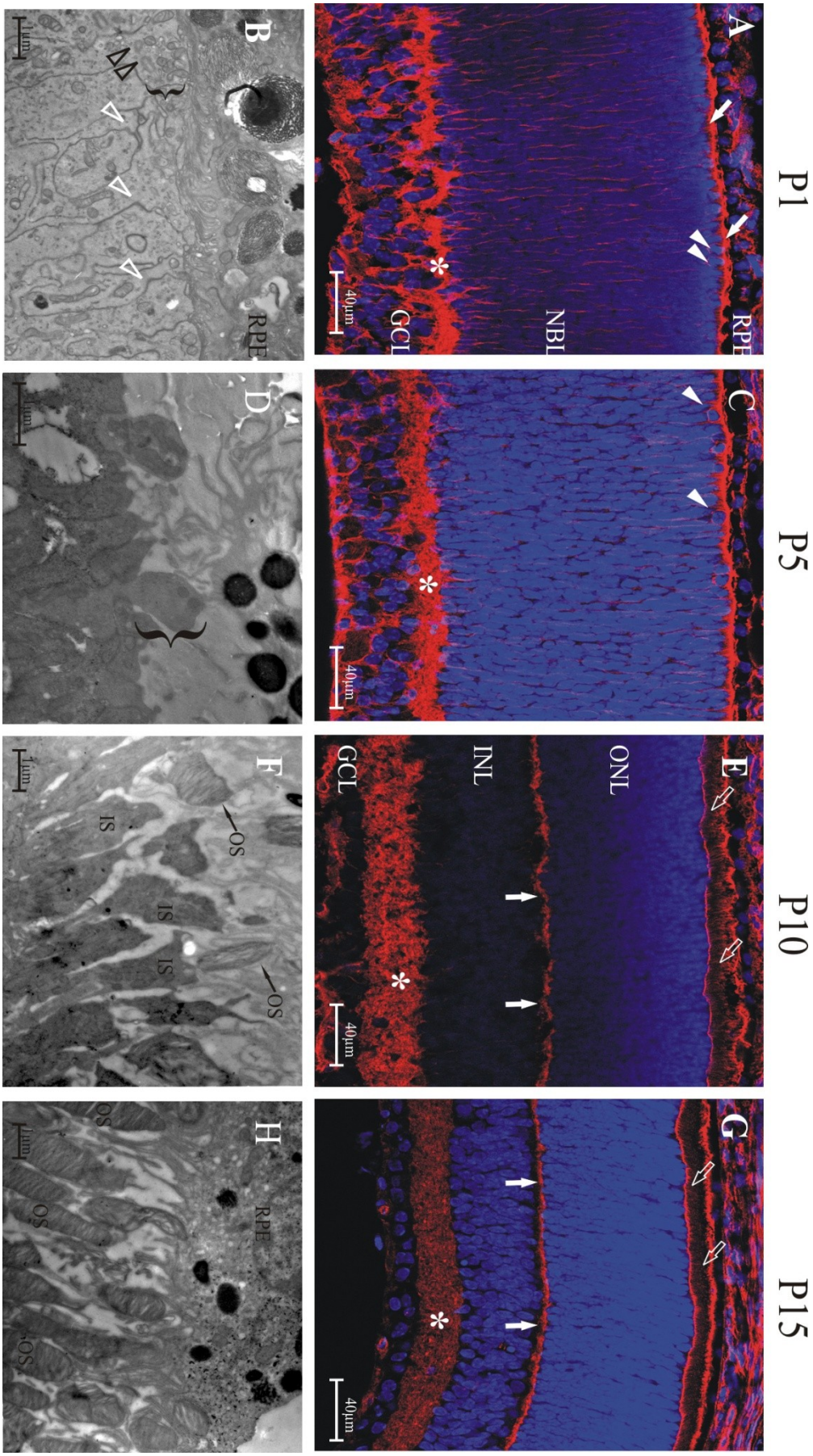

Figure 6. The development of the Syrian hamster retina.

Upper row: 10 μm cryo sections labeled with phalloidin Alexa 594, lower row: ultrathin sections for routine electron microscopy (EM). A, B: postnatal day 1 (P1); C, D: postnatal day 5 (P5); E, F: postnatal day 10 (P10); G,H: postnatal day 15 (P15). **A**: At P1 the retina has three cell layers: retinal pigment epithelium (RPE), neuroblastic layer (NBL) and the ganglion cell layer (GCL). The immature inner plexiform layer is also visible *(*)*. In the neuroblastic layer presumptive cone nuclei can be observed *(arrowheads)*. The gap between RPE and NBL is a remnant of the optic vesicle into which the apical portions of differentiating photoreceptors and apical processes of pigment epithelial cells protrude, but outer- and inner segments (OS, IS) are not yet formed. *(oblique, filled arrows)*. **B**: The outer limiting membrane is made of dense membrane junctions between photoreceptor cells *(open, white arrowheads)*. The distal portions of some rod cells begin to protrude through the outer limiting membrane *(bracket)* and immature centrioles are also visible *(open, black arrowhead)*. **C**: At P5 no difference can be noted compared to P1 with light microscopy. **D**: It is visible on the EM image at P5 that the distal regions of some photoreceptors enlarge forming primitive inner segments *(bracket)*. **E**: At P10 the NBL is separated by an immature outer plexiform layer (OPL, *vertical filled arrows*) forming the outer- and inner nuclear layers (ONL, INL). The OPL is very thin, whereas the thickness of the IPL is increasing *(*)*. The presence of OS and IS is only conjectural with light microscopy *(oblique, filled arrows)*. **F**: IS and OS are recognizable at P10 using EM. The OS are immature, discs are not yet organized in a horizontal array. **G**: At P15 the retina is already very similar to that of the adult (see Figure 4), all layers are recognizable. The OPL is still very thin, but is more straight and organized than it was at P10 (*vertical filled arrows)*. The IPL is morphologically mature (*). The OS and IS can be distinguished, however, their size is smaller, than in the adult (see Figure 4). **H**: OS and IS are small in size, but structurally formed. In the OS discs are packed parallel and are arranged horizontally.

In order to study the caveolin-1 localization during photoreceptor development, we compared it to two highly abundant, well characterized proteins, rhodopsin and rhodopsin kinase. In addition, we also investigated the distribution profile of a kinase responsible for caveolin-1 phosphorylation, c-src, as well as the phosphorylated product, phospho-caveolin-1 (Figure 7). At P1 rhodopsin, rhodopsin kinase (GRK-1), caveolin-1 and phospho-caveolin-1 are not yet detectable in the prospective photoreceptor layer. However, c-src is present in the pigment epithelium (RPE), in the neuroblastic layer (NBL) and in the apical portion of prospective photoreceptor cells (Figure 7, P1). At P5 labeling of rhodopsin and rhodopsin kinase starts to appear in the NBL. While rhodopsin is localized to a few individual cells, mainly in the plasma membrane delineating the form of the cells, rhodopsin-kinase gives only a few punctuate signals in the NBL. Caveolin-1 and phospho-caveolin-1 are present in the outer part of the NBL, assumedly in the apical portion of forming photoreceptor cells, as well as in the RPE. The labeling of c-src is similar to that of P1: c-src is present throughout the NBL, in the apical portion of forming photoreceptors and RPE (Figure 7, P5). At P10 rhodopsin and rhodopsin kinase can be detected at the level of developing OS/IS and in the outer nuclear layer (ONL). Caveolin-1 and c-src label the RPE, immature OS/IS, and the ONL. Interestingly, the localization and distribution of rhodopsin, rhodopsin kinase, caveolin-1 and c-src is very similar in the ONL. The signals are located throughout the ONL and have a granular, punctuate appearance. In contrast, phospho-caveolin-1 is present only at the level of OS/IS and in the RPE (Figure 7, P10). At P15 the distribution of the proteins is very similar to P10, however, at this time point, the OS can be more or less differentiated from IS with light microscopy. Rhodopsin, rhodopsin kinase, caveolin-1 and c-src are present throughout the ONL and in OS/IS (caveolin-1 and c-src is detectable also in the RPE), however, caveolin-1 and c-src are visibly more dominant in IS than in OS. In contrast, phospho-caveolin-1 can only be detected in the OS/IS (most probably at the level of primitive outer segments), as well as in the RPE (Figure 7, P15).

DOI:10.14753/SE.2014.1845

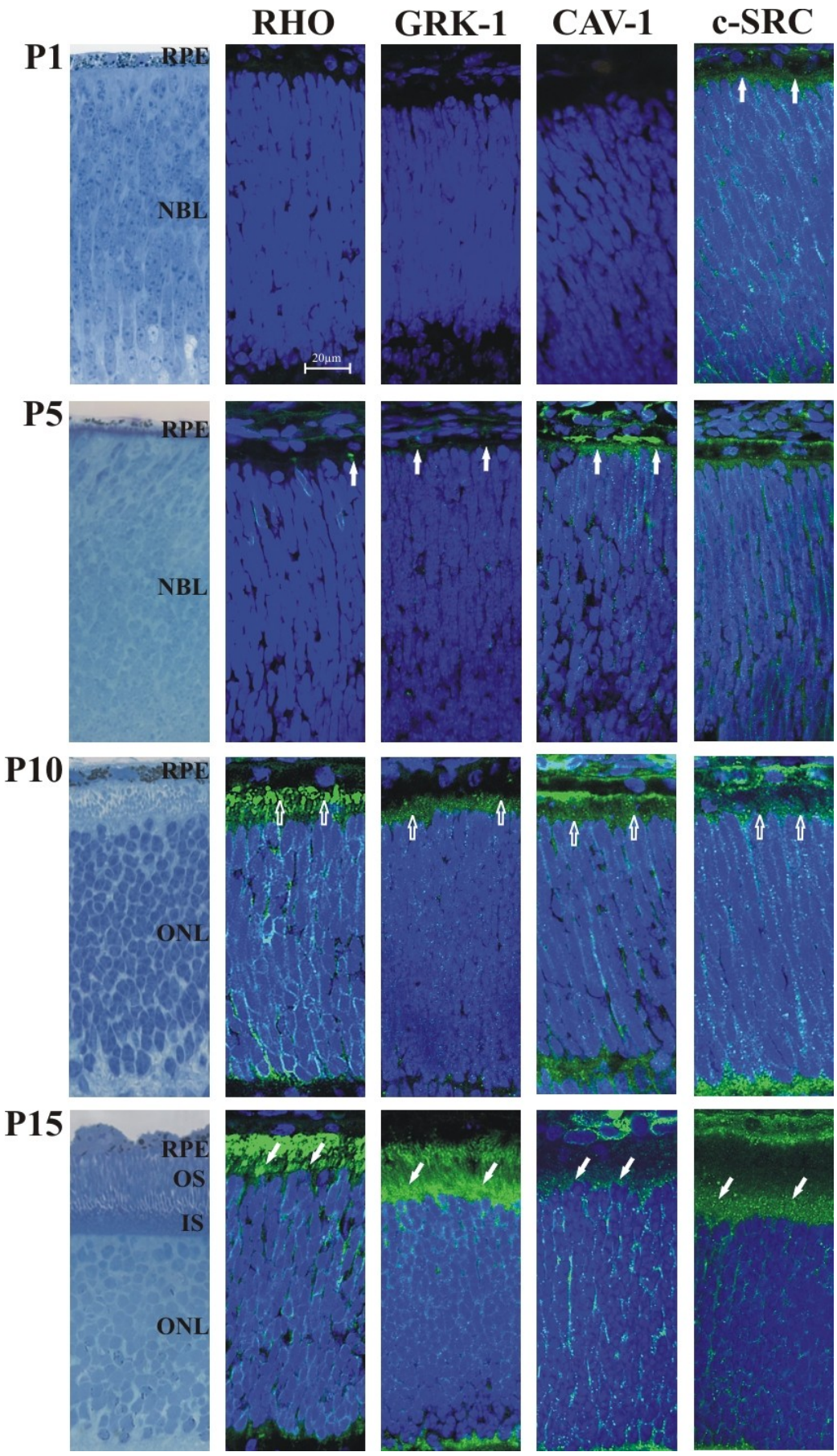

DOI:10.14753/SE.2014.1845

Figure 7. Developmental stages of the photoreceptor cell layer with immunostaining. Column 1 shows retinal structure on toluidine blue-stained semithin sections. Columns 2-5: Immunocytochemistry using different antibodies (green) against rhodopsin (RHO, column 2), rhodopsin kinase (GRK-1, column 3), caveolin-1 (CAV-1, column 4), phosho-caveolin-1 (pCAV-1, column 5) and c-src (c-SRC, column 6) at different ages, postnatal day 1, 5, 10 and 15 (P1-15). Nuclei are labeled with DAPI (blue). Arrows indicate the following areas: the apical portion of forming photoreceptor cells (*filled, vertical arrows*), the level of forming OS and IS (*open, vertical arrows*), inner segments (*filled, oblique arrows)*.

The extent of protein expression during development was followed by Western blot analysis. Rhodopsin, rhodopsin kinase, caveolin-1 and phospho-caveolin-1 were not detected at P1, while their expression gradually increased through P5, P10 and P15 until adulthood. In comparison, there is no marked change in the expression of c-src during development (Figure 8).

DOI:10.14753/SE.2014.1845

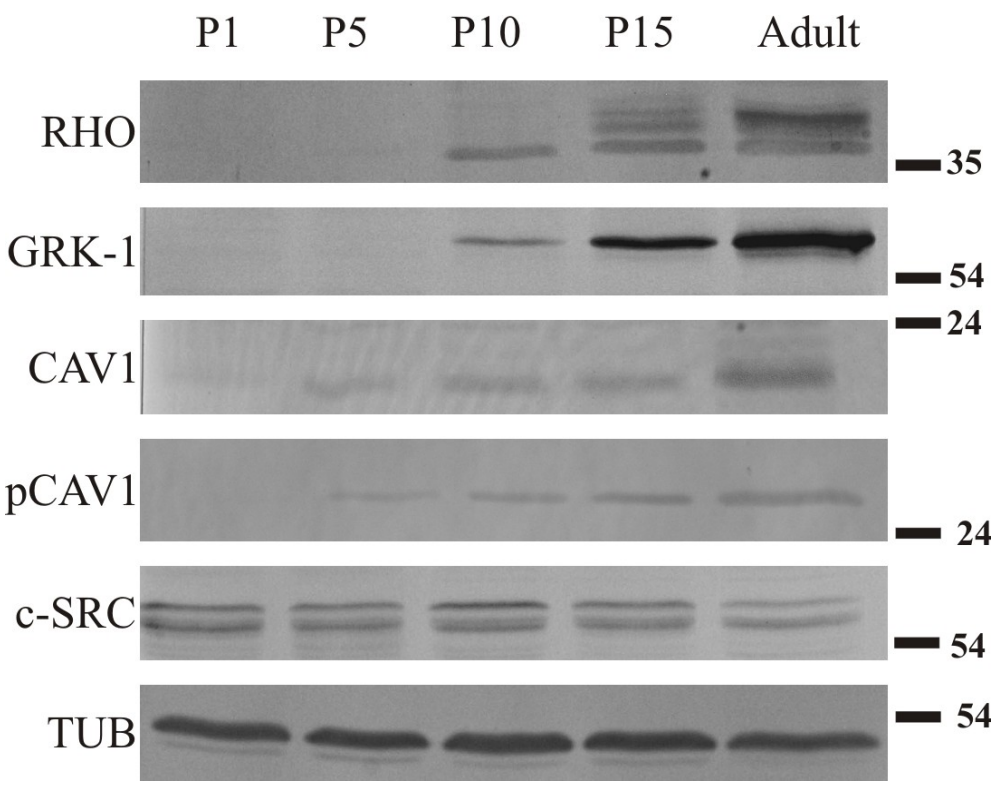

Figure 8. Western blot analysis of whole retinal homogenates from developing Syrian hamster.

P1, P5, P10, P15 and adult retinas were tested with antibodies against rhodopsin (RHO), rhodopsin kinase (GRK-1), caveolin-1 (CAV-1), phosho-caveolin-1 (pCAV-1) and c-src (c-SRC). Endogenous control: tubulin (TUB). Note the increasing expression of rhodopsin, rhodopsin kinase, caveolin-1 and phosho-caveolin-1(not or minimally expressed at P1 and their expression increases through P5, P10 and P15 until adulthood), while the expression of c-src shows no marked change during development.

DOI:10.14753/SE.2014.1845

Since the distribution of rhodopsin, rhodopsin kinase, caveolin-1 and c-src was similar at P10 and P15, the question arose whether these proteins are located in a common compartment or not. In order to test if these proteins are co-distributed, double-labeling immunocytochemistry was used. As the similarity of the distribution was most obvious at postnatal day 10, we chose this age to compare the distribution of rhodopsin and caveolin-1 (Figure 9, A) as well as the distribution of rhodopsin with c-src (Figure 9, B). Individual punctuate structures between the outer limiting membrane and outer plexiform layer were seen to be labeled by both rhodopsin and caveolin-1, indicated by yellow color in the merged images. The heavy staining of the OS/IS layer by the rhodopsin antibody made observation of an eventual colocalization difficult. A similar overall observation could be made on specimens double-labeled with rhodopsin and c-src (Figure 9).

DOI:10.14753/SE.2014.1845

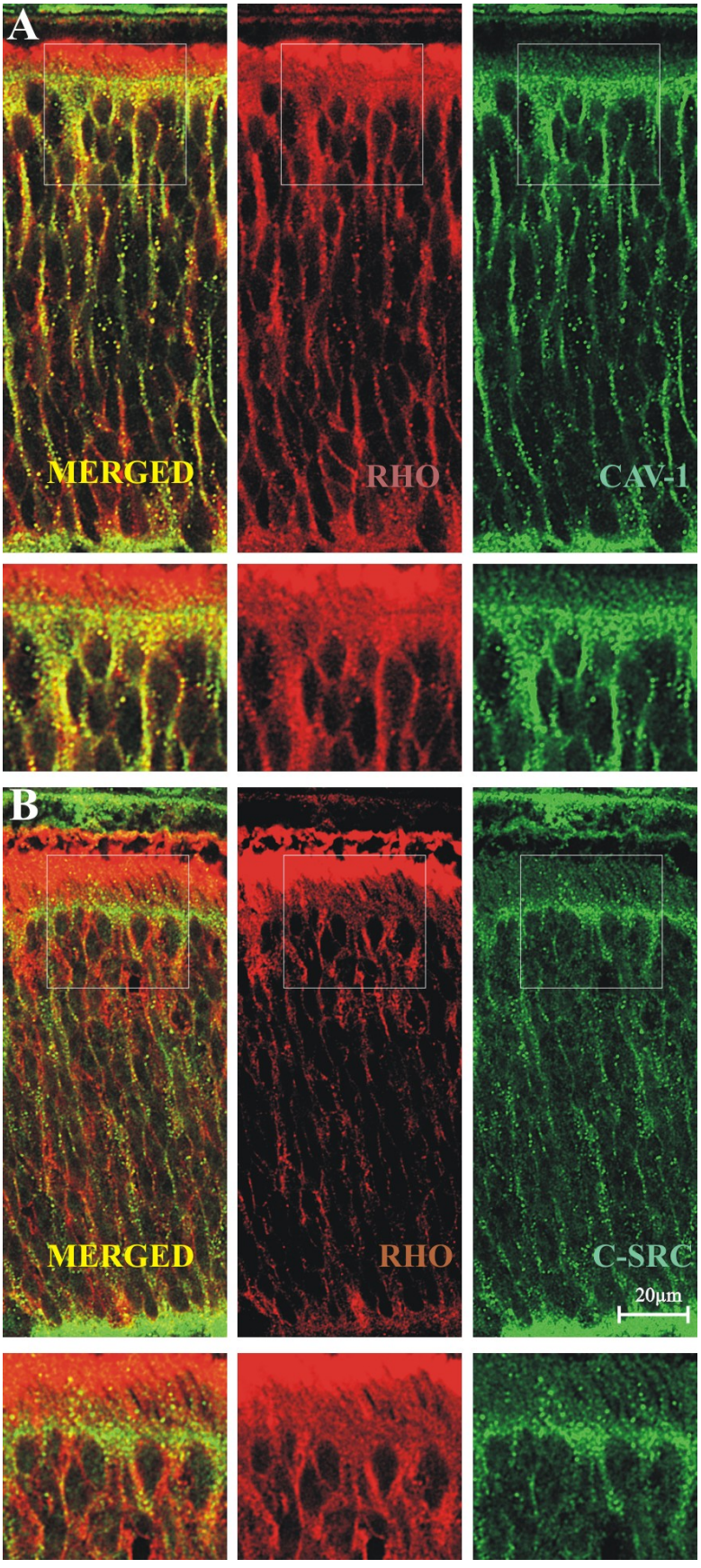

Figure 9. Double immunolabeling of rhodopsin with caveolin-1 and rhodopsin with c-src in the developing retina at P10.
A: rhodopsin (red) and caveolin-1 (green); B: rhodopsin (red) and c-src (green). Individual punctuate structures appear yellow (co-localization).

In order to determine if rhodopsin formed a complex with other raft-associated OS proteins, as identified by immuncytochemical colocalization, we used immuoprecipitation. We also investigated the co-immunoprecipitation with two other proteins of the OS: ROM-1 and RDS. Previously ROM-1 was reported to be a part of the OS raft membrane domains, but RDS was not found in this same fraction (Boesze-Battaglia et al., 2002). Whole retinal lysates from P1, P5, P10, P15 and adult were immunoprecipitated with the anti-opsin antibody. Immunoprecipitated complexes were isolated and their protein content determined by Western blots. Rhodopsin was found to co-immunoprecipitate with caveolin-1, c-src and ROM-1, but not with RDS (Figure 10), (Berta et al., 2011b).

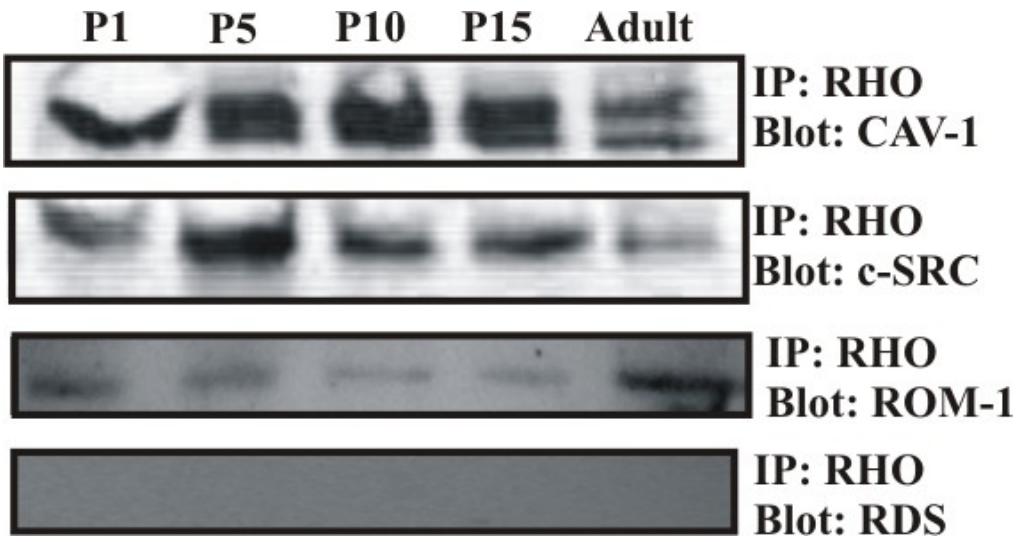

Figure 10. Immunoprecipation with rhodopsin antibody using whole retinal lysates from different stages of development (P1, P5, P10, P15) and adult Syrian hamster.
Rhodopsin co-immunoprecipitates with caveolin-1, c-src and ROM-1, but not with RDS.

DOI:10.14753/SE.2014.1845

2. Localization of raft-associated proteins in the photoreceptors of the mature retina of the Syrian hamster

The morphology of the adult hamster retina is very similar to that of other rodents. The golden hamster retina (Figure 11, Panel A) has an abundance of rods, with a relatively low number of cones. The outer- and inner segments of rods are thin (Figure 11, Panels A and B), and finer details can only be seen with electron microscopy. To characterize the rod photoreceptors with immunocytochemistry we used specific antibodies against rhodopsin, as well as rhodopsin kinase. The labeling of rhodopsin is restricted to the OS, while rhodopsin kinase is present in OS/IS and in the outer nuclear layer (Figure 11, Panel C). We determined the caveolin-1 distribution in the photoreceptor layer of the retina and also studied the localization of c-src (an enzyme that phosphorylates caveolin-1, (Schlegel et al., 1998), as well as the phosphorylated form of caveolin-1 (Figure 11, Panel C). The presence of caveolin-1 is clearly seen in the IS, however, it can only be detected in traces in the OS. The ONL, which is generally made of the cell bodies of photoreceptors and Müller cell processes, also contains caveolin-1. In contrast to caveolin-1, phospho-caveolin-1 is restricted to the OS while the IS and the ONL lacking phospho-caveolin-1 labeling. The distribution of c-src in the photoreceptor layer is analogous to that of caveolin-1: c-src is more dominant in IS, weakly stains OS and shows a scattered punctuate labeling in the ONL. The pigment epithelium also contains caveolin-1, phospho-caveolin-1 and c-src, but it is not labeled with rhodopsin or rhodopsin kinase antibodies (Figure 11, Panel C).

DOI:10.14753/SE.2014.1845

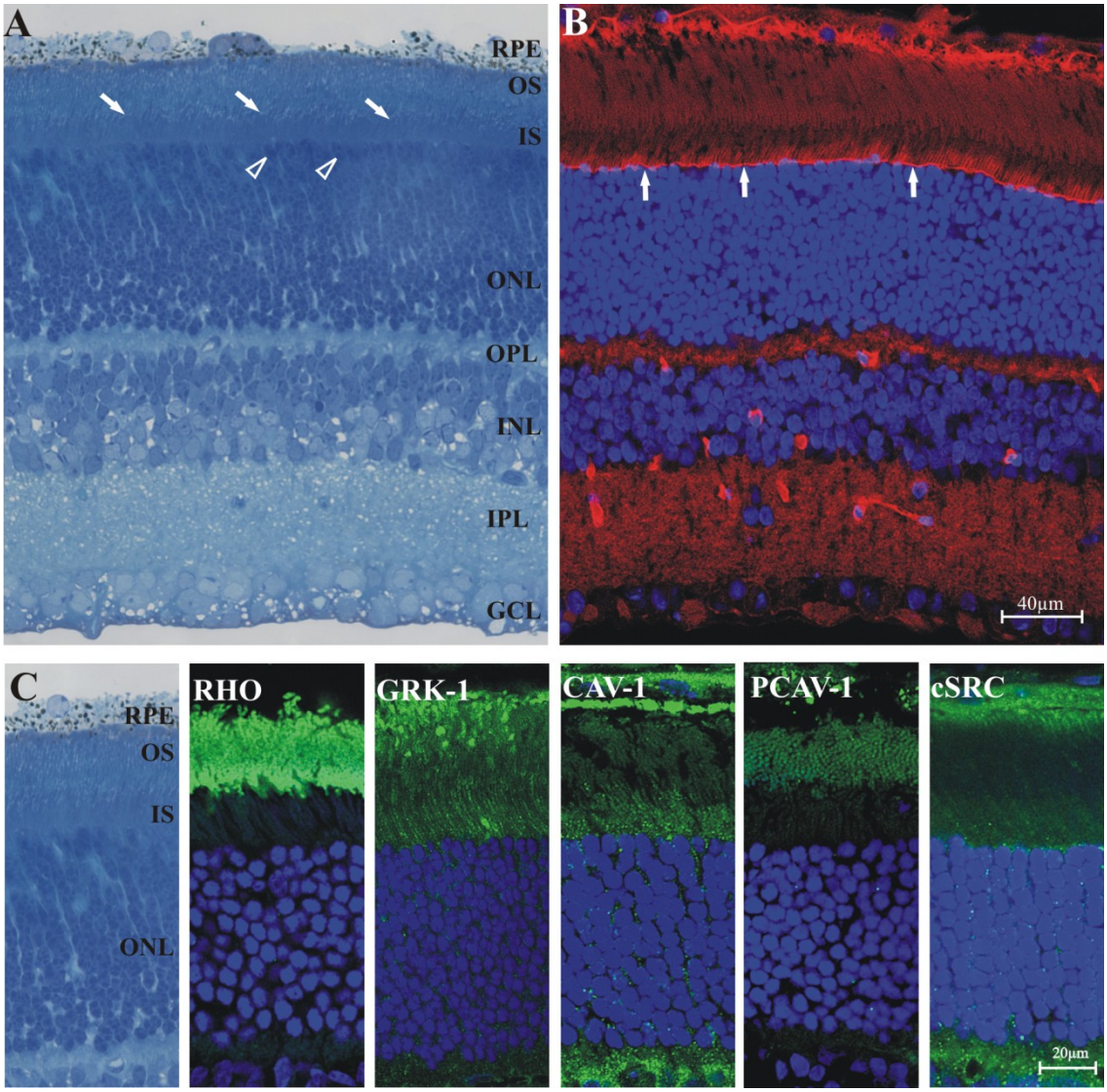

Figure 11. Immunolabeling of the adult Syrian hamster retina.
A: Semithin section with toluidin blue staining: structure of the mature hamster retina. Marked layers: retinal pigment epithelium (RPE), outer segments (OS), inner segments (IS), outer nuclear layer (ONL), outer plexiform layer (OPL), inner nuclear layer (INL), inner plexiform layer (IPL), ganglion cell layer (GCL). The hamster retina contains dominantly rods, with fewer cones *(open arrowheads show the nuclei of some presumptive cones)*. Photoreceptor OS and IS are thin and densely packed, the border between OS and IS is apparent *(oblique arrows)*. **B**: 10 μm cryo-section, phalloidin (red) labeling. Overall morphology of the retina. Phalloidin labeling enhances the outer limiting membrane *(vertical arrows)* and the blood vessels (round red structures in the OPL, INL and IPL). Nuclei are labeled with DAPI (blue). **C**: 10 μm cryo-section, localization of rhodopsin (RHO), rhodopsin kinase (GRK-1), caveolin-1 (CAV-1), phosho-caveolin-1 (pCAV-1) and c-src (c-SRC) in the photoreceptor layer of the Syrian hamster. Immunolabeling of different proteins is shown in green, nuclei are labeled with DAPI (blue).

The phospho-caveolin-1 content was determined in whole retinal lysates and isolated ROS fractions. As expected, the ROS lysate is enriched in rhodopsin and rhodopsin kinase when compared to the whole retinal lysate. Caveolin-1, phospho-caveolin-1 and c-src are all detectable in both ROS and whole retinal lysates (Figure 12).

DOI:10.14753/SE.2014.1845

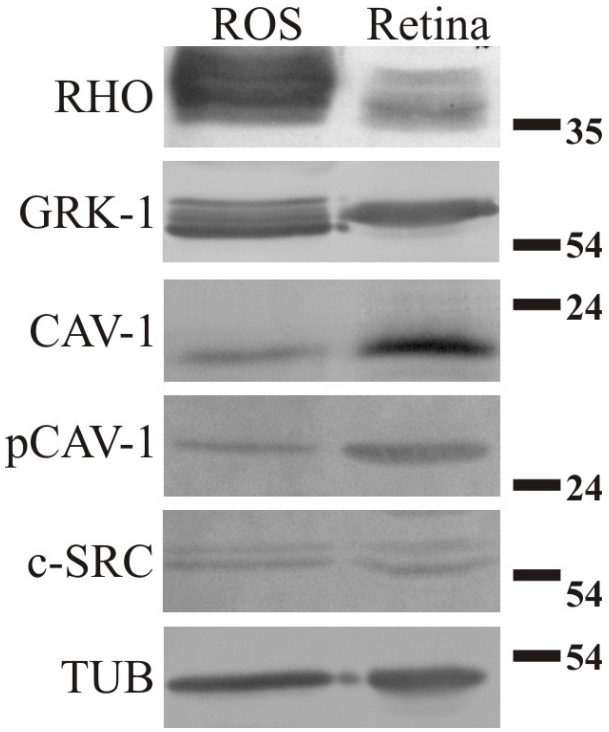

Figure 12. Detection of rhodopsin, rhodopsin kinase, caveolin-1, phosho-caveolin-1 and c-src in isolated ROS (rod outer segment) membrane lysates and in whole retinal homogenates. Tubulin (TUB) was used as an endogenous control. Note the rhodopsin (RHO) and rhodopsin kinase (GRK-1) enrichment in ROS lysates. Caveolin-1 (CAV-1), phospho-caveolin-1 (pCAV-1) and c-src (c-SRC) are all present in both lysates. While c-src protein could be detected without any marked difference in the two specimens, the expression of caveolin-1 was more prominent in the retinal lysate (Berta et al., 2011b).

DOI:10.14753/SE.2014.1845

As the hamster retina, similarly to other rodents, has very thin photoreceptors and therefore a finer localization in ROS/RIS is not possible, we made parallel immunolabeling of caveolin-1 and phospho-caveolin-1 in the large rod photoreceptors of the toad *Xenopus laevis*. The caveolin-1 antibody did not give specific labeling in this species. Phosho-caveolin-1 could be localized to the thin rim of OS and to structures likely to be cilia (Figure 13).

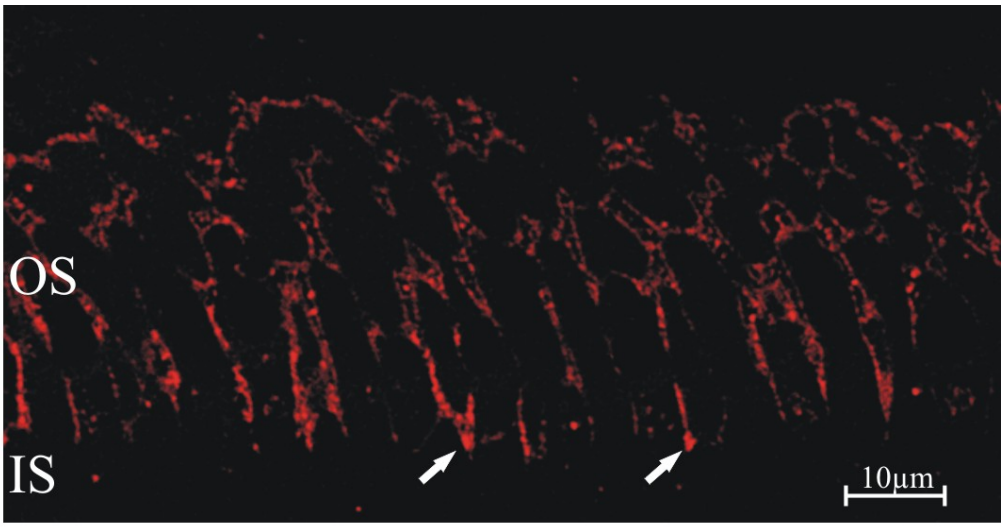

Figure 13. Phospho-caveolin labeling in *Xenopus laevis* retina, semithin section. Phospho-caveolin is localized to the rim of the OS and to the cilia *(arrows)*.

DOI:10.14753/SE.2014.1845

3. Localization of caveolins in dog retina and in inherited canine retinal degenerations

First we wanted to describe the expression of the different caveolin isoforms in the normal dog retina. Our results show that caveolin-1, caveolin-2 and c-src give a diffuse labeling throughout the ONL, indicating that the cell bodies of photoreceptors and possibly Müller cells are labeled. Horseshoe-like structures and layers of dotted signals can be observed on the border of the ONL and the OPL labeled with these antibodies. This appearance at this location is typical for rod and cone presynaptic terminals. The IS are visibly labeled, but the OS are very weakly or not labeled at all. Caveolin-3 does not label photoreceptors in this species. Phospho-caveolin-1 is restricted to the OS, while phospho-caveolin-2 gives a labeling very similar to that of caveolin-2. The pigment epithelium contains caveolin-1, caveolin-2, phospho-caveolin-1, phospho-caveolin-2 and c-src, but no caveolin-3. In the inner retinal layers caveolin-1, caveolin-2, phospho-caveolin-2 and c-src gave a very strong labeling around the blood vessels and a weaker labeling in the INL and GCL. Interestingly caveolin-3 labeled only structures that, according to their location, can be assumed to be horizontal cells (Figure 14.).

Immunocytochemistry with the same antibodies were done also in different retinal degenerations of the dog: *erd, rcd1, crd2* and *XLPRA2*. Meaningful differences could be observed, the degeneration of photoreceptors also affected the expression of the investigated raft-associated proteins (Figure 15, Figure 16). The most striking observation of all was that phospho-caveolin-1 labeling was missing in all diseases, but caveolin-1 labeling was intact, indicating the possibility that the diseased photoreceptors are not capable of phosphorylating caveolin-1. Interestingly *XLPRA2* and *crd2* (Figure 16) retinas were not labeled with the caveolin-2 antibody, while the labeling was intact in *erd* and *rcd1* (Figure 15).

DOI:10.14753/SE.2014.1845

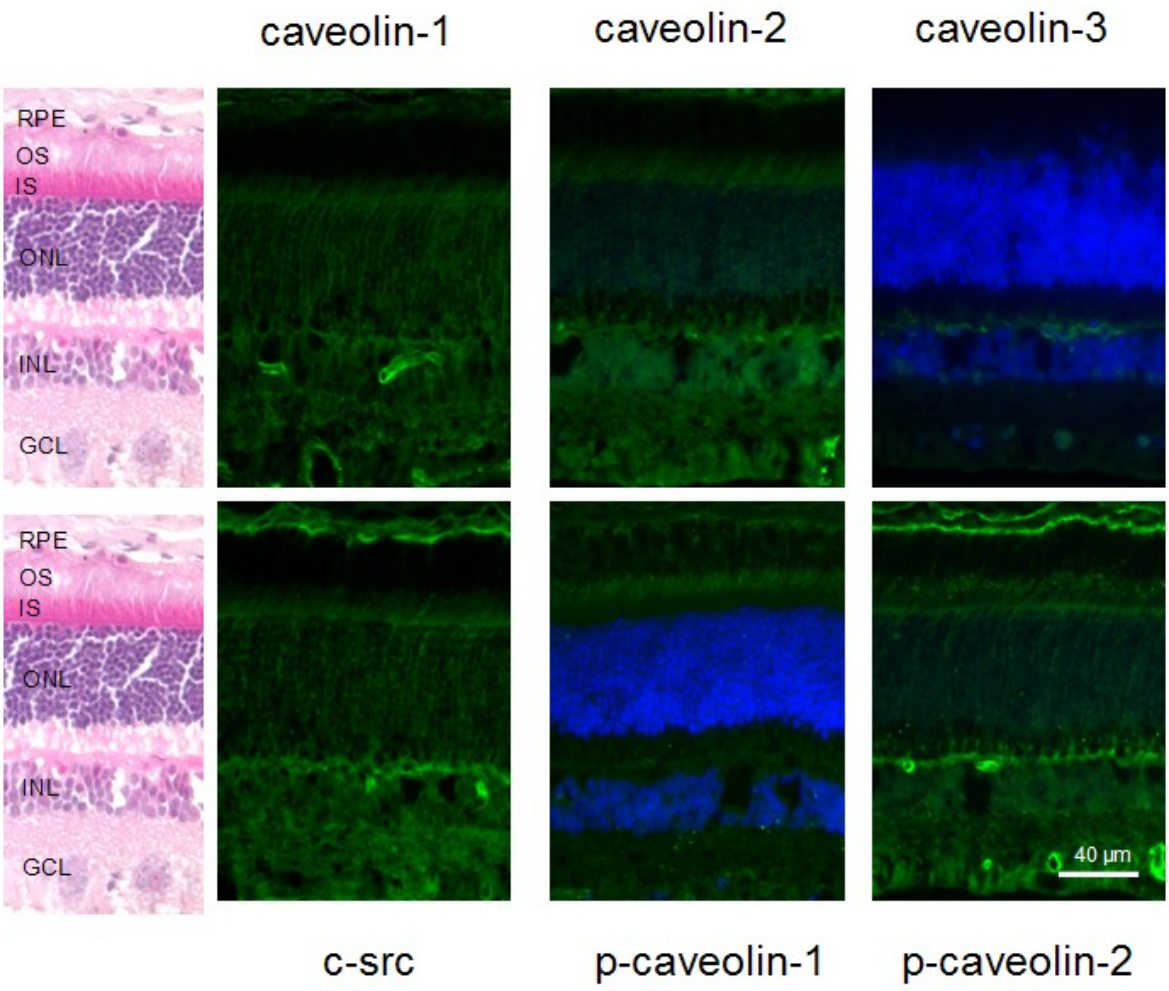

Figure 14. Immunolabeling with antibodies against different caveolin isoforms, phosphorylated forms of caveolin-1 and caveolin-2 and c-src in the dog. Caveolin-1, caveolin-2, c-src and phosho-caveolin-2 gave a diffuse labeling throughout the retina, only the OS were not labeled, in contrast, phospho-caveolin-1 labeled only the OS and OS-IS junctions. Caveolin-3 labeling is restricted to horizontal cells. Marked layers: retinal pigment epithelium (RPE), outer segments (OS), inner segments (IS), outer nuclear layer (ONL), inner nuclear layer (INL), ganglion cell layer (GCL).

DOI:10.14753/SE.2014.1845

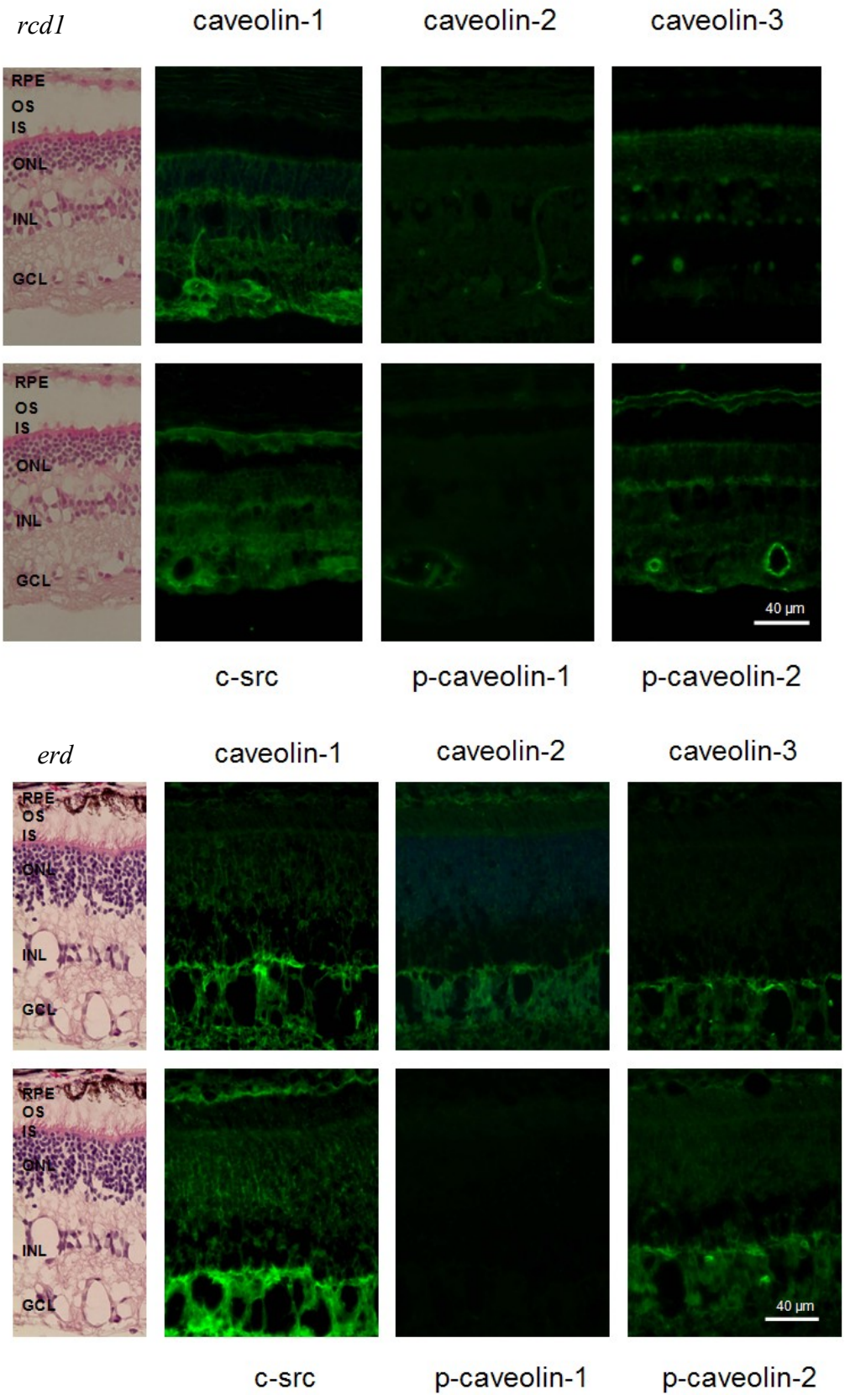

DOI:10.14753/SE.2014.1845

Figure 15. Immunocytochemistry with antibodies against caveolin-1, caveolin-2, c-src, phosho-caveolin-1 and phosho-caveolin-2 in the *erd* and *rcd1* retina (dog). Labeling with caveolin-2 and phospho-caveolin-1 is almost completely missing, while labeling with caveolin-1, c-src and phospho-caveolin-2 were very similar to that of the normal. In *erd* caveolin-3 was only detected in the inner retinal layers, in rcd1 caveolin-3 also labeled the ONL.

DOI:10.14753/SE.2014.1845

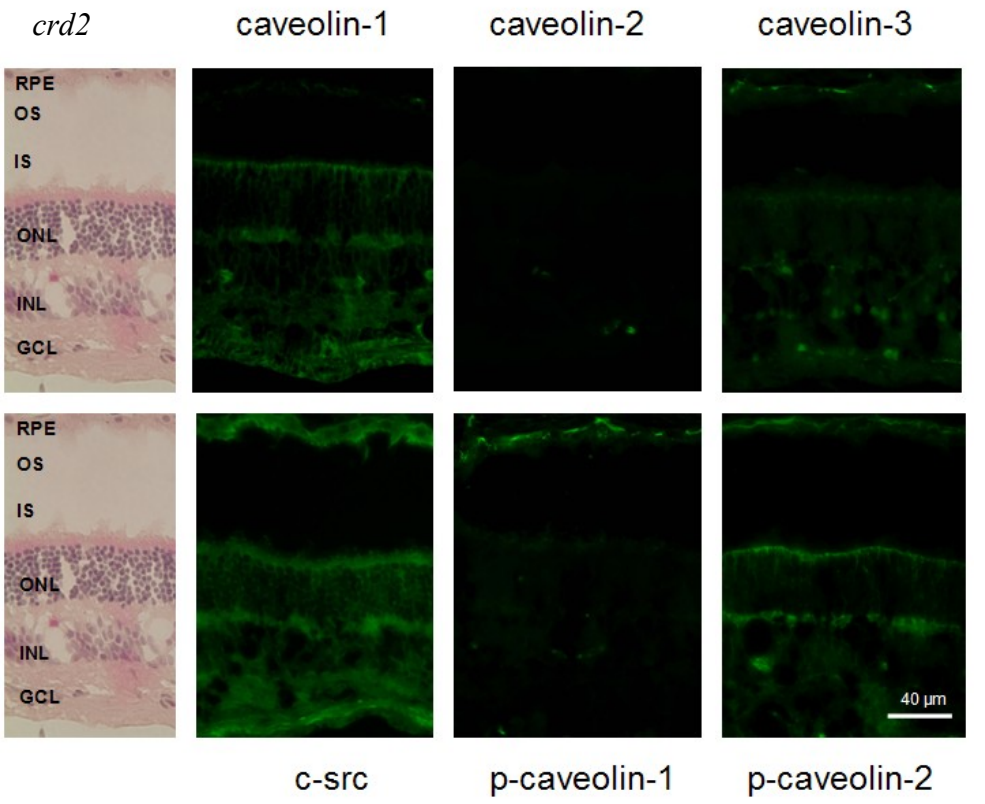

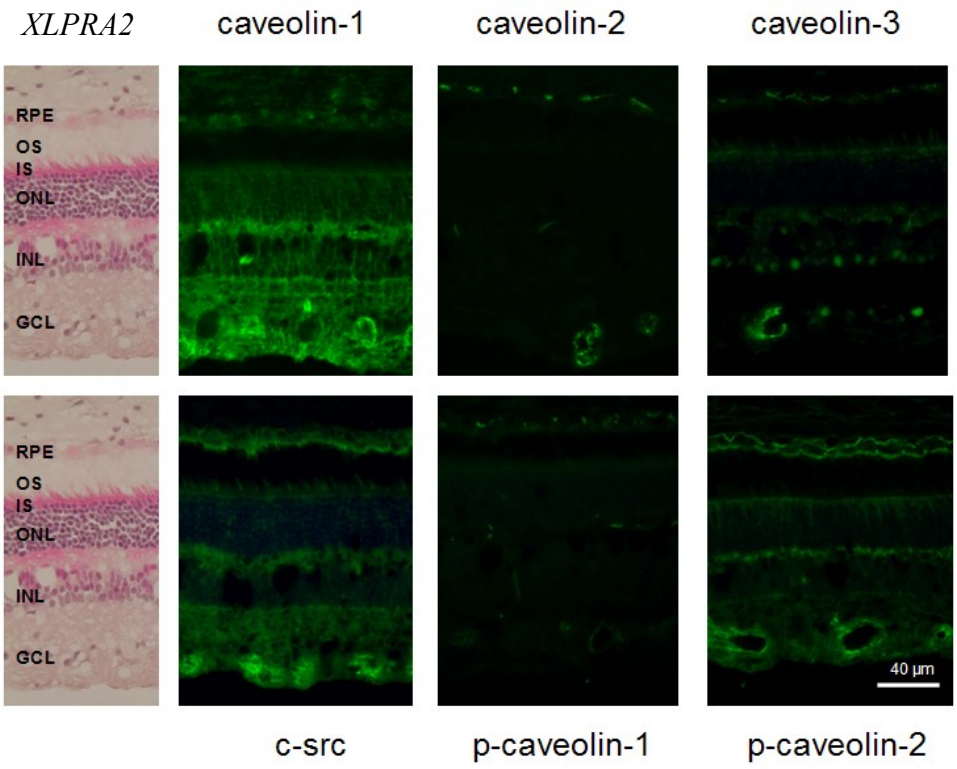

DOI:10.14753/SE.2014.1845

Figure 16. Localization pattern of caveolin isoforms, phospho-caveolin-1, phospho-caveolin-2 and c-src in the *crd2* and *XLPRA2* retinas (dog). The labeling of caveolin-1, c-src and phospho-caveolin-2 are intact, but the antibody against caveolin-2 and phospho-caveolin-1 gives very weak or no labeling. Caveolin-3 is not only expressed in the inner retinal layers, but also in the photoreceptor layer, labeling weakly the ONL and stronger the IS.

DOI:10.14753/SE.2014.1845

4. Distribution of caveolin isoforms in the lemur retina

Caveolin-1: In the macular region, caveolin-1 was detected in every layer. Among these layers, the density of immunolabeling showed only slight differences. Both the outer and inner segments harbored caveolin-1. In the outer and inner nuclear layers, caveolin-1 was localized along the cell membranes. The ganglion layer and the outer and inner plexiform layers diffusely expressed caveolin-1. In the periphery, caveolin-1 was localized in the same layers, but at lower densities. The INL and ONL both contained caveolin-1, but the immunoreactivity was weaker in the inner layer. In the ciliary body, both layers were labeled with anti-caveolin-1 (Figure 17, Table 6).

Caveolin-2: The immunostaining of caveolin-2 differed from that of caveolin-1. The lemur retina barely evidenced any caveolin-2 signals. Weak immunoreactivity was detected within the ganglion layer. The label was somewhat stronger around the blood vessels, including the vessel cells and blood cells. No signal was detected in the ciliary body samples (Figure 17, Table 6).

Caveolin-3: In the macular region and the periphery, the immunostaining pattern of caveolin-3 was similar to that of caveolin-1, but the density was significantly lower. Labeling was detected only between the ganglion cell layer and the inner limiting membrane. Immunostaining densities ranged from low to moderate. Caveolin-3 was also detected within the ciliary body (Fig. 17, Table 6), (Berta et al., 2007b).

DOI:10.14753/SE.2014.1845

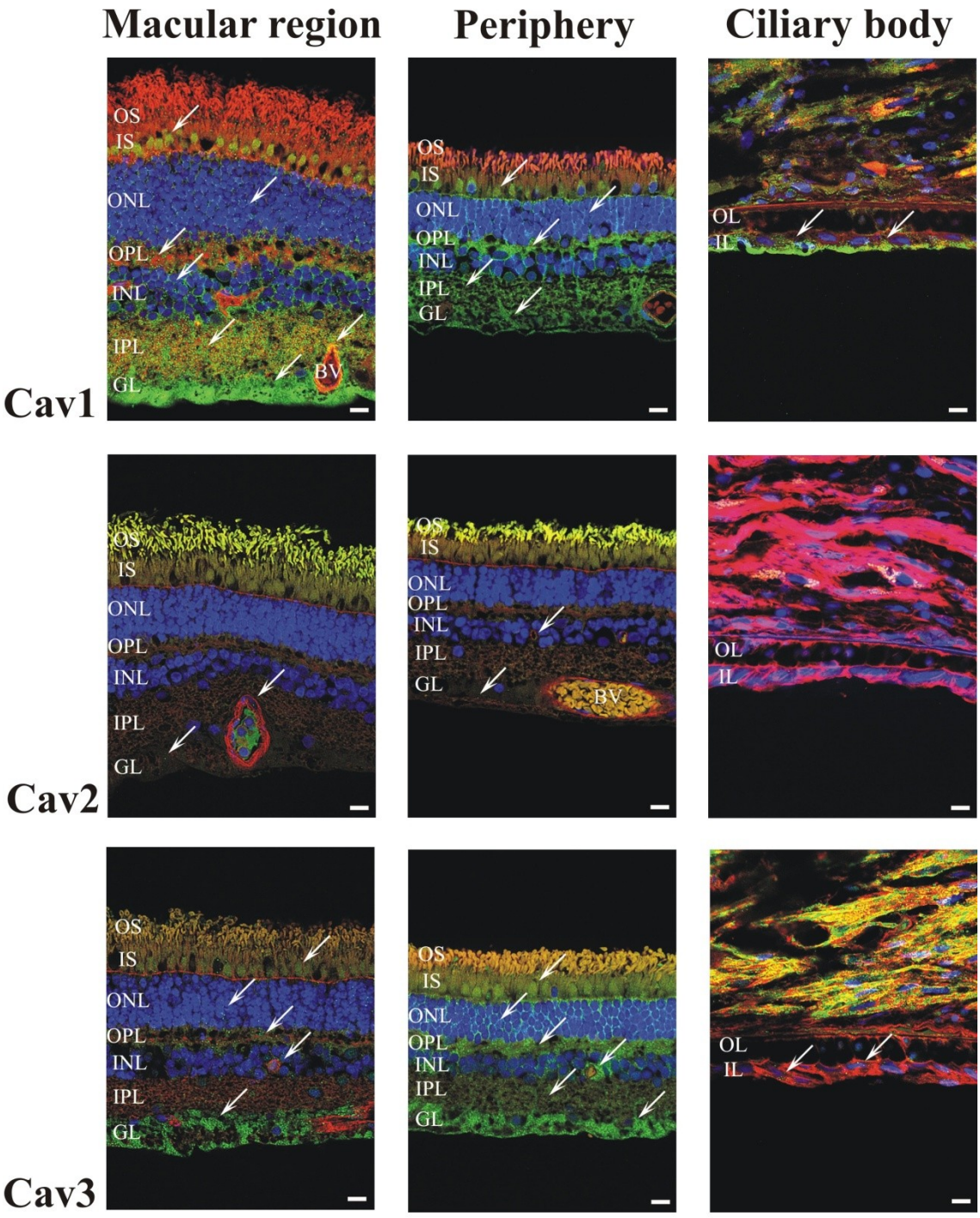

Figure 17. Immunocytochemistry analysis of caveolin-1, -2 and -3 in the lemur retina. Samples were obtained from different anatomical sites of the retina following the radial plane from the central to the peripheral retina (macular region, M; periphery, P; ciliary body, CB). Alexa fluor 488 was used to detect caveolins (green, arrows). The cytoskeleton and the nuclei were marked with Alexa fluor 594 labeled phalloidin (red) and DAPI (blue), respectively. Merged images are shown. Caveolin-1 was observed in all layers with the same density among the layers at the macular region and the periphery. At the ciliary body, caveolin-1 stained both epithelial layers. Hardly any caveolin-2 signals were observed, and were detected only in the vascular cells of the central portion and the peripheral region. No signs were observed in the ciliary body. Caveolin-3 was present in all layers at every region. *Scale bar = 10 µm. PE=pigment epithelium, OS=outer segments, IS=inner segments, OLM=outer limiting membrane, ONL=outer nuclear layer, OPL=outer plexiform layer, IPL=inner nuclear layer, INL=inner plexiform layer, GC=ganglion cells, ONF=optic nerve fibers, ILM=inner limiting membrane, OL=outer layer, IL=inner layer.*

Region	Macular region			Periphery			Ciliary body		
Caveolin	1	2	3	1	2	3	1	2	3
OS	+	-	+	+	-	+	+	-	+
IS	+++	-	++	++	-	++			
ONL	+++	-	++	++		++			
OPL	+++	-	++	++	-	++			
INL	+++	-	++	++	-	++	++	-	+
IPL	+++	-	++	++	-	++			
GCL	+++	+	++	++	+	++			

Table 6. Summary of labeling density of caveolin-1, -2 and -3 in different locations of the lemur retina. Densities were estimated in the ten retinal layers (see abbreviations at Fig. 17.) and at the ciliary body, in the pigmented (outer) and the non-pigmented (inner) epithelial layers. Caveolin-1 was present in all retinal layers. A center-to-peripheral gradient was observed: principally high density in the central portion (M), moderate level in the periphery (P), low and moderate in the ciliary body (CB). Caveolin-2 was detected only in the ganglion layer with low density. Caveolin-3 was present in every layer with moderate density, with the exception of the ciliary body, in which it evidenced low density. -, none; +, low; ++, moderate; +++, high.

DOI:10.14753/SE.2014.1845

5. Caveolins in the (melanoma malignum affected) human retina

Caveolin-1: The bound antibody was present in all layers of the retina. The weakest staining could be found in the pigment epithelium (low). The autoflourescence of the pigment granules made the assessment of the immunostaining density more difficult, but the immunoreactive structures were significantly smaller than the pigment granules, thus the formers could be clearly identified. In other layers the density was estimated to vary from low to very high. The distribution of immunolabel exhibited a characteristic center-to-peripheral gradient; increasing from very low, low, moderate and high density (M), reaching the maximum level (very high; P), then decreasing towards the extreme peripheral part of the retina (very low, low; CB). (Figure 18, Table 7).

Caveolin-2: The caveolin-2 immunoreactivities (IRs) were found to be present from the outer nuclear layer to the inner limiting membrane, showing very low, low and moderate densities (M), however at the peripheral part (P) in the inner plexiform layer, the layer of the optic nerve fibers and the inner limiting membrane no IRs could be detected. Reaching the epithelium of the ciliary body (CB) the IRs decreased to an undetectable level (Figure 19, Table 7).

Caveolin-3: In the macular region, the caveolin-3 immunoreactivity was present from the outer nuclear layer to the inner limiting membrane with very low, low and moderate densities (M). At the peripheral part (P) IRs also occured in the layer of the outer segments (low). As to the ciliary body (CB), caveolin-3 signals could be seen in both epithelial layers, with low and moderate densities (Figure 20, Table 7), (Berta et al., 2007a).

DOI:10.14753/SE.2014.1845

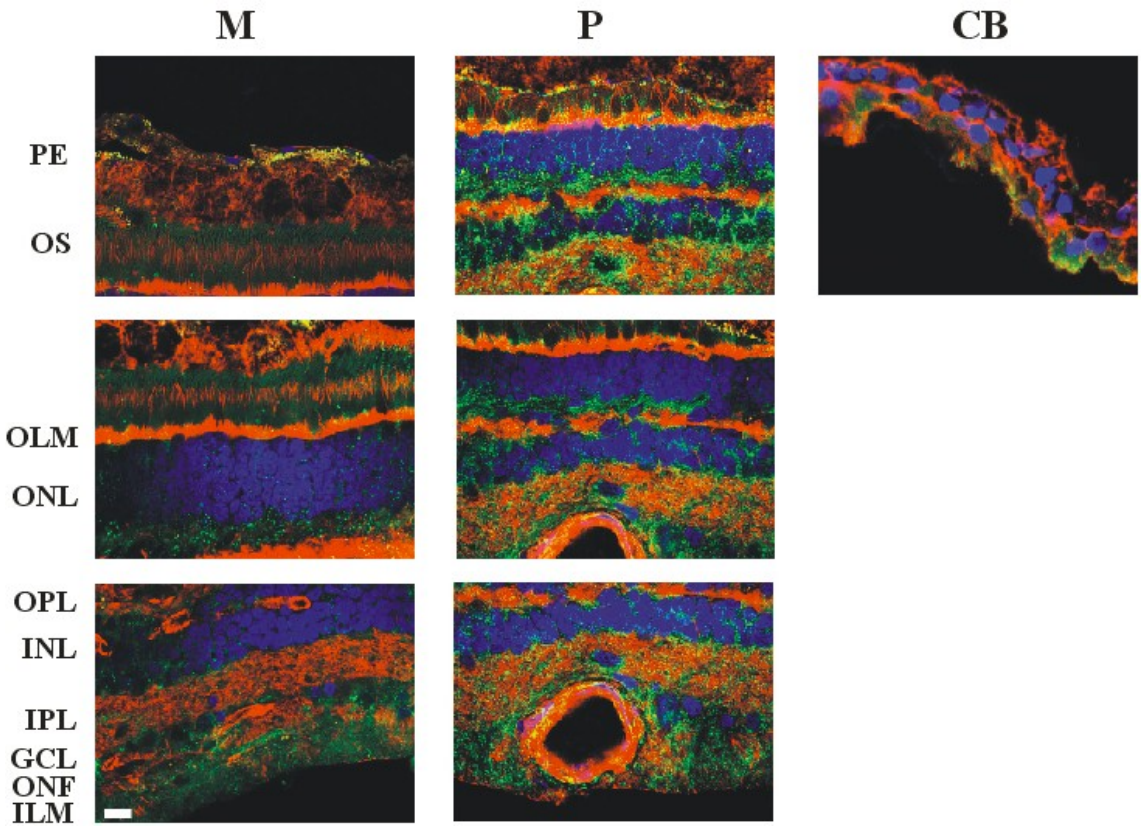

Figure 18. Immunocytochemical analysis of caveolin-1 in the human retina.

Upper row: outermost retinal layers (pigment epithelium, outer segments), middle row: outer nuclear layer and outer limiting membrane, lower row: innermost retinal layers (outer plexiform layer, inner nuclear layer, inner plexiform layer, ganglion cells, optic nerve fibers, inner limiting membrane). Samples were taken from different anatomical sites of the retina following a radial plane from the central to the peripheral retina (macular region, M; periphery, P; ciliary body, CB). Alexa Fluor 488 was used to detect caveolin-1 (green). The cytoskeleton and the nuclei were decorated with Alexa fluor 594 labeled phalloidin (red) and DAPI (blue), respectively. Merged images are presented. Caveolin-1 was present in all layers of the retina. Weakest signals could be seen in the pigment epithelium (low). The different regions of the retina showed a center-to-peripheral gradient; the immunoreactivity being higher at the periphery. Pigment granules show autofluorescence, but they can be obviously distinguished from caveolin signals. *Scale bar, 10 µm. PE=pigment epithelium, OS=outer segments, OLM=outer limiting membrane, ONL=outer nuclear layer, OPL=outer plexiform layer, IPL=inner nuclear layer, INL=inner plexiform layer, GC=ganglion cells, ONF=optic nerve fibers, ILM=inner limiting membrane*.

DOI:10.14753/SE.2014.1845

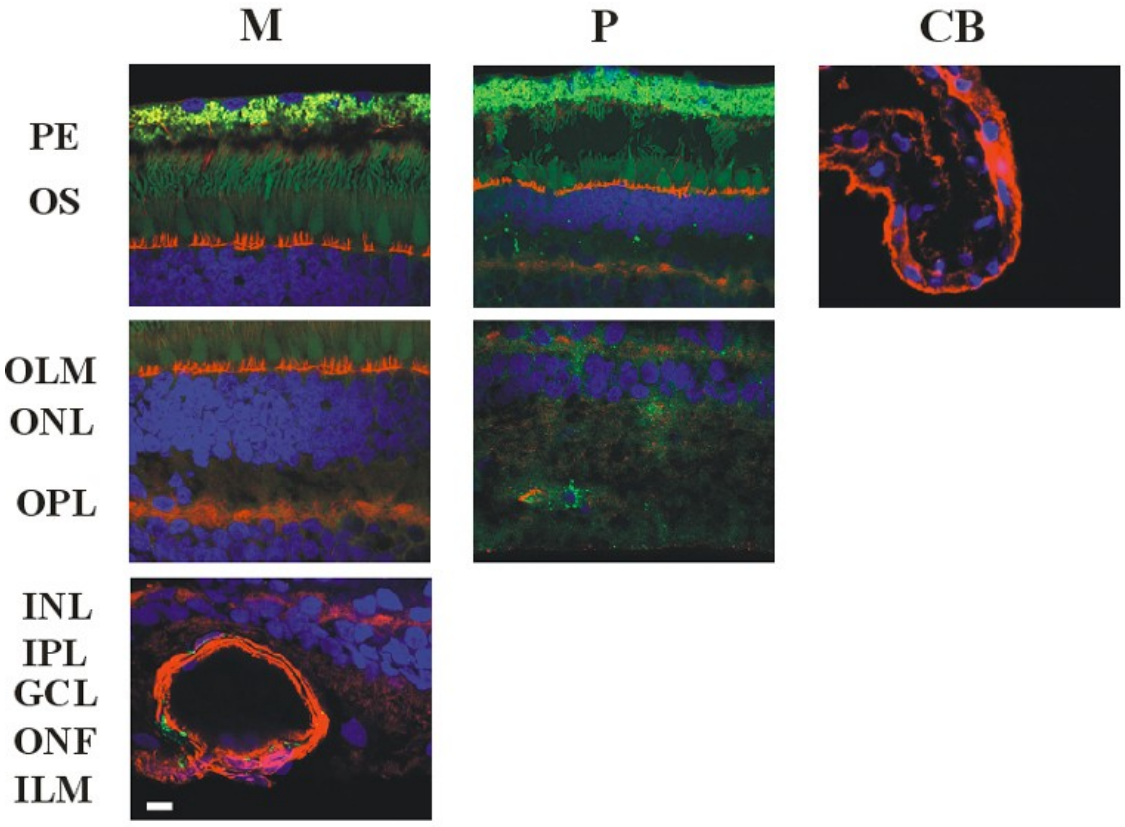

Figure 19. Immunocytochemical analysis of caveolin-2 in the human retina.

Samples were taken as described in Figure 1. Alexa Fluor 488 was used to detect caveolin-2 (green). The cytoskeleton and the nuclei were decorated with Alexa fluor 594 labeled phalloidin (red) and DAPI (blue), respectively. Merged images are shown. Caveolin-2 was found in the ONL and the ILM, including the intervening layers, showing very low, low and moderate densities (M). At the peripheral part (P) IRs (immunoreactivities) were observed only in the ONL, OPL, INL and GC (very low, low). No signals were observed at the epithelium of the ciliary body (CB). Note, that pigment granules show autofluorescence. *Scale bar, 10 µm. PE=pigment epithelium, OS=outer segments, OLM=outer limiting membrane, ONL=outer nuclear layer, OPL=outer plexiform layer, IPL=inner nuclear layer, INL=inner plexiform layer, GC=ganglion cells, ONF=optic nerve fibers, ILM=inner limiting membrane*.

DOI:10.14753/SE.2014.1845

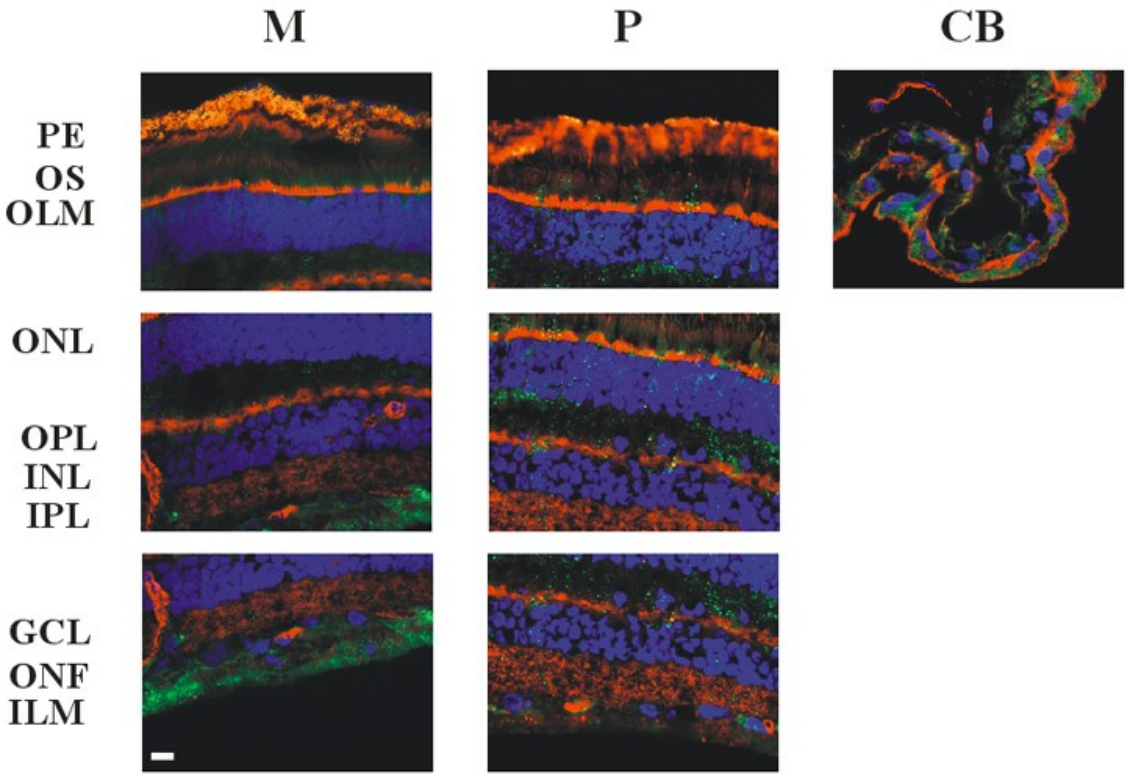

Figure 20. Immunocytochemical analysis of caveolin-3 in the human retina.

Samples were taken as described in Figure 1. Alexa Fluor 488 was used to detect caveolin-3 (green). The cytoskeleton and the nuclei were decorated with Alexa fluor 594 labeled phalloidin (red) and DAPI (blue), respectively. Presented images are merged. Caveolin-3 was observed in the ONL and the ILM, including the intervening layers, showing very low, low and moderate densities (M). At the peripheral part (P) IRs also occured in the layer of the outer segments (low). At the ciliary body (CB) caveolin-3 signals could be seen in both layers (low, moderate). Note, that pigment granules show autofluorescence. *Scale bar, 10 µm. PE=pigment epithelium, OS=outer segments, OLM=outer limiting membrane, ONL=outer nuclear layer, OPL=outer plexiform layer, IPL=inner nuclear layer, INL=inner plexiform layer, GC=ganglion cells, ONF=optic nerve fibers, ILM=inner limiting membrane*.

DOI:10.14753/SE.2014.1845

Region	M			P			CB		
Caveolin	1	2	3	1	2	3	1	2	3
PE	+	-	-	+++++	-	-	+	-	++
OS	++	-	-	+++++	-	++	++	-	+++
OLM	++	-	-	+++++	-	-			
ONL	+++	++	++	+++++	+	++			
OPL	++++	++	++	+++++	++	++			
INL	+++	+	+	+++++	++	++			
IPL	+++	+	+++	+++++	-	++			
GC	++++	++	++	+++++	++	++			
ONF	++++	+++	+++	+++++	-	++			
ILM	++++	+++	+++	+++++	-	++			

Table 7. Summary of the semiquantitativ analysis made on immunocytochemistry with the three caveolin isoforms in the human retina. -, none; +, very low; ++, low; +++, moderate; ++++, high; +++++, very high. *PE=pigment epithelium, OS=outer segments, OLM=outer limiting membrane, ONL=outer nuclear layer, OPL=outer plexiform layer, IPL=inner nuclear layer, INL=inner plexiform layer, GC=ganglion cells, ONF=optic nerve fibers, ILM=inner limiting membrane*.

DOI:10.14753/SE.2014.1845

6. Early retinal degeneration (erd)

Retinal development and degeneration in *erd* dogs

In the canine retina both photoreceptors are present at birth, but not completely differentiated. At 2 wks of age both IS and OS are visible, but are undeveloped and variable in length. With time IS and OS increase in their size and number. They also become uniform in height, densely packed and arranged parallel. The development is complete between 7 and 8 wks (Aguirre et al., 1972). In *erd* on 1 μm plastic sections and ultrathin sections using high resolution optical and electron microscopy, it was already demonstrated that ROS and RIS are variable in length and their proportions, while the size of cones remains normal at 4.2 wks (Acland and Aguirre, 1987). On 7 μm sections, using light microscopy, the retinal development appears to be normal until 7.7 wks of age, however pycnotic nuclei can be observed in the ONL at 7.1 wks. From 8.3 wks on, the irregularity of OS and IS begins to be visible, their orientation is not as parallel and they are less densely packed than before. At 12.3 wks loss of OS, shortening and loss of IS are obvious, in the inter-photoreceptor space phagocytic invasion can be observed. These details become even more pronounced at 14.1 wks, when more OS are lost, OS and IS become really short and macrophages can still be observed in the widened inter-photoreceptor space. Until this time point the ONL and INL thickness do not seem to change. By 48.1 wks OS and IS become extremely short, ONL thickness decreases dramatically, INL thickness decreases moderately. Thereafter at 62 wks degeneration becomes severe, ONL has only one layer. The retina seems to be completely degenerated at 101 wks, severe gliosis is dominant. The retina is entirely lacking both rods and cones. At 165 wks the disease progresses even more, the retina is extremely thin (Figure 21), (Berta et al., 2011a).

DOI:10.14753/SE.2014.1845

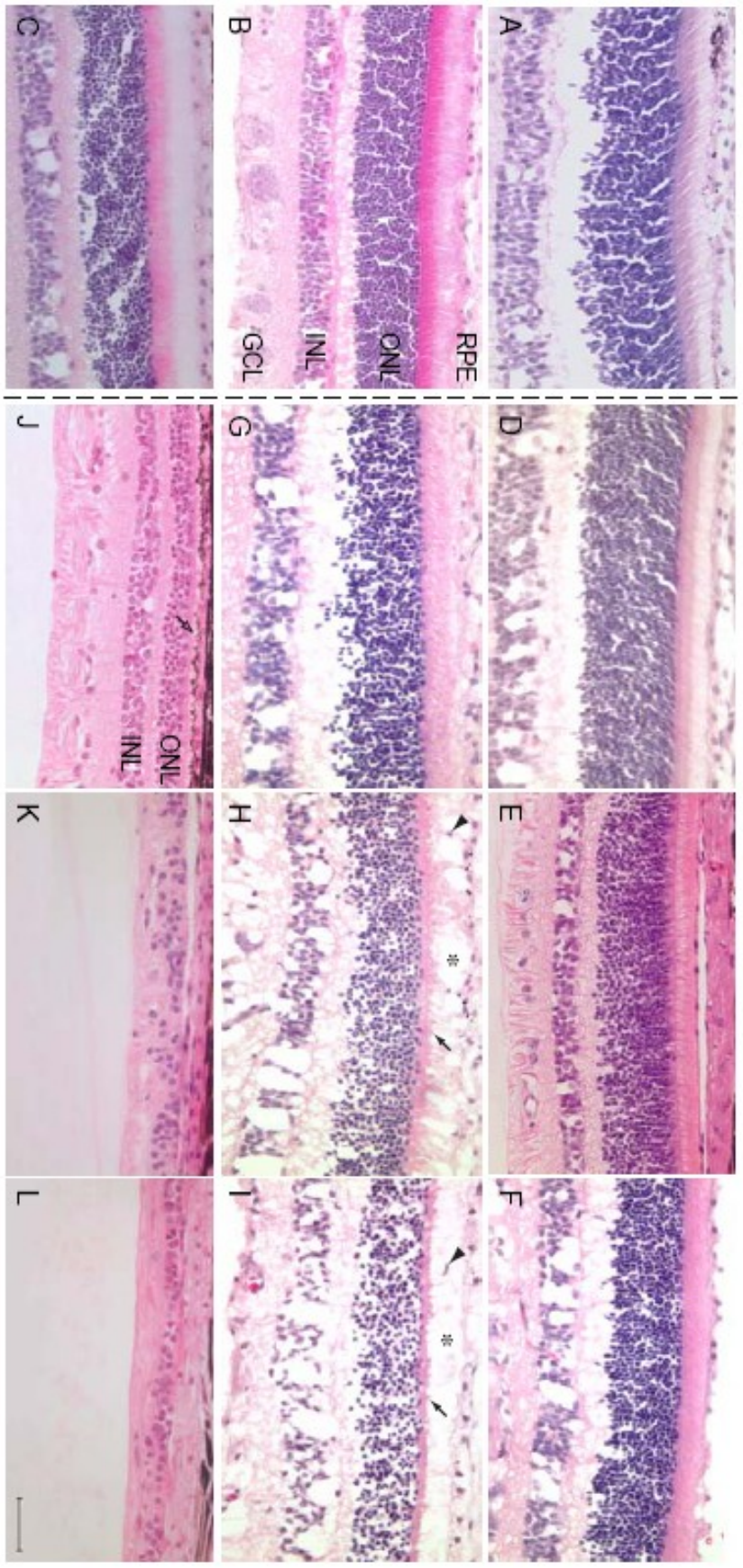

Figure 21. Steps of retinal development and degeneration in *erd* dogs
H&E stained retinal sections of control (A-C) and mutant (D-L) dogs of different ages in weeks (A-4.7; B-8.7; C-25.7; D-4.3; E-7.1; F-7.7; G-9.1; H-12.3; I-14.1; J-48.1; K-101; L-165). Structural abnormalities are recognized in mutant retina at 9.1 wks, and are progressive. Shortening of inner segments (H, I-oblique arrows) and loss of photoreceptors (H, I-*), collapse of the photoreceptor layer (J-open arrow), and invasion of cells into the interphotoreceptor space that are most probably macrophages (H, I-arrowheads) are prominent disease-associated changes. RPE=retinal pigment epithelium, ONL=outer nuclear layer, INL=inner nuclear layer, GCL=ganglion cell layer. Scale bar 40 μm.

Topography of the disease

To determine the uniformity of the disease throughout the retina, sections from different ages (age range, 4.3-165 wks) were examined from the optic nerve to the ora serrata in the superior and the inferior meridian, respectively. In young ages (4.3-14.1 wks) the disease progress is comparable in all quadrants and regions. However, previously it was described, that at 4.2 wks in the most peripheral parts the disease was less readily appreciable (Acland and Aguirre, 1987). Note that these regions are not included in our study. Interestingly at 48.1 wks in the superior retina, area 2 is more degenerated than area 1. As for the inferior meridian, area 1 and 2 appear to be in the same stage of degeneration. Later, as the disease progresses (62-165 wks), differences disappear and degeneration is uniformly present in all areas (Figure 22, 23.).

DOI:10.14753/SE.2014.1845

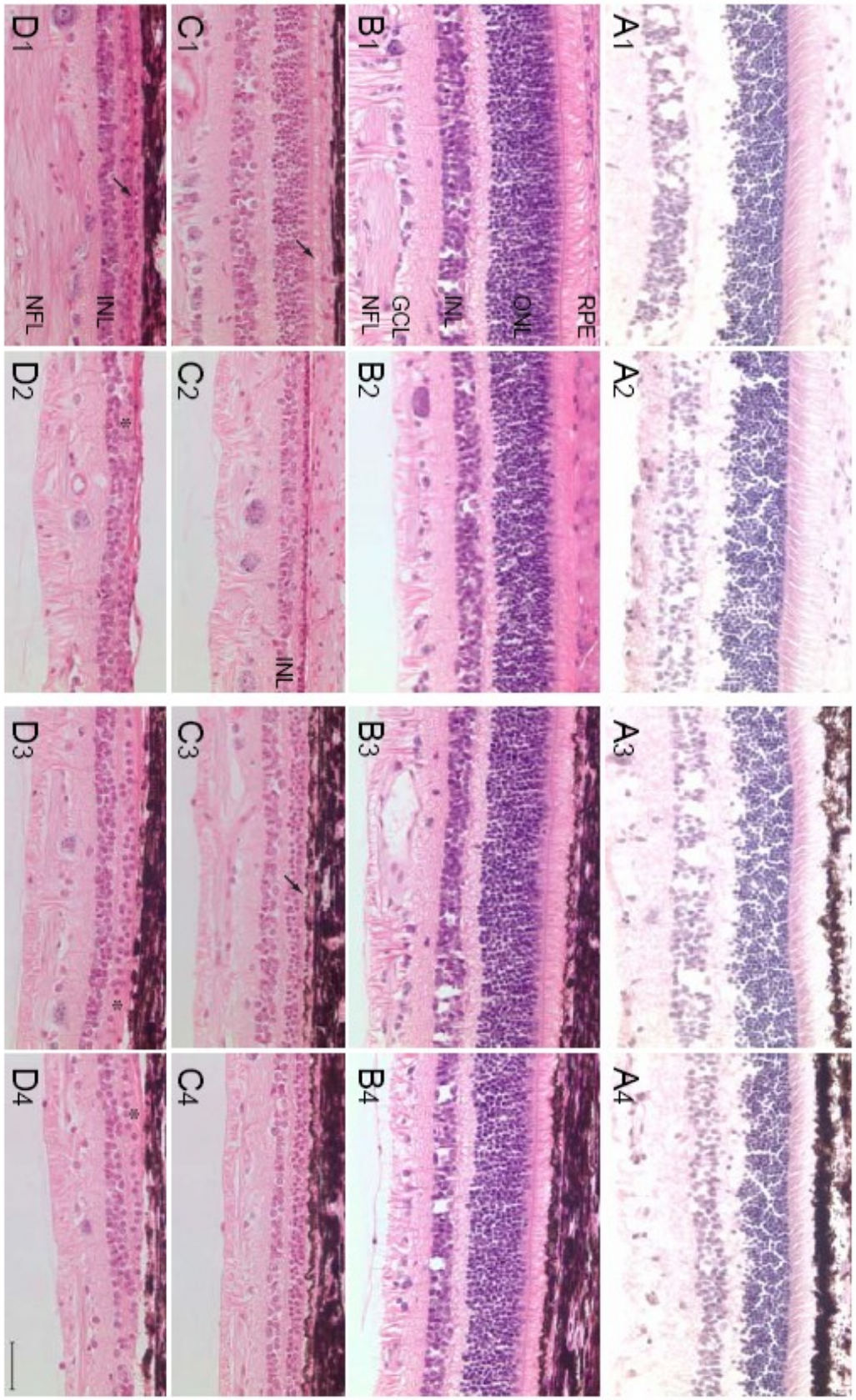

Figure 22. Topographical differences in various regions of the *erd* retina.
A1: normal retina 8.7 wks, superior retina, area 1, A2: normal retina 8.7 wks, superior retina, area 2, A3: normal retina 8.7 wks, inferior retina, area 1, A4: normal retina 8.7 wks, inferior retina, area 2, B1: *erd* retina 7.1 wks, superior retina, area 1, B2: *erd* retina 7.1 wks, superior retina, area 2, B3: *erd* retina 7.1 wks, inferior retina, area 1, B4: *erd* retina 7.1 wks, inferior retina, area 2, C1: *erd* retina 48.1 wks, superior retina, area 1, C2: *erd* retina 48.1 wks, superior retina, area 2, C3: *erd* retina 48.1 wks, inferior retina, area 1, C4: *erd* retina 48.1 wks, inferior retina, area 2, D1: *erd* retina 62 wks, superior retina, area 1, D2: *erd* retina 62 wks, superior retina, area 2, D3: *erd* retina 62 wks, inferior retina, area 1, D4: *erd* retina 62 wks, inferior retina, area 2. A1-A4: normal retina; B1-B4: at 7.1 wks area 1 (2000μm from optic nerve) and area 2 (halfway between the optic nerve and the ora serrata) are at the same stage of disease in the superior and the inferior retina, morphology yet normal; C1-2: in the superior retina of *erd* 48.1 wks area 2 is more diseased than area 1. C3-4: in the inferior retina of *erd* 48.1 wks area 1 and 2 are at the same stage of degeneration, which is in between area1 and 2 in the superior. D1-4: both areas are in the same stage of disease in the superior and the inferior retina also. *RPE= retinal pigment epithelium, ONL= outer nuclear layer, INL= inner nuclear layer, GCL= ganglion cell layer, NFL= neurofilament layer. Scale bar 40μm*

DOI:10.14753/SE.2014.1845

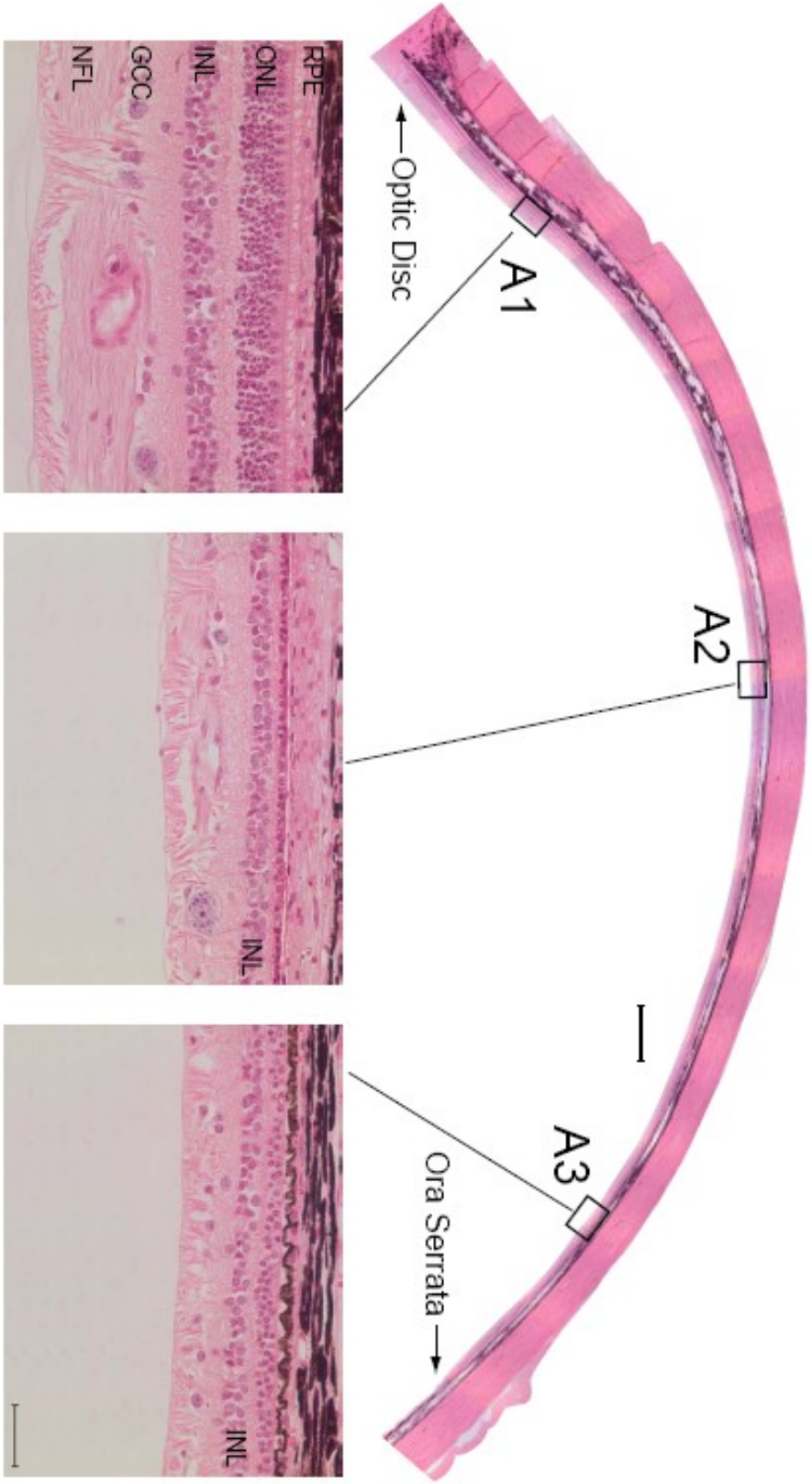

Figure 23. Mosaic image of the complete superior *erd* retina at 48.1 wks of age. A1, 2000 ± 500 μm from the optic nerve and A2, middle point ±500 μm of the retina A3, 2000 ± 500 μm from the ora serrata. Regional differences of the disease: A2 is more diseased than A1 or A2. *Scale bar 500μm.*

Immunohistochemistry of the disease

We characterized degeneration properties in the ONL and INL using immunocytochemistry. Although the RPE appeared normal on H&E sections, we also labeled them for RPE65 and found them intact at 9.1 wks of *erd* (data not shown). In order to evaluate the affects of disease in rods, double-fluorescence immunolabeling was carried out for rod opsin (labeling rod OS in normal retina) and synaptophysin (labeling the synaptic terminals). As early as 4.3 wks a partial mislocalization of rhodopsin is visible in the ONL. The OS appear to be of variable length and already have irregular contours. There is no loss of synaptophysin immunoreactivity at this age and it stays unchanged until 14.1 wks of age. Between 7.7-14.1 wks progressive rod disease develops: OS become more disorganized, more variable in shape and length, they also shorten, and some disappear. Rod opsin mislocalization becomes severe, staining the thin rod cytosol around soma in the ONL, throughout the entire length and height of the *erd* retina. However the delocalization is not uniform: photoreceptor synaptic terminals are heavily labeled. From 7.7 short rod-opsin-positive neurites can be observed reaching to the inner retina, as the as the INL. Neurite sprouting of cones was not observed (Berta et al., 2011a). Cone degeneration properties are discussed later.

DOI:10.14753/SE.2014.1845

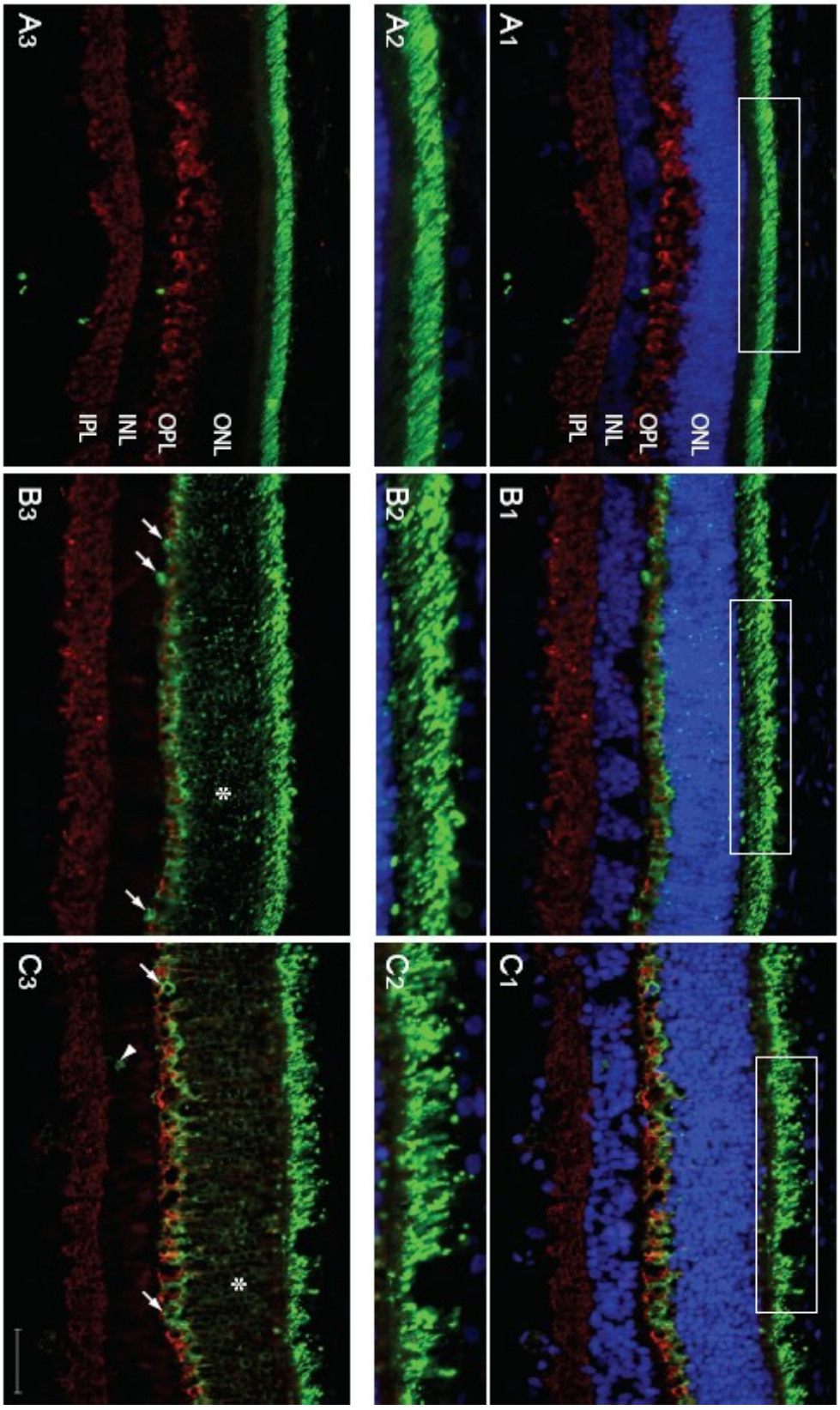

Figure 24. Characterization of rod disease in the *erd* retina.

Immunofluorescence labeling with the anti-rod opsin antibody (green) shown with (A1,B1,C1) and without (A2,B2,C2) the blue DAPI nuclear stain in normal (A1,A2) and *erd*-mutant (B1,B2,C1,C2) retinas. A1: normal retina 12.3 wks, rhodopsin (green), synaptophysin (red) and DAPI (blue) labeling, A2: normal retina 12.3 wks, magnified rhodopsin- labeled OS (green), A3: normal retina 12.3 wks, rhodopsin (green) and synaptophysin (red) labeling, B1: *erd* retina 7.7 wks, rhodopsin (green), synaptophysin (red) and DAPI (blue) labeling, B2: *erd* retina 7.7 wks, magnified rhodopsin (green) labeled OS, B3: *erd* retina 7.7 wks, rhodopsin (green) and synaptophysin (red) labeling, C1: *erd* retina 12.3 wks, rhodopsin (green), synaptophysin (red) and DAPI (blue) labeling, C2: *erd* retina 12.3 wks, magnified rhodopsin (green) labeled OS, C3: *erd* retina 12.3 wks, rhodopsin (green) and synaptophysin (red) labeling. In A1-A3 (normal retina) only OS are labeled with the rhodopsin antibody. B1-B3: *erd* 7.7wks, irregular OS that are variable in length, rhodopsin mislocalization, neurite sprouting can be observed, in the diseased retina C1-C3: disease progresses (12.3 wks), extremely variable OS and OS loss. The rhodopsin delocalization is visualized best without DAPI. Rhodopsin delocalizes to the inner segments, ONL (*) and OPL synaptic terminals (oblique arrows).

ONL= outer nuclear layer, OPL= outer plexiform layer, INL= inner nuclear layer.IPL= inner plexiform layer. Scale bar 40μm for principial panels.

Because beside ONL loss, INL thinning was also observed during the development of the disease, we used several markers to label the inner retina. Bipolar cells were exceptionally in the focus of our interest, because inner retinal response was found to be abnormal in the ERG of *erd* dogs. Both PKC-α labeling of ON bipolars and Go-α signals of rod bipolars are strongly decreased in all examined ages (4.3, 7.7, 9.1 11.6 14.1 wks). However, the reduction of Go-α is moderate, compared to PKC-α, which shows only a slightly visible labeling. In order to visualize the presence of the weak PKC-α signal, we increased antibody concentration, by which it was possible to reveal the presence of the signal. These findings indicate the malfunction of ON bipolars (Go-α) and rod bipolars (PKC-α). Calretinin and calbindin (data not shown) labeling of horizontal, amacrine and ganglion cells showed that these neurons developed normally (examined age range: 4.3-14.1 wks), however at 14.1 wks horizontal cells show an irregular shape. Until 9.1 wks of age vimentin and GFAP labeling of Muller cells and astrocytes remains normal. Later the reactivity of these cells increases, the cell processes reach first the inner, later the outer border of ONL. Note that the cell processes only reach the outermost part of INL in normal (Figure 25).

DOI:10.14753/SE.2014.1845

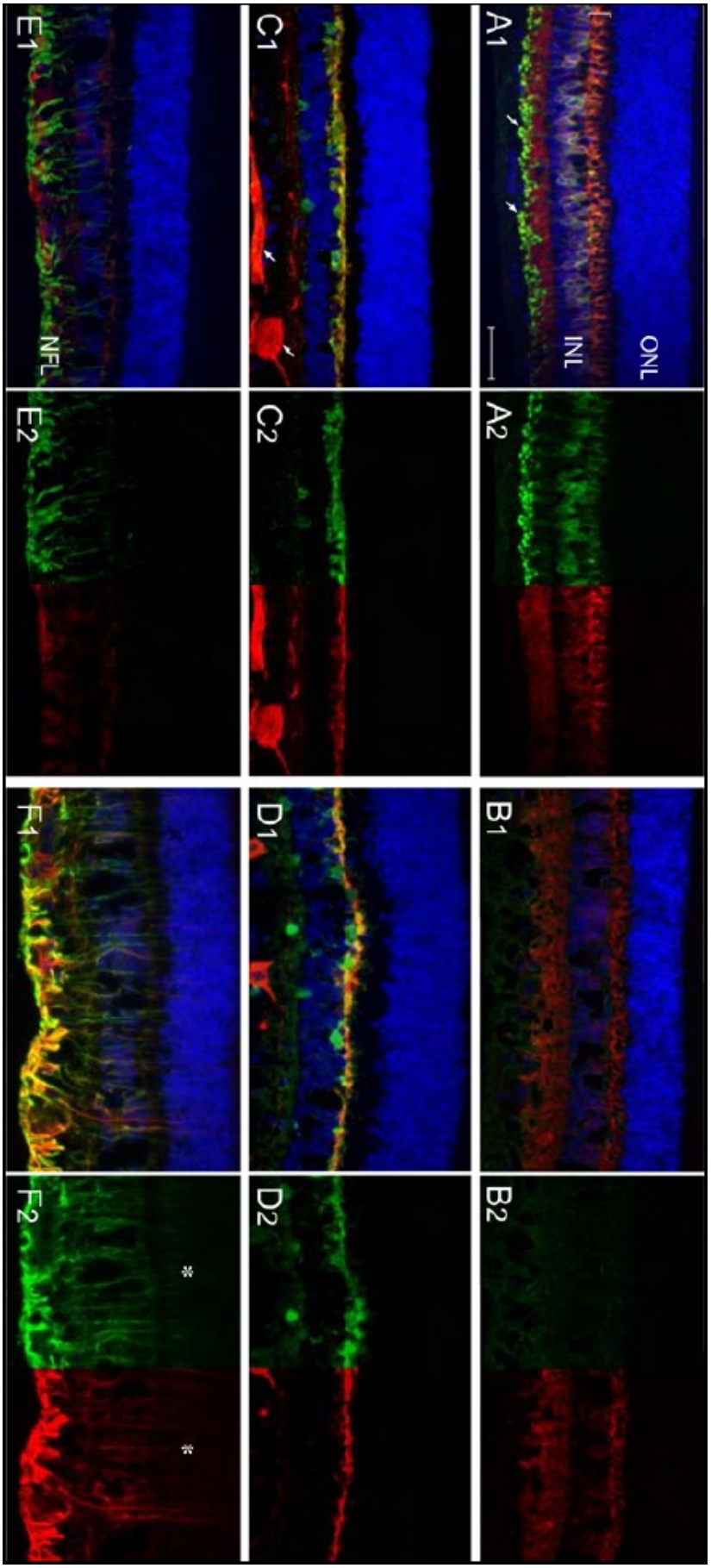

Figure 25. Morphological changes in the inner retina in *erd*.
A1: PKCα (green), Goα(red), and DAPI (blue) labeling in 9-week-old normal retina. A2: tiled image from A1 without DAPI staining, (PKCα green, left, Goα red, right, B1: PKCα (green), Goα(red), and DAPI (blue) labeling in *erd* 7.7 wks, B2: tiled image from B1 without DAPI, (PKCα green, left, Goα red, right); C1: calretinin (green), neurofilament 200kDa (NF,red), and DAPI (blue) labeling in 9-week-old normal retina C2: tiled image from C1 without DAPI, (calretinin green, left, neurofilament 200kDa red, right), D1: calretinin (green), neurofilament 200kDa (NF,red), and DAPI (blue) labeling in *erd* 9.1 wks, D2: tiled image from D1, (calretinin green, left, neurofilament 200kDa red, right; E1: vimentin (VIM,green), GFAP (red), and DAPI (blue) labeling in 12-week-old normal retina, E2: tiled image from E1, (vimentin green, left, GFAP red, right), F1: vimentin (VIM,green), GFAP (red), and DAPI (blue) labeling in *erd* 12.3 wks, F2: tiled image from F1, (vimentin green, left, GFAP red, right). A1-B2: Goα (ON bipolar) and PKCα (rod bipolar) signals are decreased in *erd* (B1-B2) compared to normal (A1-A2). C1-D2: no difference between calretinin (horizontal and amacrine cells) and neurofilament labeling of normal (C1-C2) and *erd* (D1-D2). E1-F2: vimentin and GFAP labeling of Müller cells are increased in *erd* compared to normal. The dendrites reach the outer nuclear layer (*). *ONL= outer nuclear layer, INL= inner nuclear layer, NFL= neurofilament layer. Scale bar 40μm.*

Early retinal degeneration was previously described to be a photoreceptor disease, with abnormal development and degeneration of not only rods, but also cones (Acland and Aguirre, 1987). Therefore we followed rod and cone disease characteristics exceptionally carefully and in detail (Figure 26) and found that although rods showed several signs of disease, including mislocalization and neurite sprouting, neither of them were observed in the case of cones. Both red/green (COS-1) and blue opsin (OS-2) were expressed in the hCAR-labeled cones. Both the number and distribution pattern of blue- and red/green cones were similar to normal in all ages examined (4.3-14.1 wks). As for their morphology, cone outer segments progressively started to have irregular contours, similarly to rods. Surprisingly, labeling of different cone subtypes lead us to a new aspect of the disease, in rods mAb OS-2 not only localized to the blue cones, but also to

the rod outer segments in the age range of 7.7-14.1 wks. In the 4.3-week-old *erd* retina no rods were labeled with OS-2. At 7.7 wks the rod label of OS-2 was yet homogeneous and faint, but at 12.3 wks the rod OS contours very clearly outlined by OS-2 (Figure 26). This finding was however not confirmed by using other, polyclonal antibodies directed against the blue opsin. PNA and hCAR immunolabeling were used to identify both cone classes, and evaluate their structure and distribution during development and degeneration. Control cones were uniformly elongated, and PNA labeled the insoluble matrix domain around cone OS's. Labeling with hCAR also was distinct in all cone compartments, but variable in the axons coursing through the ONL (Figure 26). Mutant cones, on the other hand, appeared shorter in younger animals (Figure 26), and some failed to show hCAR labeling even though the cells were readily identifiable in transmitted light with or without DIC optics. Qualitative assessment of cone numbers based on PNA labeling was normal, but cone pathology was progressive, and the OS's of older animals became disoriented; in parallel, cone pedicles became distorted and irregular, and hCAR labeling was reduced or lost (Berta et al., 2011a).

The COS-1 and OS-2 antibodies labeled the L/M- and S-cone classes respectively, both in control and mutants, and labeling was restricted to the OS (Figure 26). To determine intensity differences between normals and mutants, an antibody dilution series was carried out. The minimal dilution required for labeling S-cones was the same for both groups for the 3 antibodies (monoclonal OS-2, goat sc-14363, rabbit AB5407). In contrast, polyclonal antibodies sc-22117 and AB5405 against the L/M-cones resulted in distinct labeling at dilutions of 1:20,000 and 1:80,000 respectively in *erd*, but required double the concentration (1;10,000 and 1:40,000) to label normal cones.

DOI:10.14753/SE.2014.1845

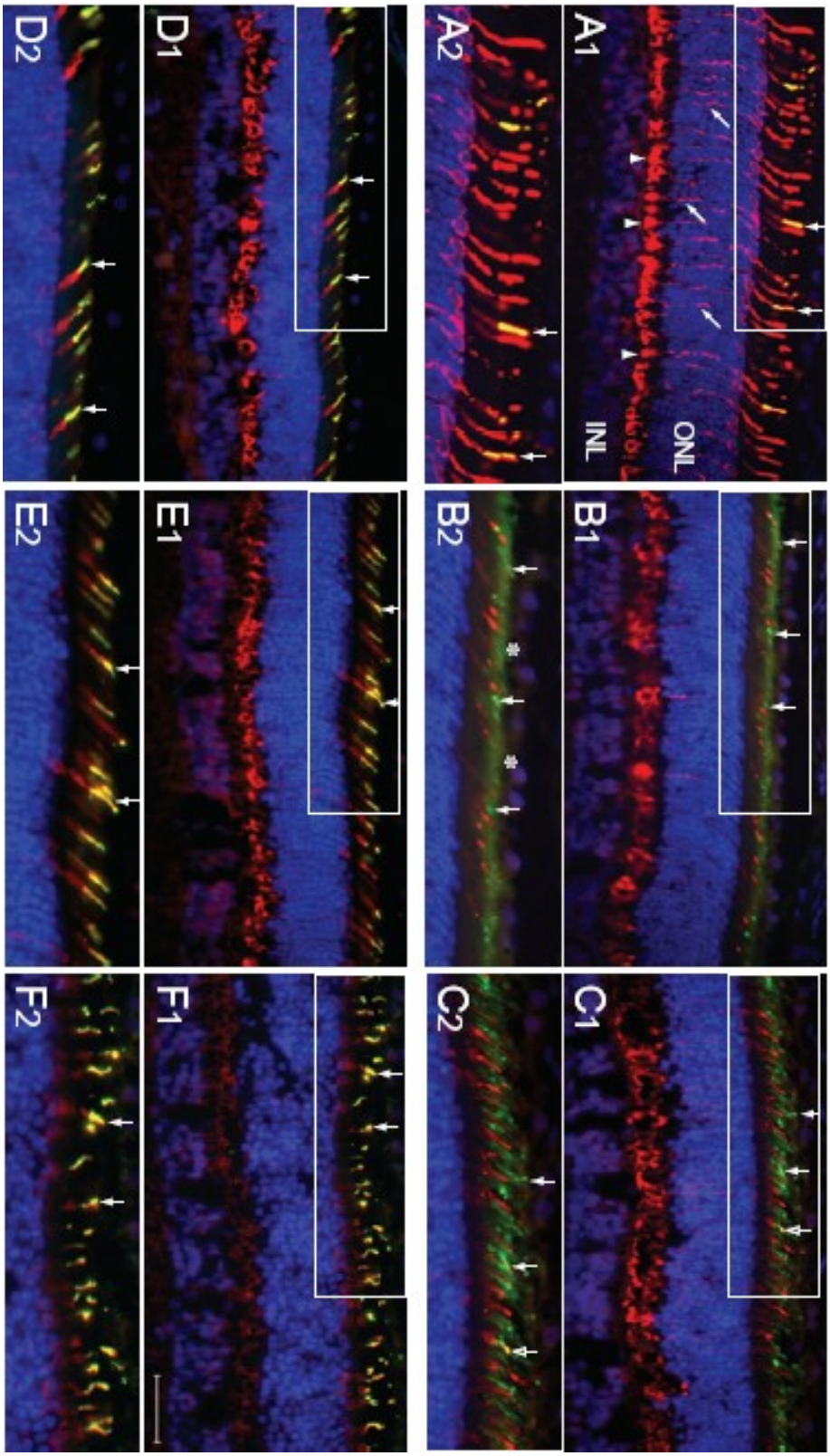

Figure 26. Cone disease characteristics in the *erd* retina.

Expression of rod and cone molecular markers in *erd* in early development. Sections from normal dogs of 9 wks **(A)**, 8.7 wks **(D)** of age and from mutant animals 7.7 wk **(B)** 11.6 wks **(C)**, 8.4 wks **(E)**, 14.1 wks **(F)** of age, labeled with antibodies against S cone opsin (OS-2, green)/hCAR (red) **(A-C)** and L/M cone opsin (COS-1, green)/hCAR (red) **(D-F)**, and with a DAPI (blue) nuclear stain. The boxed areas are presented at higher magnification in the panels below, and vertical arrows identify the same cells. Control cones label distinctly but variably with hCAR; L/M cones make up the majority of cones, and only few S-cones are present. Other than cone outer segment disorientation in the older *erd* retina, L/M-cone opsin labeling is normal and restricted to the outer segments of these cells. The OS-2 antibody distinctly labels S-cone outer segments, and also there is more diffuse and faint labeling over the rod outer segments. Oblique arrows indicate cone cell bodies, open arrowheads cone pedicles. *ONL= outer nuclear layer, INL= inner nuclear layer. Scale bar 40µm.*

DOI:10.14753/SE.2014.1845

Cell death and cell proliferation in *erd*

TUNEL labeling was used to examine the kinetics of photoreceptor apoptosis/cell death in the disease during (4.3 wks), or after (7.7-14.1 wks) the completion of postnatal retinal differentiation. As this could only be done in paraformaldehyde-fixed cryosections, analysis was limited to 4.3-14.1 wks. As the distribution of disease is not completely uniform, we determined cell death in both the superior and inferior meridian, respectively. TUNEL labeled cells were counted only in ONL. In the control retinas (age range, 4.7-12 wks) the TUNEL labeled cells/ 1M μm² are lower than 13. At the earliest *erd* age the number is close to normal, approximately 14 TUNEL labeled cells/ 1M μm². The amount of TUNEL positive cells gets rapidly very high at 7.7 wks. The labeled nuclei vary in their size and they are distributed evenly throughout the ONL (including the outermost level, where cone somas are located). Their number gets high as 332 in the superior and 192 TUNEL labeled cells/ 1M μm² in the inferior meridian. Later (after 7.7 wks) the amount decreases reaching the lowest point in both meridians, 135 in the superior, 185 TUNEL labeled cells/ 1M μm² in the inferior retina. Their number reaches a high level again at 11.6 wks, approximately 280 TUNEL labeled cells/ 1M μm² in both meridians. This number decreases rapidly by the age of 14.1 wks. The course of the cell death period is therefore prolonged and is bimodal. The two peaks occur earlier in the superior (7.7 and 11.6 wks), and later in the inferior meridian (8.3 and 12.3 wks, see Figure 27).

DOI:10.14753/SE.2014.1845

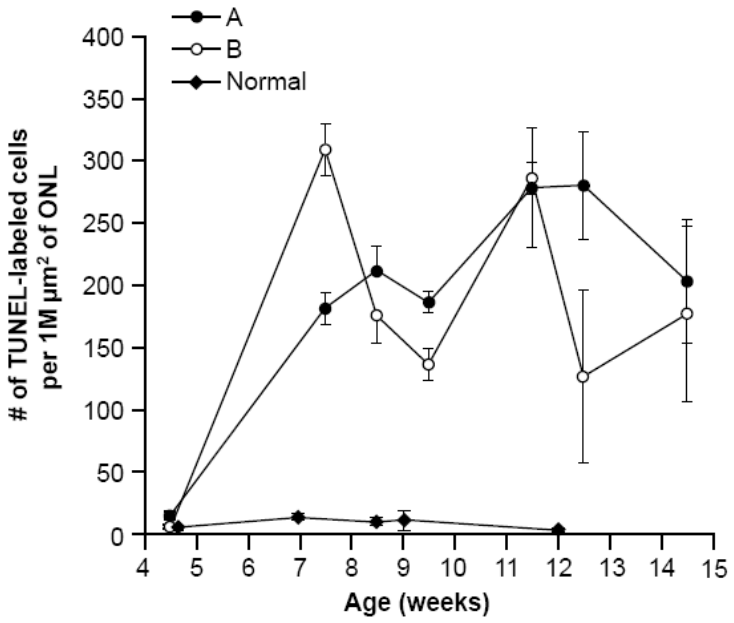

Figure 27. Number of TUNEL-labeled photoreceptor cell nuclei per 1 million (M) µm² of ONL in the superior and inferior retina, respectively, indicating the cell death rate in the *erd* retina. The period of cell death is prolonged and has two peaks: 7.7 and 11.6 wks in the superior retina, 8.3 and 12.3 wks in the inferior retina. Compare the high amount of cell death in the *erd* retina to normal. *A= superior retina, B= inferior retina.*

To quantify the changes of ONL and INL thickness observed during *erd* retinal development, the number of cell rows was counted, and the thickness (µm) was measured in the ONL and INL, respectively. Because no major differences were observed between the two types of measurements, we are only displaying the number of cell rows, in both the superior and inferior meridian. The ONL thickness represents the presence or the loss of photoreceptors. After a small decrease between 4.3 and 7.7 wks the ONL thickness stays constant until 14.1 wks of age. Note that until this age the *erd* retinal thickness follows course of the normal. Thereafter the ONL decreases dramatically by 48.1 wks and gets even thinner at 62 wks. The changes in INL thickness were not as prominent as in the ONL. The number of INL cell rows in *erd* also stays close to normal until 14.1 wks. But still, by 48.1 wks there is a 50% decrease and even more at 62 wks (Figure 28).

DOI:10.14753/SE.2014.1845

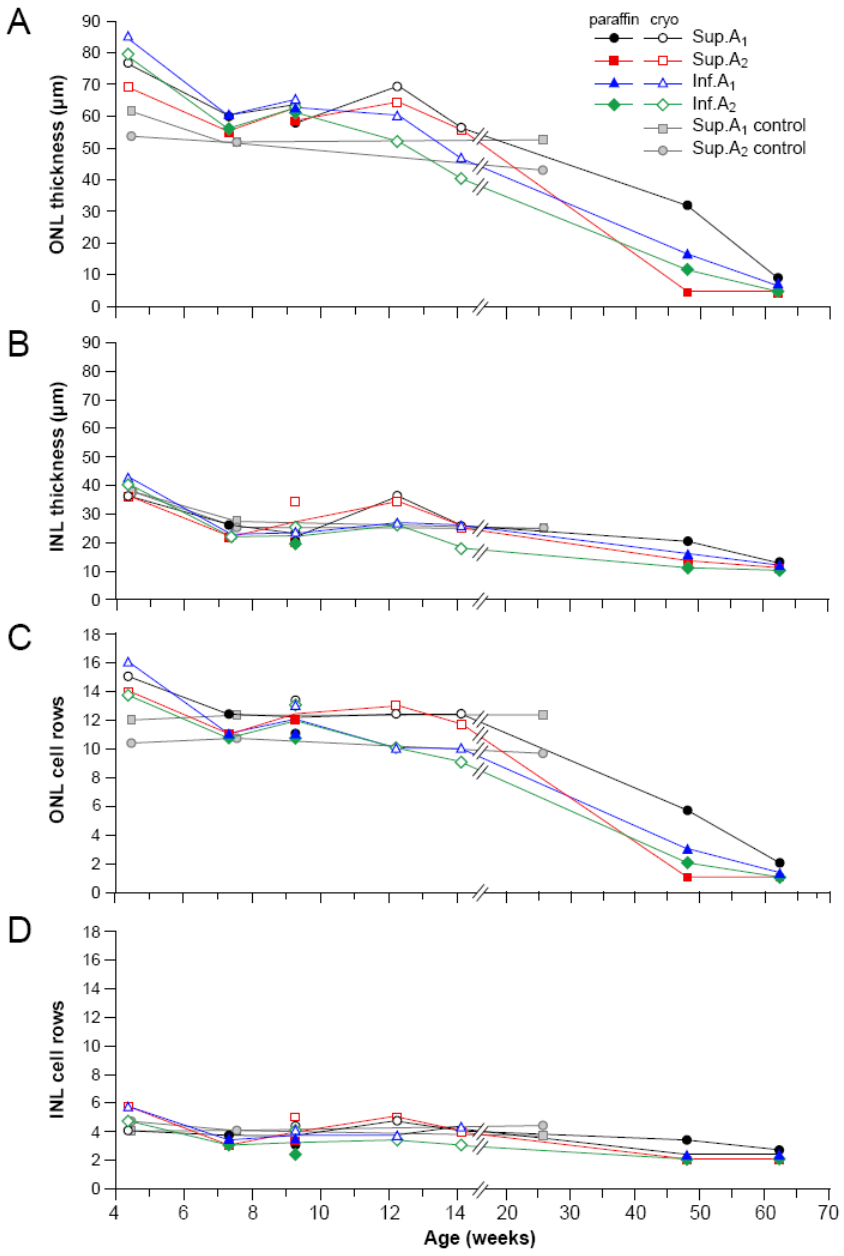

Figure 28. The rate of cell loss in the *erd* retina. Changes in ONL, INL thickness and the number of cell rows, in area 1 and area 2 from the superior and inferior retina, respectively. The ONL and INL thickness and also the number of cell rows remain normal until 14.1 wks. By 48.1 wks their thickness is strongly reduced. Note the difference between the ONL thickness of area 1 and area 2 in the superior retina at 48.1 wks. *Sup A1.= area 1 (2000 ± 500 µm from the optic nerve) in the superior retina, Sup A2= area 2 (middle point of the retina ±500 µm) in the superior retina, Inf A1= area 1 in the inferior retina; Inf A2= area 2 in the inferior retina.*

DOI:10.14753/SE.2014.1845

PCNA labeling was used to determine cell proliferation in the ONL of the *erd* retina. PCNA (proliferating cell nuclear antigen) is expressed in cells in proliferating cells(Waseem and Lane, 1990). In spite of the high rate of cell death between 4.7 and 14.1 wks, ONL thickness did not decrease in this period, which suggested the possibility of cell proliferation in the ONL. As the course of cell death was different in the superior and inferior retina, cell proliferation was determined in both meridians. In controls (7-12 wks) the amount of PCNA labeled cells/ 1M μm² is very low. In *erd* 4.3 wks, the number was similar to the normal (less than 3 PCNA labeled cells/ 1M μm²). However between 7.7 and 14.1 wks high amount of PCNA positive cells were observed in the *erd* retina. This is the same period, when high cell death kinetics were observed. Interestingly, the course of cell proliferation also has two peaks, occurring at the same time points as cell death peaks (7.7, 11.6 wks in the superior and 8.3, 12.3 wks in inferior meridian). Note that the number of dividing cells varied between 40-133 PCNA labeled cells/ 1M μm², while number of TUNEL labeled cells varied between 125-308 cells/ 1M μm² in the *erd* retina of ages 7.7-14.1 wks (Figure 29.). The PCNA labeled nuclei were smaller than other nuclei, but evenly distributed throughout the ONL. The specificity of PCNA labeling was confirmed by KI67 (Beltran et al., 2007) at two time points (8.4 and 141 wks). The expression of PCNA in the *erd* retinas was also studied using qRT-PCR. The relative quantity of PCNA was 66.3% higher at 9.6 wks than control (8 wks) at 99% confidence (data not shown). There was no significant difference between PCNA expression in control and *erd* at 12 wks.

DOI:10.14753/SE.2014.1845

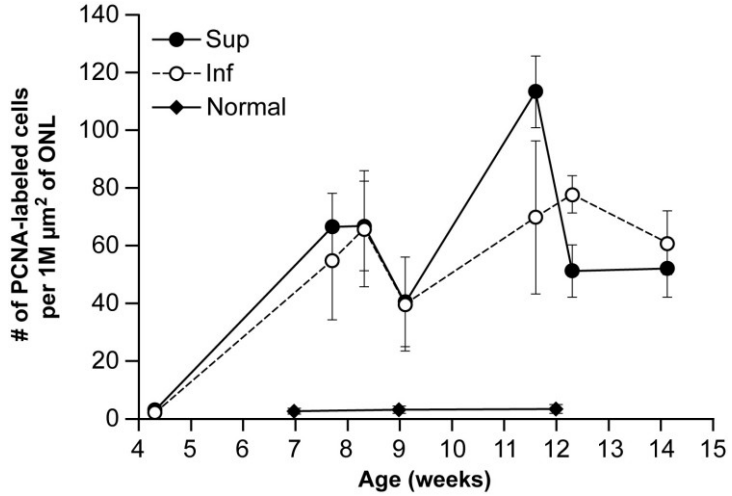

Figure 29. Number of PCNA-labeled photoreceptor cell nuclei per 1 million (M) µm² of ONL in the superior and inferior retina, respectively, indicating the cell proliferation rate in the *erd* retina. The course of cell proliferation follows the kinetics of cell death: it is prolonged and has two peaks at 7.7 (8.3) and 11.6 wks in the superior retina, and at 8.35 and 12.3 wks in the inferior retina. Compare the high level of cell proliferation in the *erd* retina to normal, *A= superior retina, B= inferior retina.*

In order the preclude the possibility, that the PCNA-labeled cells are microglial cells or Müller cells, that migrated into the ONL, CD18 and CRLABP labeling were used. Sections from two ages of *erd* were labeled, 8.3 wks and 11.6 wks, parallel with normal controls, 9wks and 12 wks. In normal, the detected few microglias are dominantly in the inner part of ONL. In *erd* very few microglias do appear in the outer part of ONL. The total number of microglial cells were negligible compared the PCNA positive cells in *erd*. Also PCNA positive cells were distributed evenly throughout the ONL, on the contrary CD18 positive cells were dominantly in the inner part of ONL. CRLABP labeling was the same in *erd and* control sections. The CRLABP labeling showed, that there are no migrated Müller cells in the ONL of control or *erd* sections, their cell bodies were all located in the inner part of the retina.

To investigate if this cell proliferation period is a unique characteristic of *erd* retinas or not, we also counted PCNA labeled nuclei in the ONL of other inherited retinal degenerations, including *rcd1*, *crd2* and *XLPRA2*. The high rate of cell proliferation could only be observed in *erd*, but not in the other three diseases, where the number of PCNA positive cells in the ONL was not or only slightly higher than in normal (Figure 30), (Berta et al., 2011a).

DOI:10.14753/SE.2014.1845

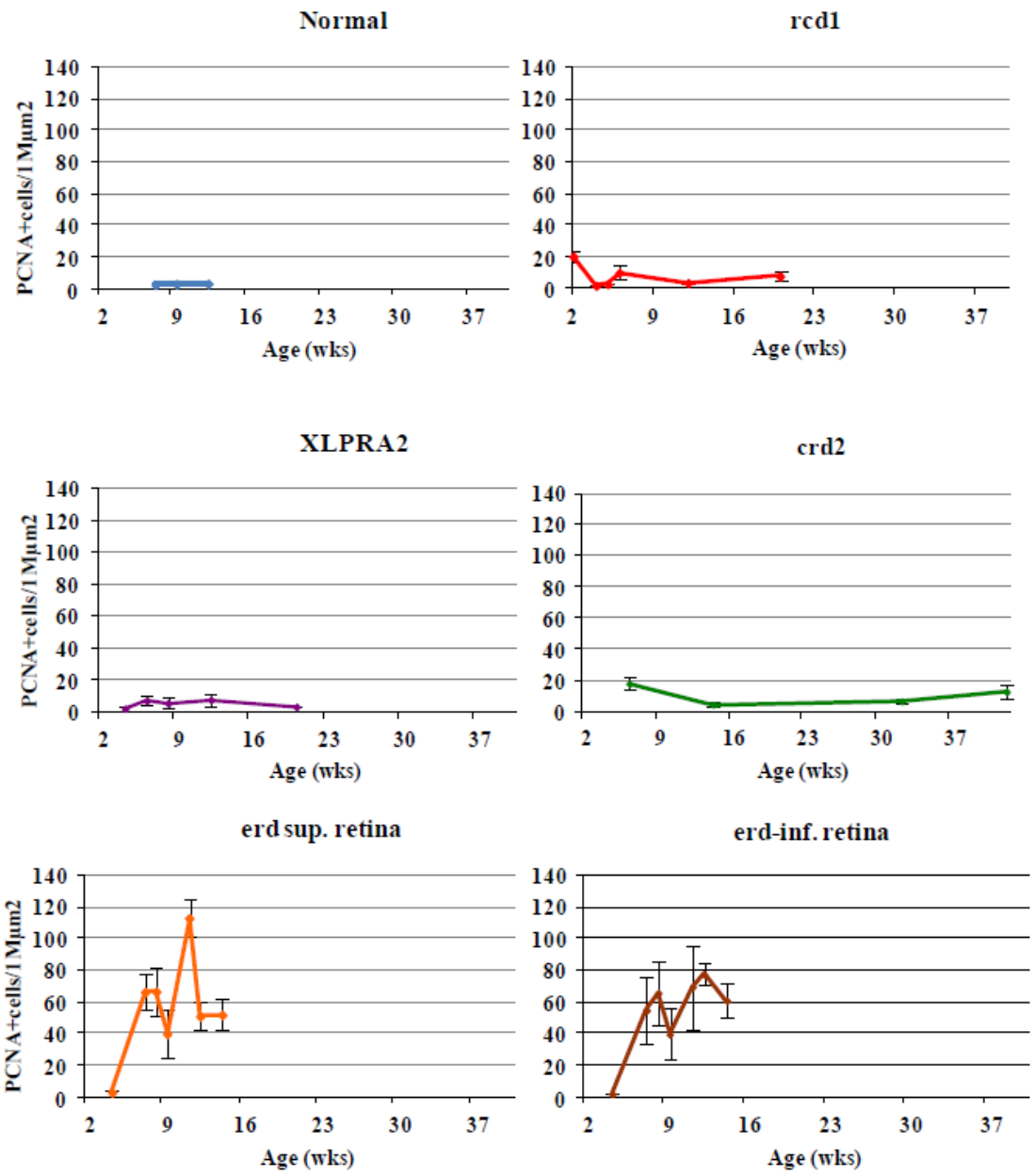

Figure 30. Number of PCNA-labeled photoreceptor cell nuclei per 1 million (M) μm² in different inherited canine retinal degenerations, showing separately the superior and inferior retina in *erd*. The high rate of cell proliferation could only be observed in *erd*, in the other diseases it was comparable to that of the normal.

PHH3 labeling was used to differentiate mitotic cells from those undergoing DNA repair that labeled with PCNA. In normals, PHH3 labeled nuclei were located

adjacent to the external limiting membrane, and, in the immediate postnatal period, limited to the retinal periphery at the time when the outer neuroblastic layer was separating, and the outer plexiform layer (OPL) had just formed (Figure 31 A, arrows). In control dogs 4 wks or older, there were almost no PHH3 labeled cells in ONL. In mutants, on the other hand, PHH3 labeled nuclei only were present at different levels of the ONL, and these were small, round and distributed uniformly from the center to the periphery; labeled cells were distinct from those undergoing apoptosis (Figure 31 B–E). Rod opsin and PHH3 labeling clearly demonstrated colocalization, and labeled nuclei were enclosed by a rod opsin positive cytoplasmic rim (Figure 31 F,G,G1–4). We have examined a subset of samples and calculated the number of PHH3 positive cells applying the same method used for counting PCNA positive cells (see Materials and Methods). The results indicate that comparable numbers of labeled nuclei in the ONL, expressed as labeled cells/106 mm2, were present with both PCNA (7 wk control=261; *erd*-7.7 wk=61616 and 11.6 wk=91630) and PHH3 (7 wk control=462.3; *erd*-7.7 wk=153656 and 11.6 wk=100611) labeling. Double labeling with PHH3 and glutamine synthetase (GS) was used to rule out Müller cell contribution to the dividing cell population. Distinct and comparable GS labeling was present in the normal and mutant retinas, and extended from the external to the internal limiting membranes. In *erd*, GS labeling was not associated with PHH3 labeled nuclei in the ONL (Figure 32). An antibody against nestin, expressed in neuronal stem cells, was used to label the normal and mutant retinas in the 4.3–14.1 wk time period. In both groups, comparable nestin labeling was found only in the retinal periphery and ciliary margin region, the site of retinal stem cells, but not in the ONL (Figure 32 A1, A2 illustrate the finding for 9 and 8.3 wk control and *erd*, respectively). Nestin, PCNA and PHH3 gave similar labeling results for the periphery/ retinal ciliary margin region of normal and mutants (data not shown). Antibodies against CD18 or PAX6, respectively, labeled microglia (CD18) or Müller cells and inner retinal neurons (PAX6), and the results were comparable between *erd* and control (Figure 32 B1,B2 and C1,C2). Taken together, the results show that the PCNA or PHH3 labeled cells in the ONL could not be accounted for by dividing Müller cells, stem cells, microglia or macrophages responding to the degenerative events in the photoreceptor layer, (Berta et al., 2011a).

DOI:10.14753/SE.2014.1845

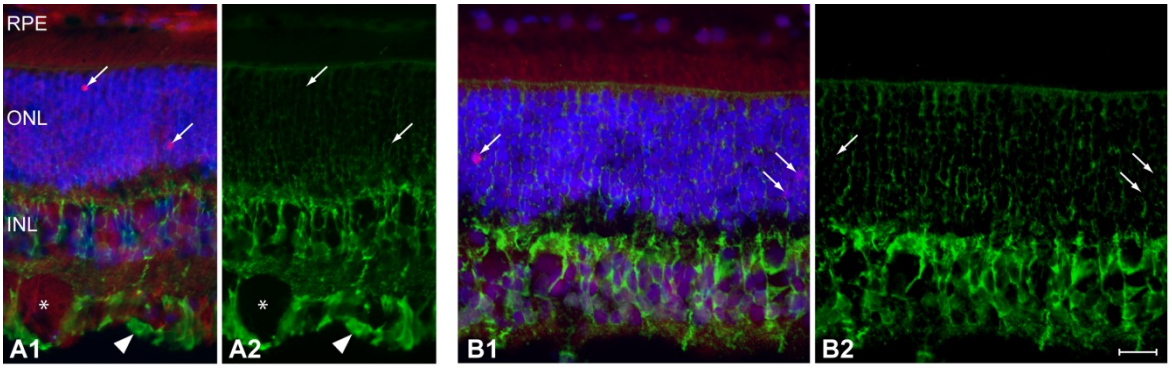

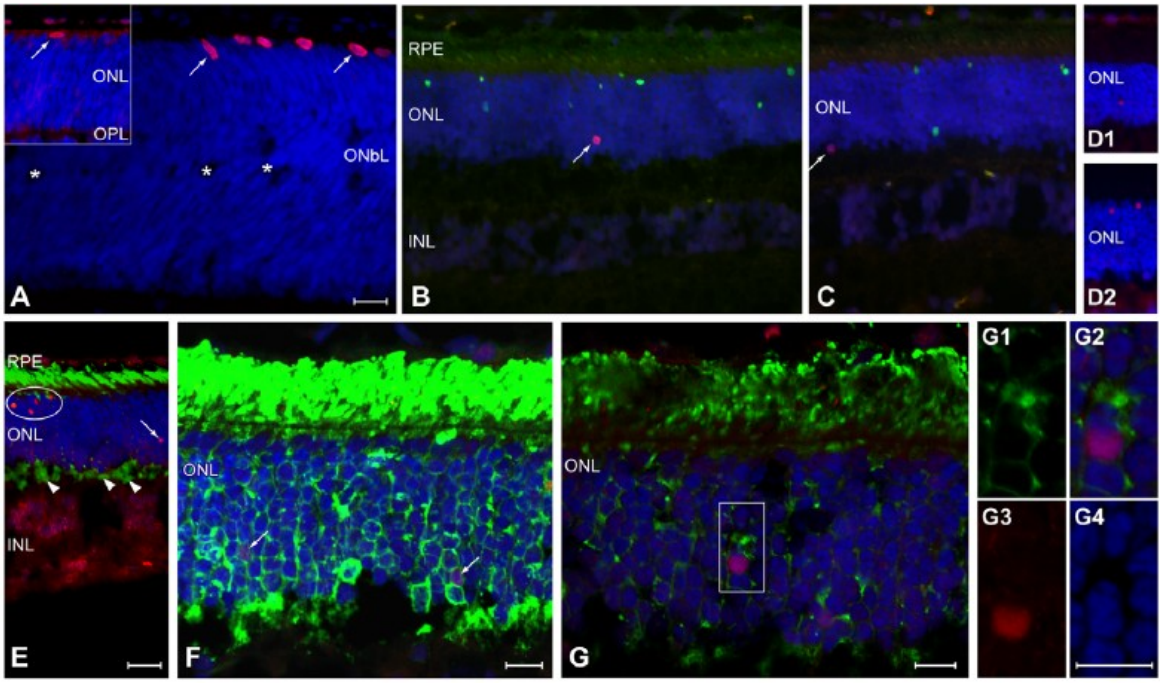

Figure 31. Phospho-histone H3 (PHH3) labeling of mitotic cells. Sections examined by epifluorescence **(A-E)** or confocal **(F-G)** microscopy using single **(A, D1, D2)** or double labeling **(B, C** -TUNEL; **E, F, G** -rod opsin), and DAPI (blue) nuclear staining. **(A)** Cell division occurs in the retinal periphery of normal young dogs [1 and 1.6 (inset) weeks] as the outer neuroblastic layer (ONbL) begins to separate (*), and the outer and inner nuclear (ONL, INL) and outer plexiform (OPL) layers form. Labeled nuclei (arrows) are large, ovoid and located at the external edge of the retina. **(B, C, D1, D2)**. In *erd*, PHH3 labeled nuclei are round (arrows), located at all levels of the ONL, and labeling does not co-localize with TUNEL labeled (green) nuclei (**B,C** and **D1, D2** are different dogs at 11.6 wk of age). **(E, F)** Epifluorescence (**E**, 11.6 wks of age) and projection confocal image (**F**, 7.7 wks of age) shows individual or clustered (arrows or oval, respectively) PHH3 labeled nuclei (orange or purple nuclei) in the ONL, and rod opsin (green) delocalization into the ONL and synaptic terminals (**E**, arrowheads). **(G, G1-G4)** Single optical sections from a different region of the same retina as (**F**) using rod opsin (green), PHH3 (red-purple), and DAPI (blue) labeling. **(G1-G4)** Higher magnification of the boxed region showing colocalization of rod opsin labeling surrounding PHH3 (purple) labeled nucleus (**G2**), and the individual channels for rod opsin (**G1**), PHH3 (**G3**) and DAPI (**G4**). Scale bars: a-e=20 μm, f-g4=10 μm.

DOI:10.14753/SE.2014.1845

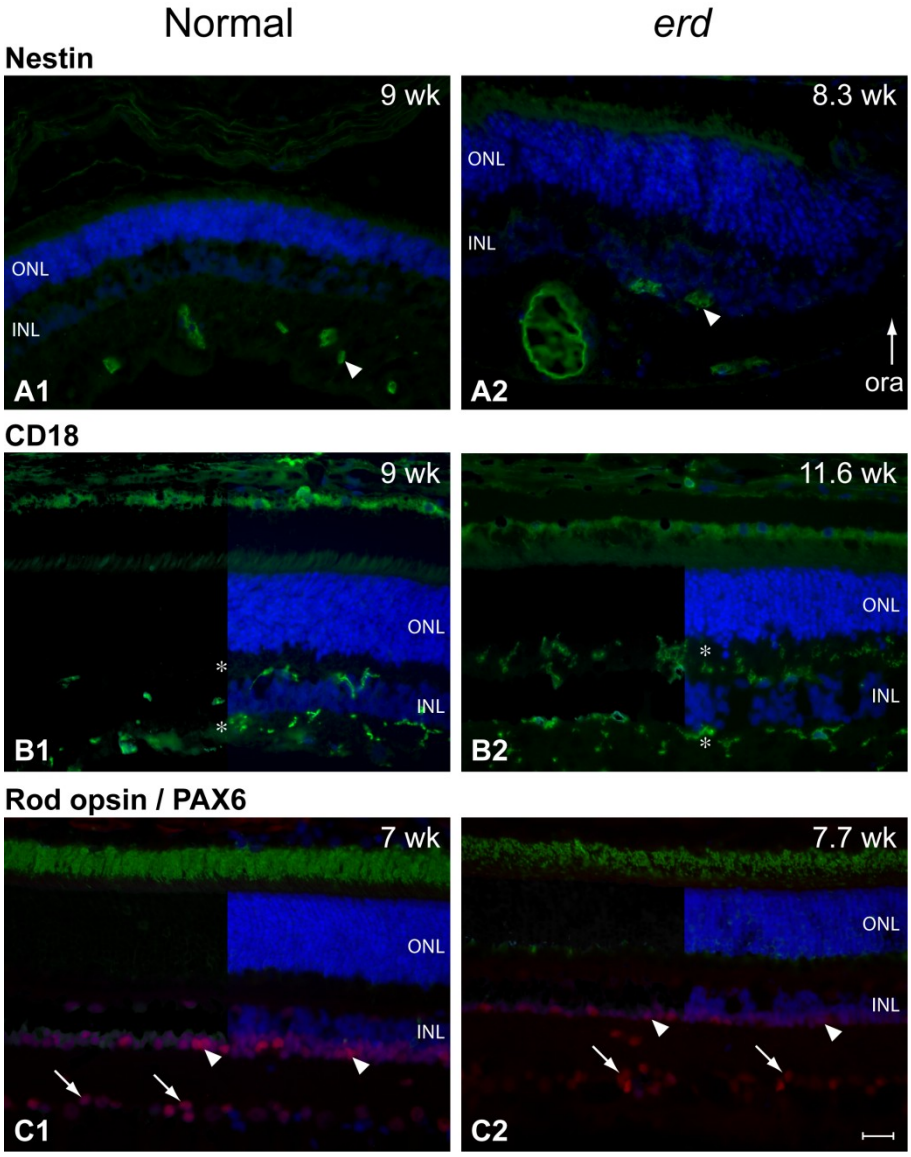

Figure 32. Nestin, cd18 and PAX6 labeling. Representative single (A1, A2-Nestin, B1, B2-CD18; green) or double (C1, C2-PAX6- red, rod opsin-green) labeling, with DAPI (blue) nuclear staining of normal or *erd* retinas of different ages. (A1, A2) Nestin labels cells only in the retinal periphery (arrowhead) near the ora serrata (ora). (B1, B2) CD18 labeling of microglia is limited to the outer and inner plexiform layers (*). (C1, C2) A population of cells in inner border of the INL, presumably Müller cells, labels intensely with PAX6 (arrowheads); labeling is also present in the ganglion cell layer (arrows). Note rod opsin delocalization in the mutant ONL (C2). Scale bar= 20 μm.

Gene and protein expression in the *erd* retina

We used qRT-PCR to characterize retinal expression of the mutated gene, STK38L, and another member of the NDR family, LATS1, at different ages during normal development and disease (Figure 33 A). STK38L expression in control retinas was unchanged during development. Although mutant mRNA lacked exon 4, the altered transcript showed a slight increase in expression at the 2 older disease time periods (8.3/9.9wks, 11.9/14.1wks) examined when using an exon 6 probe ($0.05 \leq p \leq 0.1$). LATS1 expression was increased at the 3 wk time point in normals, and at the 2 older disease time points (8.3/9.9wks, 11.9/14.1wks). As well, we examined by qRT-PCR the expression pattern of two cell cycle genes. The expression pattern of CCNA1 was similar to LATS1, but CCND1 expression was minimally reduced or unchanged at the three disease stages examined (Figure 33 B), (Berta et al., 2011a).

Expression of photoreceptor specific proteins in mutant retinas

Immunoblotting demonstrated increased expression of three of four photoreceptor-specific proteins evaluated (S-opsin, L/M-opsin, RDS peripherin) in lysates from 6.4 and 9.9 wk *erd*-retinas compared to 8wk normal control (Figure 34 a,c). The CRX transcription factor was unchanged, but NR2E3 was significantly increased at 6.4 wks, whereas NRL levels were elevated only at 9.9 wks (Figure 34 b,c). The NR2E3 results differed from those obtained by immunocytochemistry, and could be the result of different antibodies used in the blots and tissue sections (Berta et al., 2011a).

DOI:10.14753/SE.2014.1845

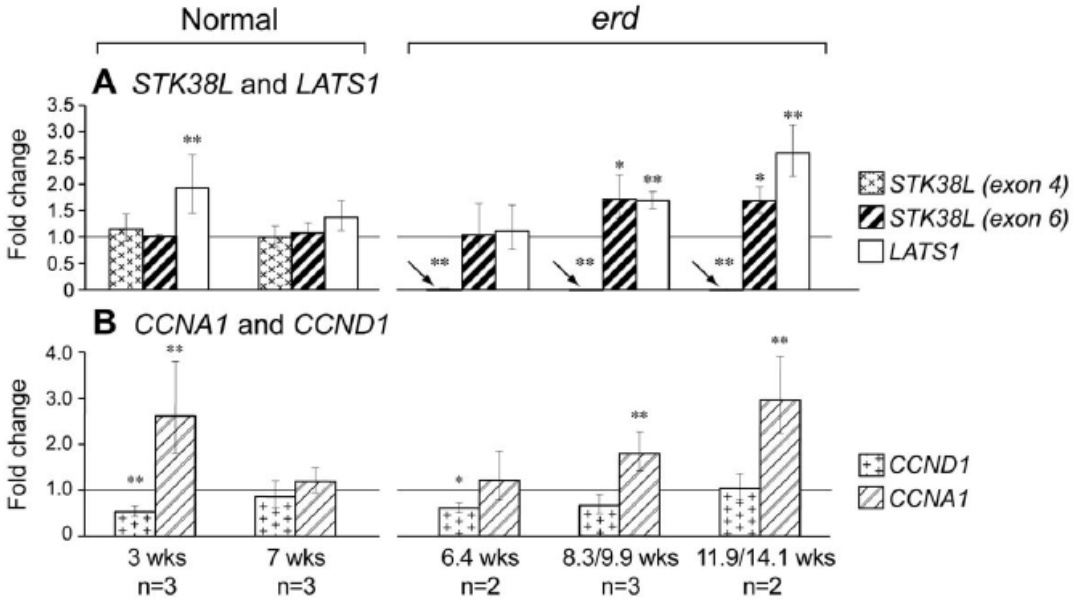

Figure 33. Retinal gene expression changes during normal development and disease. Expression was analyzed for genes that are (A) causally associated with the mutation or are part of the same gene family, or (B) involved with the cell cycle. Statistical significance between different groups in comparison to the 16 wks old normal control retinas (n = 3), depicted by horizontal line at 1.0 Fold Change, was assessed with an unpaired t-test, and expressed as statistically significant (** = $p \leq 0.05$) or towards statistical significant (* = $0.05 \leq p \leq 0.1$). For STK38L, one probe was located within the exonic deletion [STK38L (exon 4)], and the second in exon 6, 39 to the splicing defect [STK38L (exon 6)]. Noted below each time point are the number of different samples used (n =) at each time point.

DOI:10.14753/SE.2014.1845

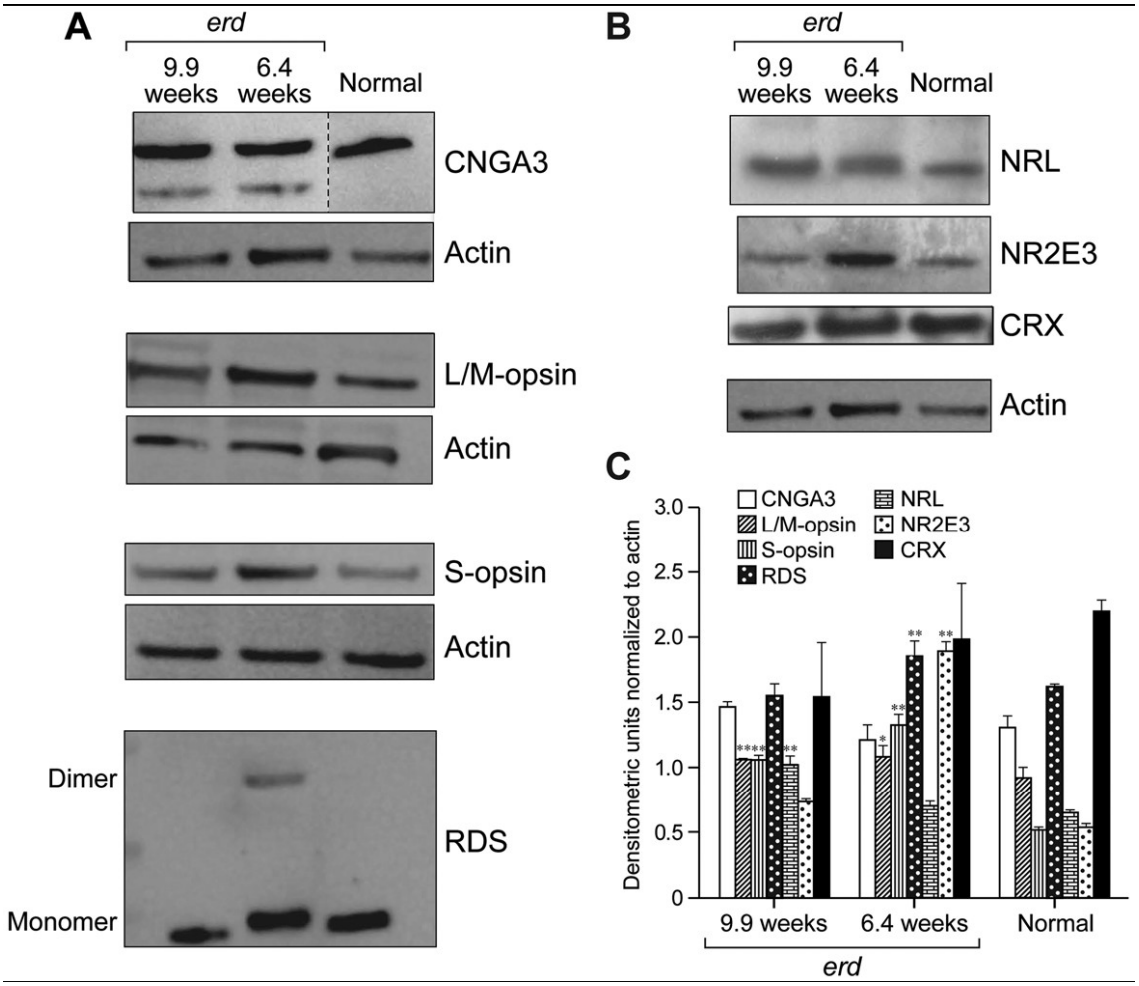

Figure 34. Protein expression in *erd* retina. Expression of (A) CNGA3, L/M-opsin, S-opsin, RDS, and (B) NRL, NR2E3, CRX proteins in cleared whole retinal lysates. (C) Net intensity densitometric values are expressed as corrected net intensity of the sample normalized to corrected net intensity of actin loading controls. Actin loading control is the same for S-opsin and RDS, and for NRL, NR2E3 and CRX, respectively. Results are the mean 6 SD of four independent densitometer scans of two individual Western blots. Confidence levels: * = 95%, ** = 99%.

DOI:10.14753/SE.2014.1845

Mutant rod outer segment renewal is diffuse rather than by band displacement

Rod OS renewal in control and mutant retinas was examined by autoradiography at different time points (1, 2, 3 and 4 days) following the intravitreal injection of ^{3}H-leucine or ^{3}H-fucose; both precursors have been used extensively in prior renewal studies in dogs, and gave the same measure of OS renewal in normal retinas (Aguirre and Andrews, 1987; Aguirre and O'Brien, 1986; Buyukmihci and Aguirre, 1976). As expected, normal rod renewal was by band displacement, and calculated renewal rates were 2.13$\pm$ 0.08 μm/day for central and mid peripheral regions. Based on the ~14-16 μm length of the average canine rod OS, it would take approximately 7 days to renew each rod. In mutant rods, however, a distinct band of radioactivity was not present, and a renewal rate could not be established. Diffuse label was present at all levels of the OS layer, and the labeling pattern was similar in rods and cones. The differences in renewal between controls and mutants was visualized best at the 4 day post injection interval when the band of radioactivity, and a trailing label tail, was clearly just distal to the rod OS midpoint in controls, but diffuse label and no band was present in mutants (Figure 35 A), (Berta et al., 2011a).

Normal rod opsin biosynthesis in mutant retina, but abnormal disposal kinetics

To complement the autoradiographic renewal studies, a series of biochemical experiments were carried out to examine rod opsin biosynthesis and disposal kinetics in control and mutant retinas at 1, 2 and 4 days following the intravitreal injection of ^{3}H-fucose/^{14}C-leucine. At different time points following injection, dark adapted eyes were collected, and crude rod OS preparations isolated, solubilized and the labeled proteins run on 10% PAGE and radioactivity determined at the opsin peaks.

Relative incorporation of ^{3}H-fucose/^{14}C-leucine label into control and mutant rod opsin differed between control and mutant animals (Figure 35 B). In normals, opsin labeling with both precursors increased at post injection days 2 and 4 as the labeled precursor pool in the vitreous was incorporated into newly synthesized protein. Regression analysis of combined ^{3}H-fucose and ^{14}C-leucine data from controls yielded a slope (daily increase in label) of 0.225 $\pm$ 0.0746. In contrast, after the 1 day time point,

DOI:10.14753/SE.2014.1845

the mutant retinas demonstrated abnormal kinetics of label incorporation into opsin, and the intensity decreased at 2 and 4 days. Regression analysis on combined ^{3}H-fucose and ^{14}C-leucine data for affecteds yielded a slope of -0.296 $\pm$ 0.0459. The difference between control and affected slopes was highly significant (Z = 5.9401, p =1.43E-09), (Berta et al., 2011a).

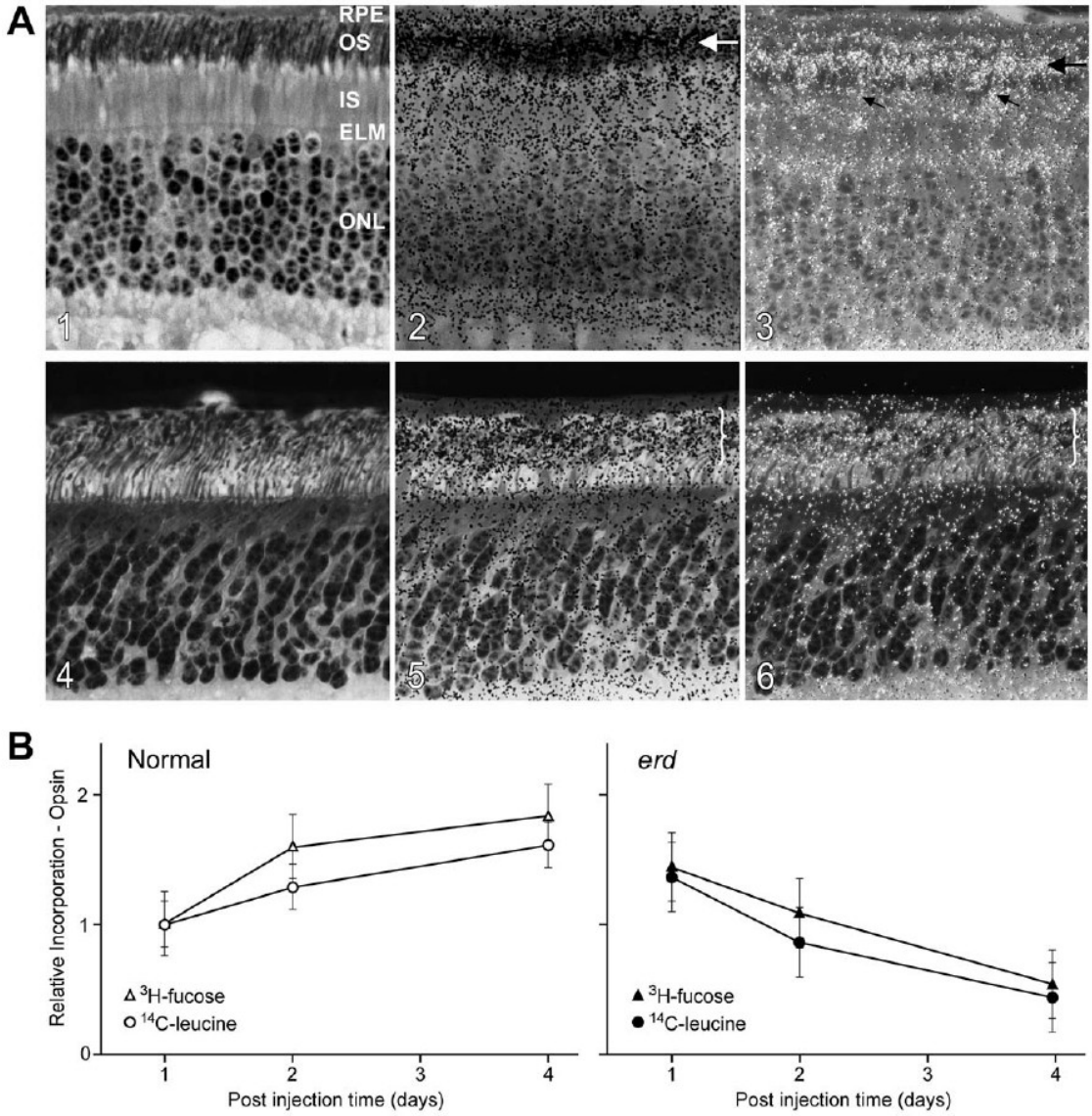

Figure 35. Cone outer segment like renewal in *erd* (***A)*** Rod outer segment renewal examined 4 days following intravitreal injection of ^{3}H-fucose in 10.9 week old normal

(*A1-3*) and *erd*-affected (*A4-6*) dogs. The images (*A1*, *A2* and *A4*, *A5*) are serial sections taken from the posterior pole of the superior retinal areas. The transmitted bright-field autoradiogram (*A2*, *A5*) shows in the normal a band of labeling whose leading edge extends to 2/3 of the rod OS (*A2*, horizontal arrow) with a trailing tail of radioactivity. This is better visualized in the combined transmitted/epipolarizing image (*A3*, arrow) that also shows diffuse label in areas where cone OS are present (oblique arrows). The mutant retina (*A4-6*) shows diffuse label at all levels of the OS layer (*A5, A6*; brackets). RPE=retinal pigment epithelium; OS=outer segments; IS=inner segments; ELM=external limiting membrane; ONL=outer nuclear layer. ***(B)***, Relative incorporation of ^{3}H-fucose/^{14}C-leucine into opsin at different time points following intravitreal injections. All data are normalized to incorporation of label at day 1. *erd* outer segments initially take up both labels (day 1), but label intensity decreases at later post injection times.

DOI:10.14753/SE.2014.1845

VI. Discussion

Despite the widespread expression in many tissue and cell types, initially it was believed that caveolin expression in the central nervous system is limited to glial cells. However, more recent studies showed that all three caveolin isoforms are expressed in neurons of the central nervous system (Head and Insel, 2007). Interestingly their expression in neuronal cells has been detected independently without any conclusive evidence for caveolae, even though detergent-resistant, low-density membranes (lipid rafts) can be isolated from these cells. It is now widely accepted that caveolins do exist and function also independent from caveolae. Typical examples are neurons and leukocytes, which cells express caveolins, but lack caveolae (Head and Insel, 2007).

Generally caveolins have two significant functions in neuronal cells. First, they play a role in synaptic maintenance and stabilization, partly acting cooperatively with post-synaptic density proteins and partly through binding cholesterol. Second, they have a crucial function in regulating intracellular signaling in neurons: physically interacting with and sequestering the appropriate signaling molecules, trafficking the molecules to and from the membrane surface and influencing the modulators of this pathway (Stern and Mermelstein, 2010).

Despite their inter-species differences, based on recent publications and our studies, caveolin isoforms seem to be inherent components of the vertebrate retinas. Our research group was first to investigate the expression and localization of caveolin isoforms in the human and the primate retina – previously only common laboratory animals (mouse and rat) were used in such studies. Since normal human retina is not available for research, the lemur retina can be used as a suitable model for caveolin distribution it the normal human retina, supposing that the retina of a primate shows a considerable morphological and functional similarity to that of humans. Previous studies about caveolins in the retina were detailed from various aspects, but were not extended to peripheral regions of the retina and ignored one of the three isoforms, caveolin-3 completely.

The localization of caveolin-1 in the retina was first studied in rodents. It was found to be present in the outer plexiform layer in mouse retina at the synaptic ribbon in photoreceptor terminals (Kachi et al., 2001), and also detected in Müller cells and

pigment epithelial cells of the rat retina (Bridges et al., 2001; Ueda, 2002). Although caveolin-1 is known to be most abundantly expressed in adipocytes, endothelial cells, fibroblasts and smooth muscle cells, these latter observations and our studies also confirm that, similarly to the brain, caveolin-1 is also expressed in retinal neuronal and glial cell types. No data are available about the distribution of caveolin-1 in the healthy human retina yet and such retinal samples for research are not to be expected in the future either. Consequently, inter-species comparison is likely the only way of modeling this problem. Studies on mammalian retinas suggest, that the different caveolin types occur less frequently than the ones found in our sections from melanoma malignum-affected human eyes, as caveolin-1 was only observed in a few cell types in rodents (Bridges et al., 2001; Kim et al., 2006; Ueda, 2002). Our observations show, that caveolin-1 is evenly distributed in the different layers of not just the lemur, but also of the human retina. We did not identify the different cell types with specific markers, but it is still obvious, that caveolin-1 is expressed in many cell types, including pigment cells, photoreceptors, ganglion cells and probably also in all the other cell types as well. Interestingly, the density of caveolin-1 exhibited a characteristic center-to-peripheral variation in both species; after an increase towards the mid-periphery it reached a maximum level in the middle periphery and then it started to decrease towards the ora serrata. Comparing the human to the primate retina the same pan retinal pattern has been found in both species, but with an obviously higher density in the human as estimated in our semiquantitative analysis (Berta et al., 2007a; Berta et al., 2007b).

Regarding caveolin-2, previous studies described this protein to be present only around blood vessels of the retina (Ueda, 2002). This correlates with the fact, that caveolin-2 is known to be co-expressed with caveolin-1 mainly in adipocytes, endothelial cells, fibroblasts and smooth muscle cells. Our observations about caveolin-2 distribution in the lemur retina confirm these facts: caveolin-2 was localized mainly around blood vessels. It has to be noted, that the most peripheral part of the lemur retina also expressed caveolin-2, and this region of the retina has not been examined earlier by others. In the human retina caveolin-2 was also localized in several layers: between and including the ONL and the ILM. It was also present in the extreme peripheral part, but the density was found to be higher. Drawing a parallel between analogous retinal regions of the two species, one can conclude that the distribution was similar, however

the estimated densities were markedly higher in the human (Berta et al., 2007a; Berta et al., 2007b).

No studies were previously performed on the presence of caveolin-3 in the retina in any species. Traditionally, caveolin-3 was thought to be muscle-specific, recently however it was also detected in astroglial cells and vegetative ganglions (Kiss et al., 2002). It is also known that the expression of caveolin-3 is intense in the central nervous system in early embryonic stages in the chicken (Shin et al., 2003). Comparing the human and the lemur retina the estimated expression density of caveolin-3 did not show such obvious differences, as seen at caveolin-1 and -2. Still, caveolin-3 was expressed in more layers of the human retina compared to those of the lemur. The density and intensity of the caveolin-3 immunoreactivity was found to be just between the other two isoforms, higher than those of caveolin-2, but lower than those of caveolin-1. The distribution of caveolin-3 in the human retina was similar to caveolin-2: immunoreactive labeling was present between and including the ONL and the ILM. In comparison, the lemur retina contained caveolin-3 specific labeling only in the ganglion cell layer and the ILM. At the most peripheral parts the labeling density was prominent in both species. It is very interesting that caveolin-3 gives the highest density in this special, two layered ciliary epithelium, which, containing stems cells in many species, can be thought to represent an early developmental stage of the retina (Berta et al., 2007a; Berta et al., 2007b). This is in good agreement with previous observations about chicken retinal development (Shin et al., 2003). Further studies have to be made to reveal the presence and function of caveolin-3 in retinal development, our studies did not aim to investigate this problem.

Summarizing these results, the distribution and the quantity of the caveolin isoforms were different in the two species. The densities, estimated with semiquantitative analysis, depending on the strength of immunolabeling in the different retinal layers and cells, were apparently higher in the human retina. It was also obvious, that they were present in more regions and in more layers in the human retina. Although caveolin is a conservative protein, the amount and distribution of caveolin in different tissues may alter across species. No data are available to support or preclude this possibility. We also cannot rule out, that other factors, i.e. sample fixation or other effects during sample preparation also influence the results. We already emphasized that the human

retinal specimen available for this study presumably contained pathological retinal conditions. As so, it is also possible that differences observed in the localization pattern and densities between the human and lemur retina may be attributed to the vicinity of the tumor. It is well known that some potentially meaningful changes take place in the ocular cytoskeleton in various ocular diseases: in corneal dystrophies, degenerations and inflammatory diseases, in opacification of the lens, in diseases characterized by proliferation of the retinal pigment epithelium, and in intraocular tumors (Kivela and Uusitalo, 1998). Choroidal tumors are associated with several degenerative changes in the overlying tissues, including proliferation, detachment, atrophy, and metaplasia of the retina, first and foremost the retinal pigment epithelium (Damato and Foulds, 1990). Therefore, provoked by the choroidal tumor, such pathologic conditions cannot be precluded in the human retinal tissues used in our study.

Parallel to the first morphological findings other study groups also investigated the retinal caveolin content with biochemical methods and confirmed the presence of caveolin-1 in the retina of various species. Boesze-Battaglia et al. (2002) were first to describe caveolin-1 in bovine rod outer segment (ROS) -derived detergent-resistant membranes (DRMs), just a year after Seno et al. first isolated DRMs from bovine photoreceptors and proved the existence of these domains in ROS (Boesze-Battaglia et al., 2002; Seno et al., 2001). Among other proteins, involved in the visual transduction, rhodopsin was detected in ROS DRMs (Seno et al., 2001). Later on rhodopsin kinase and c-src, a regulatory enzyme of caveolin-1 (Schlegel et al., 1998), were also described in ROS DRMs (Martin et al., 2005; Senin et al., 2004). Since rhodopsin and rhodopsin kinase are important participants in the phototransduction process, while caveolin-1 and c-src are characteristic markers of lipid rafts (Pike, 2003), their presence in the same membrane domains (DRMs) initiated speculations about functional connections between the two systems. It was shown, that light conditions affect the protein content of DRMs caveolin-1 being more abundant in dark adapted DRM fractions (Boesze-Battaglia et al., 2002).

Although previous biochemical data suggest the enrichment of caveolin-1 and c-src in the DRM fraction of ROS (Boesze-Battaglia et al., 2002; Martin et al., 2005), their localization using immunocytochemistry is more pronounced in the IS and in the ONL than in the OS. In all morphological studies until present, caveolin-1 was localized

to various components of photoreceptor cells: in the synaptic endings, in inner segments and perikarya, however outer segments were very weakly or practically not labeled at all (Berta et al., 2007a; Berta et al., 2007b; Elliott et al., 2008; Kachi et al., 2001; Kim et al., 2006). We described a similar distribution of these proteins in photoreceptors of the Syrian hamster with immunocytochemistry: they were mainly located in the IS and the cell body, showing a punctuate labeling pattern. To strengthen and supplement previous biochemical data, we isolated OS membranes from whole retinal samples and compared their protein content to each other. Our OS samples also contained caveolin-1 (and c-src), however in comparison to whole retinal lysates, OS contained only a minority of src and caveolin-1 (Berta et al., 2011).

Caveolin-1 is phosphorylated on tyrosine 14 and it has been proposed that the phosphorylated form of caveolin-1 may play a role in membrane domain internalization processes similar to those observed during OS disc formation (del Pozo et al., 2005). Yet until now, there have been no publications devoted to phosphorylation of caveolins in retinal photoreceptors. In our studies we also followed the labeling pattern of a specific antibody directed against phosphorylated caveolin-1 (phospho-caveolin-1) during development and compared it to that of the adult. We found that phospho-caveolin-1 was almost exclusively localized to photoreceptor outer segments of the hamster, but precise localization was not possible due to the thinness of the photoreceptor OS (Berta et al., 2011). The large photoreceptors of the *Xenopus laevis* made it possible to more precisely localize this protein. In the *Xenopus laevis* phospho-caveolin-1 is located in the photoreceptor OS rim and the cilia. We also confirmed the presence of phospho-caveolin-1 biochemically in the isolated OS membranes. These results are at least thought-provoking and the idea that caveolin-1 entering the OS is phosphorylated seems reasonable. This phosphorylation event may take place either in the OS or at the IS/OS junction. This latter option seems a little more plausible, since c-src, the kinase that phosphorylates caveolin-1 (Li et al., 1996) is preferentially present in the inner segment (Berta et al., 2011). In vitro experiments also support this idea (Elliott and Ghalayini, 2008).

The idea of caveolin-1 as a passive or active participant of rhodopsin transport originated from the fact that the localization pattern of rhodopsin and caveolin-1 during hamster retinal development was very similar. This at least raises the question whether

caveolin-1 is colocalized with rhodopsin in the same compartment on the way to the outer segment or not. For investigating this possibility, the developmental period of photoreceptors when OS are formed and the transport to the OS is most pronounced, seemed to be the ideal time for analysis (in the hamster approximately between postnatal day 5-15). In this time period of hamster retinal development, we have found that not only rhodopsin and caveolin-1, but also rhodopsin kinase and c-src showed a rather similar distribution in photoreceptor cells. To investigate whether some or all of these molecules form a complex, we used double immunolabeling visualized with confocal microscopy to compare the localization of rhodopsin and caveolin-1 as well as rhodopsin and c-src. Our results have shown that most of the punctuate structures that were positive for rhodopsin were also labeled with caveolin-1 and c-src. This was most evident in the ONL where punctuate structures could be identified individually. Additionally morphological colocalization was supported by immunoprecipitation performed with rhodopsin antibody at various developmental time points. Rhodopsin was shown to co-immunoprecipitate with caveolin-1 and c-src not only at different developmental stages, but also in the adult (Berta et al., 2011).

The rhodopsin content and distribution of these punctuate structures in the photoreceptor cytoplasm led us to the concept that they represent rhodopsin transport carriers (Deretic, 2006), delivering rhodopsin, a characteristic transmembrane protein, to the outer segment. If so, rhodopsin transport carriers should contain such lipid rafts that scaffold caveolin-1, c-src, ROM-1 and other molecules on the way to the base of the connecting cilium. This is in good agreement with recent finding (Baker et al., 2008), that integral membrane proteins or proteins anchored to the membrane by geranyl-geranylation or palmitoylation move collectively along a default pathway to the outer segment and raises the possibility of caveolin-1 mediating and/or regulating rhodopsin transport mechanism in photoreceptor cells.

The exact function of lipid rafts or caveolin-1 in photoreceptors is still not clear and probably longer discussion has to be expected in the future. Function of lipid rafts in trafficking of membrane proteins or in the regulation of phototransduction are possible options, as lipid rafts have been implicated in many important cellular processes, such as polarized sorting of apical membrane proteins in epithelial cells and signal transduction (Kurzchalia and Parton, 1999). Then again, it seems that the OS is a

default destination during the transport of membrane proteins in photoreceptors (Baker et al., 2008), which questions the necessity of a such a protein sorting mechanism. As for the caveolins, among many other functions caveolin-1 and phospho-caveolin-1 can suppress or inhibit enzyme activity through bounding and releasing enzymes in their scaffolding domain (Schlegel et al., 1998; Swaney et al., 2006). In the bound position the enzymes are active, while in the released form they have an inactive state. There are several enzymes in phototransduction that are possible candidates to have interactions with caveolin-1 or phospho-caveolin-1, but this issue remains unresolved. Further studies are also needed to specify the exact role of caveolin-1 and its phosphorylated form in the primary photoreceptor processes in the OS. Especially intriguing is the question, why and by what mechanism is caveolin phosphorylated on its way at the IS/OS border.

Comparative morphological studies are essential in order to understand the distribution and function of raft-associated proteins in the retina. In our studies, we also examined the expression of caveolins in the normal dog retina, but great differences in comparison to the Syrian hamster were not seen. Limited samples were available to study the dog retinal development, and in the 4-week-old dog rhodopsin mislocalization could be detected, in a way strengthening the rhodopsin localization pattern seen in rodents during development. It must be mentioned however, that this developmental age of the dog retina represents a much more mature state than what we described in the hamster. Also, the two species have a generally different time course in retinal development.

The mutation in *STK38L* results in the *erd* phenotype in abnormal photoreceptor development, particularly and primarily affecting rods. The morphological and functional alterations in photoreceptors can be detected in early developmental stages. These abnormalities were studied detailed using electron microscopy: aberrant rod OS and IS, pathologic alterations of the rod and cone synaptic terminals and abnormal second order neurons. These obvious morphological changes in *erd* are reflected in characteristic visual functional deficits (Acland and Aguirre, 1987). The early retinal degeneration is unique among other retinal degenerations in animal models and human patients. The extensive variation in length between rod IS and OS, and the lack of a

synchronized developmental plan between adjacent groups of photoreceptors are such characteristics, that until now were not seen in other retinal disorders.

The normal mature mammalian retina has its own elegant structure: neighboring groups of rods and cones are consistent both in their lengths, and in the proportions of their IS to their OS. However, the structural and functional order of photoreceptors is not an implicit property of the retinal structure, as the immature, developing retina is not yet ordered, and uniformity of photoreceptor dimensions appears only with further development; in dogs, this takes place by 7 weeks of age (Acland and Aguirre, 1987). Synchronized events in photoreceptor/retinal development could occur through the zonulae adherentes of the external limiting membrane (ELM), however candidate proteins that would mediate such processes are not well known. As the Crumbs homologue *CRB1* is essential for maintenance of this "membrane" and for photoreceptor morphogenesis, it is a plausible candidate protein (Mehalow et al., 2003). However in *CRB1* mutant mice, the photoreceptors fail to show the disparities in OS and IS length characteristic of *erd*, although focal regions of photoreceptor loss and retinal folding, together with retinal degeneration, do occur (Richard et al., 2006).

In *erd*, the impairment of cross-talk between adjacent photoreceptors is apparent and theoretically could be mediated directly by the *STK38L* mutation altered protein expression, or indirectly through influencing other proteins interacting in these processes. *STK38L* and other members of the *NDR* subfamily have a conserved N-terminal S100B binding site, and activation through S100B and Mob (Mps one binder) proteins with subsequent autophosphorylation has been described (Devroe et al., 2004; Stegert et al., 2004). S100 proteins are enriched in astrocytes and Müller cells (Vecino et al., 1997), and an effect on regulation of cell size could be through Müller cell participation in the ELM zonulae adherentes. Alternatively, as actin is enriched in photoreceptor cells, and *STK38L* regulates actin phosphorylation and actin filament dynamics, the rod abnormalities could be a direct effect of the mutation on the actin cytoskeleton (Stork et al., 2004).

Opsin mislocalization is characteristic of photoreceptor disease, and cell-class specific effects are presumed to reflect the expression of the mutated gene in rods or cones (Beltran et al., 2006; Rohrer et al., 2005). Although the functional significance of this event is unknown, it is proposed that light activation of mislocalized rhodopsin kills

rod cells by stimulating normally inaccessible signaling pathways (Alfinito and Townes-Anderson, 2002). This latter argument can be questioned by mislocalization-like expression of rhodopsin seen during retinal development. In *erd* immunolabeling with the anti-opsin antibody clearly demonstrated not only the disparate lengths of the rod OS, but also neurite sprouting and mislocalization of rhodopsin. Based on prior electron microscopic studies (Acland and Aguirre, 1987), the OS irregularities were expected, but the degree of opsin mislocalization at the 4.3 wk time point indicated that the degree of rod disease was higher than what was evident in the histological sections. That opsin mislocalization and neurite sprouting is a feature of rods, but not cones would suggest that *STK38L* is a rod-specific gene, and that the apparent cone abnormalities, e.g. failure of pedicles to fully mature, and cone cell death, are secondary to the rod disease and degeneration. Cone pedicles labeled with hCAR appeared to become irregular and distorted with disease, and markedly reduced labeling was present when cone degeneration was apparent.

In older animals not only the ONL, but both the OPL and INL were thinned. Some abnormalities could be observed early in the mutant retina, suggesting that these changes are progressive. The mutant retina showed a restricted distribution of synaptophysin labeling in OPL, while in the normal retina OPL and IPL synaptic vesicles are strongly labeled (Kivela et al., 1989; Sun et al., 2006). Further characterization of the synaptic terminal abnormalities will require antibodies that label their different components, e.g. synaptic ribbons, provided that these recognize comparable epitopes in the canine retina.

More striking, however, was the altered bipolar cell immunoreactivity with PKCα and Goα antibodies. All rod bipolars showed a marked reduction in label, and apparent retraction of dendritic and axonal processes, while the ON rod and cone bipolars failed to label with the antibody concentrations used. Based on the apparent integrity of the mutant INL during the first 14.1 wks of life, the altered immunolabeling does not represent bipolar cell loss, but, instead, a change in the expression of these proteins and/or their subcellular localization. Regardless, the OPL changes are in agreement with electroretinography studies that show an a-wave dominated ERG with impaired b-wave generating mechanism (Acland and Aguirre, 1987). The b-wave generators are the bipolar cells that require, as well, a functional photoreceptor synapse.

Apoptosis detected by TUNEL labeling occurs in terminally differentiated photoreceptors after retinal development is completed (Acland and Aguirre, 1987). Comapared to other retinal degenerations the cell death kinetics observed in *erd* is different. In such diseases cell death occurs usually in a short peak period, but interestingly, in *erd* it is sustained, and a relative large number of dying cells are present throughout the ONL between 7.7-14.1 wks of age. An unexpected finding, however, is that the mutant ONL remains at a constant thickness until after 14.1 wks of age, in other words the high levels of TUNEL labeling is not accompanied by concomitant photoreceptor loss. A possible explanation for this observation could be that, concurrently with cell death, a compensatory proliferative event might be occurring in mutants. The existence of this proliferation event was confirmed by labeling with two different cell proliferation markers, PCNA and KI-67. Both antibodies labeled many cells in the *erd* ONL, but almost none in controls. It must be mentioned here that some cell types (Müller cells, microglia, retinal progenitor cells), located in the ONL of the diseased or healthy retina, may be capable of division and could also be labeled with PCNA or KI67. To rule out this possibility we labeled the *erd* retinas with antibodies against CD18, GS and PAX6 (specific markers for microglia, Müller cells and neuronal progenitor cells). Based on our results, we conclude that the cells labeled with proliferation markers are not or only partly microglia or Müller cells and that the observed proliferating cells are decisively photoreceptors. Colocalization with PHH3 and rod opsin labeling, using confocal microscopy, confirmed that photoreceptor cells were undergoing mitosis, rather than DNA repair, as the number of labeled cells were comparable, and there was no co-localization of TUNEL and PHH3 labeling.(Essers et al., 2005; Kelly et al., 2010).

Thus between 7.7 and 14.1 wks of age, mutant photoreceptors are undergoing apoptosis or cell division. As the ONL thickness remains unchanged during this time, the magnitude of both events has to be comparable, otherwise decreases or increases in ONL cell number would occur. Because rods are uniformly distributed throughout the ONL and outnumber cones 22:1 outside the area centralis (Mowat et al., 2008), it is likely that rods are the predominant cells that are dying and proliferating. As TUNEL or PCNA labeled cells were not identified at the earlier time points, it is reasonable to

conclude that terminally differentiated albeit mutant photoreceptors can be committed to cell death or proliferation.

Neurogenesis in the developed mammalian retina or central nervous system is limited. In the brain, the subventricular zone of the lateral ventricle, and the dentate gyrus of the hippocampus show low levels of neurogenesis from neuronal progenitors (Belvindrah et al., 2002; Luzzati et al., 2006). In the retina, and under specific circumstances (Karl et al., 2008), a limited number of photoreceptors and other neurons are generated from presumably terminally differentiated Müller cells that dedifferentiate, proliferate and express neuronal progenitor markers; this has been reported in the adult rat, mice, chicken and fish (see (Lamba et al., 2008) for review). In contrast, rod photoreceptor replacement in zebrafish is dependent on the extent of injury. Total rod ablation results in robust Müller cell proliferation and formation of neuronal progenitor clusters, while ablation of a subset of rods results in proliferation of rod precursors (Montgomery et al., 2010).

Other than the present study, generation of new photoreceptors in a naturally occurring retinal degeneration has not been demonstrated. Our study has excluded neural stem cells, microglia, macrophages and Müller cells as contributing to the appearance of cells showing signs of cell proliferation. Distinguishing microglial cells from photoreceptors in the ONL is critical in determining the potential for photoreceptors to proliferate during the degenerative process. For example, a previous study of *rd1* mice suggested the possibility of photoreceptor proliferation based on PCNA and BrdU labeling. (Menu dit Huart et al., 2004). However, specific labeling for microglia showed that all dividing cells in the ONL were microglia rather than photoreceptors. (Zeiss and Johnson, 2004) Thus the *STK38L* mutant retina appears to be unique in having terminally differentiated photoreceptors undergoing cell proliferation.

What is not clear at this time are the signals that commit terminally differentiated photoreceptors to die or divide. While apoptosis is the final common pathway in retinal degenerative diseases, there are multiple potential pathways that link the mutation to the apoptotic event, and these are yet to be defined for dogs (Lohr et al., 2006; Portera-Cailliau et al., 1994); a recently developed canine-specific profiling array has the potential of providing this information and define the cell death pathways in *erd* and other retinal diseases.(Genini et al., in press). Cell proliferation, however, likely results

from loss of part of the N-terminal regulatory region that is highly conserved in all NDR subclass of AGC protein kinases (Hergovich et al., 2006). The exonic SINE insertion removes exon 4 from the mature RNA, and eliminates the binding sites for S100B and Mob proteins, part of the protein kinase domain, and a Thr-75 residue critical for autophosphorylation.(Goldstein et al., 2010) We propose that in the normal retina, the terminally differentiated photoreceptors are kept from dividing by *NDR2-Mob1* interaction. Removing this control in mutants allows the cell to re-enter the cell cycle and divide, and this is supported by increased *cyclin A1* expression.(Hergovich et al., 2006). The increased expression of *LATS1* presumably is an attempt to suppress this proliferation. Photoreceptor cell division, however, is temporally limited as the ONL thins after 14.1 wks. The cell division events are similar to what has been observed with the transgenic expression of SV40 large tumor antigen in the mouse retina which results in postnatal DNA synthesis and mitosis. A major difference from *erd*, however, is that after mitosis, the transgenic photoreceptors do not progress to a viable postmitotic stage and die (al-Ubaidi et al., 1992).

Coincident with the photoreceptor cell death and proliferation phase is a change in the visual cell population. Although both cone types remain, most rod cells (presumably generated after the proliferation event in the ONL) also have cone-like features, based on immunocytochemistry, they are labeled with OS-2, which is an antibody generated to label S-cones. Concurrently, biochemical studies show increases of the cone-specific L/M-opsin and S-opsin (the latter one 2x higher) in protein lysates, but not by qRT-PCR. This supports the idea that more S-opsin is expressed in the *erd* retina, namely located not in cone, but rod photoreceptor cells. It has to be mentioned that the OS-2 antibody shows aspecific labeling of rod photoreceptor cells when higher concentrations are used. Although we made a series of control sections during our immunochemistry to rule out this possibility, the OS-2 labeling of rods has to be viewed critically.

Further evidence to support our theory about rod photorecptors being "cone-like" came from the rod OS renewal and opsin synthesis studies. A fundamental difference between rods and cones is in the renewal of OS membrane proteins that results from rod discs isolated from the OS membrane, while cone discs are continuous with the plasma membrane (Young, 1969). Renewal in the *erd* retina was diffuse, and, unlike normal

controls, a distinct labeled band could not be identified at any time point. Simultaneous complementary biochemical studies showed comparable incorporation of both radiolabeled precursors into mutant and control rod opsin at the initial one day time point. At subsequent time points, however, labeling in the normal retina showed the expected accumulation of label, but a decreased one in mutants. This suggests that newly synthesized radiolabeled opsin redistributes rapidly throughout the mutant OS's, and loss of label occurs associated with the daily shedding of discs from the distal tips of the rod OS (LaVail, 1976). Thus the *erd* rods have a different OS structure: the membranous discs is become continuous with the plasma membrane (cone like property). This could require not only a change in expression of the membrane associated proteins, but possibly also the expression of a new repertoire of genes and proteins that determine photoreceptor OS structure. One such protein, RDS, is involved in cone OS biogenesis and maintenance, and appears to require formation of covalently linked RDS dimers to carry out this function (Conley et al., 2010). Although levels of RDS levels were only modestly elevated at 6.4 wks, distinct dimer formation was evident in the western blots. It is exceptionally interesting that in the *STK38L* mutant retina, terminally differentiated photoreceptors undergo cell division. We hypothesize that they differentiate into such photoreceptors that are rods, but have properties similar to cones. Afterwards just like in other retinal degenerations the loss of photoreceptors becomes dominant and leads to the unstoppable damage of the whole retinal structure. Still the proliferation event is exceptionally interesting and may represent a hidden capability of the retina of self renewal or regeneration possibly controlled by the *STK38L* gene. This might have consequences not only on further basic research in this topic, but also on clinical studies developing new strategies to heal or prevent retinal degenerations.

Retinal degenerations are presently thought to be incurable. Studies about photoreceptor development and degeneration are essential to find such photoreceptor differentiation mechanisms that might be manipulated experimentally in the future to reconstitute and preserve a diseased photoreceptor layer. In our work we described that a new protein, caveolin-1 may have a crucial function in photoreceptor development and that a new gene, *STK38L* may the control of cell division and morphogenesis in photoreceptors and possibly other retinal neurons.

DOI:10.14753/SE.2014.1845

VII. Conclusions

1. Using double immunolabeling and co-immunoprecititation we showed that rhodopsin colocalizes with caveolin-1 and c-src in small punctuate structures during retinal development, raising the possibility that they play a role in early outer segment formation. In addition, we also investigated the distribution profile of the phosphorylated product, phospho-caveolin-1. Interestingly in the adult Syrian hamster outer segments were only minimally labeled with the anti-caveolin-1 antibody, but they were positive for phospho-caveolin-1. The idea that caveolin-1 is phosphorylated before entering the OS seems reasonable.

2. Among other species we investigated caveolin-expression in the human retina, where relevant data on the topic were until now completely missing. Here we used enucleated eyes affected by melanoma malignum choroideae. The retina of the black-and-white ruffed lemur was utilized as a control, because we could not rule out that the expression of these proteins is altered in the presence of the tumor. Caveolins were present in many regions and layers in the human and primate retina, including both neuronal and glial cell types, however the distribution pattern was different. We also compared degenerated and normal retina of the dog to reveal a possible role of caveolin and caveolin-related proteins in these retinal disorders. Meaningful differences could be observed, so probably the degeneration of photoreceptors also affected the expression of the investigated raft-associated proteins.

3. We described the morphological characteristics of early retinal degeneration (*erd)* is an autosomal recessive canine retinal disorder caused by a mutation in the STK38L gene. After abnormal photoreceptor differentiation is completed there is a period of sustained photoreceptor proliferation and cell death. These events lead to the formation of a new photoreceptor population. We hypothesize that in *erd* terminally differentiated photoreceptors are able to proliferate and it suggests a role for STK38L in the control of cell division and morphogenesis in photoreceptors and possibly other retinal neurons.

4. We evaluated the cell proliferation rate in other canine retinal degenerations *(rcd1, crd2* and *XLPRA2)*. The high rate of cell proliferation could only be observed in

DOI:10.14753/SE.2014.1845

erd, in the other diseases it was comparable to that of the normal. The cell proliferation period seems to be unique characteristic of early retinal degeneration.

DOI:10.14753/SE.2014.1845

VIII. Summary

In order to understand their potential function in photoreceptor development, we studied the localization and expression pattern of caveolin-1 and c-src (responsible for caveolin-1 phosphorylation) during retinal development and compared it to two well characterized proteins, rhodopsin and rhodopsin kinase. We used the Syrian hamster as a model animal with a developmental series between P1 and P15. Using double immunolabeling and co-immunoprecititation we showed that rhodopsin colocalizes with caveolin-1 and c-src in small punctuate structures, raising the possibility that they play a role in early outer segment formation. In addition, we also investigated the distribution profile the phosphorylated product, phospho-caveolin-1. Interestingly in the adult Syrian hamster outer segments were only minimally labeled with the anti-caveolin-1 antibody, but they were positive for phospho-caveolin-1.

Among other species we investigated caveolin-expression in the human retina, where relevant data on the topic were until now completely missing. Here we used enucleated eyes affected by melanoma malignum choroideae. The retina of the black-and-white ruffed lemur was utilized as a control, because we could not rule out that the expression of these proteins is altered in the presence of the tumor. Caveolins were present in many regions and layers in the human and primate retina, including both neuronal and glial cell types, however the distribution pattern was different. We also compared degenerated and normal retina of the dog to reveal a possible role of caveolin and caveolin-related proteins in these retinal disorders.

We described the morphological characteristics of early retinal degeneration (*erd)* is an autosomal recessive canine retinal disorder caused by a mutation in the STK38L gene. After abnormal photoreceptor differentiation is completed there is a period of sustained photoreceptor proliferation and cell death. These events lead to the formation of a new photoreceptor population. We hypothesize that in *erd* terminally differentiated photoreceptors are able to proliferate and it suggests a role for STK38L in the control of cell division and morphogenesis in photoreceptors and possibly other retinal neurons.

DOI:10.14753/SE.2014.1845

IX. Összefoglalás (Summary in hungarian)

Mivel azt feltételeztük, hogy a lipid raftokhoz kötött fehérjéknek szerepe lehet a fotoreceptorok fejlődésében, ezért vizsgálatainkban a caveolin-1 és c-src (a caveolin-1-et foszforiláló enzim) expressziójával foglalkoztunk, összehasonlítva két jól ismert protein, a rodopszin és rodopszin kináz kifejeződésével. Modellállatként a Szíriai aranyhörcsögöt választottunk és egy fejlődési sort használtunk fel 1 és 15 napos kor között. Kettős jelölésű immuncitokémia és immunprecipitáció segítségével kimutattuk, hogy a rodopszin kolokalizál mind a caveolin-1-el, mind a c-src-vel kis pontformájú struktúrákban, ami felveti utóbbi molekulák szerepét a rodopszin és rodopszin kináz transzportjában a fotoreceptorok kültagja felé a fejlődő fotoreceptorokban. Ezen kívül kimutattuk, hogy a felnőtt állatok fotoreceptorainak kültagjaiban a caveolin-1 foszforilált formában van jelen. Ez alapján feltételezhető, hogy a caveolin-1 a kültag/beltag határon történő foszforilálás után tud bejutni a kültagba.

Más fajok vizsgálata mellett különös figyelmet fordítottunk az emberi retinára, mivel itt a caveolinok expressziójával kapcsolatban eddig nem volt irodalmi adat. Vizsgálatainkhoz melanoma malignum choroideae miatt enukleált szemek álltak rendelkezésünkre. Mivel nem kizárható, hogy a tumor jelenléte megváltoztatta ezen proteinek kifejeződését a retinában, kontrollként a fekete-fehér örvös makimajom retináját használtuk. A caveolinok a humán és a maki retina számos regiójában és rétegében jelen voltak, mind idegsejtekben, mind gliasejtekben, habár a két fajban az expressziós mintázat különbözött. Továbbá összehasonlítottuk normál és örökletes retinadegenerációban szenvedő kutyák retináját, felvetve ezen proteinek lehetséges szerepét a degenerációk patomechanizmusában.

Részletesen leírtuk az ún. korai retinadegeneració (erd= early retinal degeneration) morfológiai mozzanatait. Ezt az autoszómális recesszív módon öröklődő betegséget kutyákban a STK38L gén mutációja okozza. Megállapítottuk, hogy a kóros fotoreceptorok kifejlődését követően olyan periódus következik, amikor nagyszámú sejthalál és ugyanakkor sejtosztódás is történik a fotoreceptorok rétegében. Ez arra utal, hogy a degenerációs folyamatok restitutív módon egy új fotoreceptor populáció kialakulásához vezetnek, feltételezésünk szerint kifejlett fotoreceptorok osztódása révén, és így a STK38L génnek fontos szerepe lehet a fotoreceptorok, és esetleg más idegsejttípusok fejlődésének és osztódásának szabályozásában.

DOI:10.14753/SE.2014.1845

X. References

1. Acland, G.M., and Aguirre, G.D. (1987). Retinal degenerations in the dog: IV. Early retinal degeneration (*erd*) in Norwegian elkhounds. Experimental Eye Research *44*, 491-521.
2. al-Ubaidi, M.R., Hollyfield, J.G., Overbeek, P.A., and Baehr, W. (1992). Photoreceptor degeneration induced by the expression of simian virus 40 large tumor antigen in the retina of transgenic mice. Proc Natl Acad Sci U S A *89*, 1194-1198.
3. Alfinito, P.D., and Townes-Anderson, E. (2002). Activation of mislocalized opsin kills rod cells: A novel mechanism for rod cell death in retinal disease. Proceedings of the National Academy of Sciences, USA *99*, 5655-5660.
4. Baker, S.A., Haeri, M., Yoo, P., Gospe, S.M., 3rd, Skiba, N.P., Knox, B.E., and Arshavsky, V.Y. (2008). The outer segment serves as a default destination for the trafficking of membrane proteins in photoreceptors. J Cell Biol *183*, 485-498.
5. Beltran, W.A., Hammond, P., Acland, G.M., and Aguirre, G.D. (2006). A frameshift mutation in RPGR exon ORF15 causes photoreceptor degeneration and inner retina remodeling in a model of X-linked retinitis pigmentosa. Invest Ophthalmol Vis Sci *47*, 1669-1681.
6. Belvindrah, R., Rougon, G., and Chazal, G. (2002). Increased neurogenesis in adult mCD24-deficient mice. J Neurosci *22*, 3594-3607.
7. Berta, A.I., Boesze-Battaglia, K., Magyar, A., Szel, A., and Kiss, A.L. (2011). Localization of caveolin-1 and c-src in mature and differentiating photoreceptors: raft proteins co-distribute with rhodopsin during development. J Mol Histol *2011*, 22.
8. Berta, A.I., Kiss, A.L., Kemeny-Beke, A., Lukats, A., Szabo, A., and Szel, A. (2007a). Different caveolin isoforms in the retina of melanoma malignum affected human eye. Mol Vis *13*, 881-886.
9. Berta, A.I., Kiss, A.L., Lukats, A., Szabo, A., and Szel, A. (2007b). Distribution of caveolin isoforms in the lemur retina. J Vet Sci *8*, 295-297.

10. Boesze-Battaglia, K., Dispoto, J., and Kahoe, M.A. (2002). Association of a photoreceptor-specific tetraspanin protein, ROM-1, with triton X-100-resistant membrane rafts from rod outer segment disk membranes. J Biol Chem *277*, 41843-41849.
11. Bridges, C.C., El-Sherbeny, A., Roon, P., Ola, M.S., Kekuda, R., Ganapathy, V., Camero, R.S., Cameron, P.L., and Smith, S.B. (2001). A comparison of caveolae and caveolin-1 to folate receptor alpha in retina and retinal pigment epithelium. Histochem J *33*, 149-158.
12. Conley, S.M., Stricker, H.M., and Naash, M.I. (2010). Biochemical analysis of phenotypic diversity associated with mutations in codon 244 of the retinal degeneration slow gene. Biochemistry *49*, 905-911.
13. Damato, B.E., and Foulds, W.S. (1990). Tumour-associated retinal pigment epitheliopathy. Eye (Lond) *4 (Pt 2)*, 382-387.
14. del Pozo, M.A., Balasubramanian, N., Alderson, N.B., Kiosses, W.B., Grande-Garcia, A., Anderson, R.G., and Schwartz, M.A. (2005). Phospho-caveolin-1 mediates integrin-regulated membrane domain internalization. Nat Cell Biol *7*, 901-908.
15. Deretic, D. (2006). A role for rhodopsin in a signal transduction cascade that regulates membrane trafficking and photoreceptor polarity. Vision Res *46*, 4427-4433.
16. Devroe, E., Erdjument-Bromage, H., Tempst, P., and Silver, P.A. (2004). Human Mob proteins regulate the NDR1 and NDR2 serine-threonine kinases. J Biol Chem *279*, 24444-24451.
17. Elliott, M.H., and Ghalayini, A.J. (2008). Phosphorylation of caveolin-1 in bovine rod outer segments in vitro by an endogenous tyrosine kinase. Adv Exp Med Biol *613*, 335-341.
18. Elliott, M.H., Nash, Z.A., Takemori, N., Fliesler, S.J., McClellan, M.E., and Naash, M.I. (2008). Differential distribution of proteins and lipids in detergent-resistant and detergent-soluble domains in rod outer segment plasma membranes and disks. J Neurochem *104*, 336-352.

19. Essers, J., Theil, A.F., Baldeyron, C., van Cappellen, W.A., Houtsmuller, A.B., Kanaar, R., and Vermeulen, W. (2005). Nuclear dynamics of PCNA in DNA replication and repair. Mol Cell Biol *25*, 9350-9359.
20. Fang, P.K., Solomon, K.R., Zhuang, L., Qi, M., McKee, M., Freeman, M.R., and Yelick, P.C. (2006). Caveolin-1alpha and -1beta perform nonredundant roles in early vertebrate development. Am J Pathol *169*, 2209-2222.
21. Genini, S., Beltran, W.A., and Aguirre, G.D. (in press). Development and validation of a canine-specific profiling array to examine expression of pro-apoptotic and pro-survival genes in retinal degenerative diseases.
22. Goldstein, O., Kukekova, A.V., Aguirre, G.D., and Acland, G.M. (2010). Exonic SINE insertion in STK38L causes canine early retinal degeneration (erd). Genomics *96*, 362-368.
23. Head, B.P., and Insel, P.A. (2007). Do caveolins regulate cells by actions outside of caveolae? Trends Cell Biol *17*, 51-57.
24. Hergovich, A., Stegert, M.R., Schmitz, D., and Hemmings, B.A. (2006). NDR kinases regulate essential cell processes from yeast to humans. Nat Rev Mol Cell Biol *7*, 253-264.
25. Hnasko, R., and Lisanti, M.P. (2003). The biology of caveolae: lessons from caveolin knockout mice and implications for human disease. Mol Interv *3*, 445-464.
26. Kachi, S., Yamazaki, A., and Usukura, J. (2001). Localization of caveolin-1 in photoreceptor synaptic ribbons. Invest Ophthalmol Vis Sci *42*, 850-852.
27. Karl, M.O., Hayes, S., Nelson, B.R., Tan, K., Buckingham, B., and Reh, T.A. (2008). Stimulation of neural regeneration in the mouse retina. Proc Natl Acad Sci U S A *105*, 19508-19513.
28. Kelly, A.E., Ghenoiu, C., Xue, J.Z., Zierhut, C., Kimura, H., and Funabiki, H. (2010). Survivin reads phosphorylated histone H3 threonine 3 to activate the mitotic kinase Aurora B. Science *330*, 235-239.
29. Kim, H., Lee, T., Lee, J., Ahn, M., Moon, C., Wie, M.B., and Shin, T. (2006). Immunohistochemical study of caveolin-1 and -2 in the rat retina. J Vet Sci *7*, 101-104.

30. Kiss, A.L., Turi, A., Muller, N., Kantor, O., and Botos, E. (2002). Caveolae and caveolin isoforms in rat peritoneal macrophages. Micron *33*, 75-93.
31. Kivela, T., Tarkkanen, A., and Virtanen, I. (1989). Synaptophysin in the Human Retina and Retinoblastoma (An Immunohistochemical and Western Blotting Study). Investigative Ophthalmology and Visual Science *30*, 212-219.
32. Kivela, T., and Uusitalo, M. (1998). Structure, development and function of cytoskeletal elements in non-neuronal cells of the human eye. Prog Retin Eye Res *17*, 385-428.
33. Kurzchalia, T.V., and Parton, R.G. (1999). Membrane microdomains and caveolae. Curr Opin Cell Biol *11*, 424-431.
34. Lamba, D., Karl, M., and Reh, T. (2008). Neural regeneration and cell replacement: a view from the eye. Cell Stem Cell *2*, 538-549.
35. LaVail, M.M. (1976). Rod outer segment disk shedding in rat retina: relationship to cyclic lighting. Science *194*, 1071-1074.
36. Li, S., Seitz, R., and Lisanti, M.P. (1996). Phosphorylation of caveolin by src tyrosine kinases. The alpha-isoform of caveolin is selectively phosphorylated by v-Src in vivo. J Biol Chem *271*, 3863-3868.
37. Lohr, H.R., Kuntchithapautham, K., Sharma, A.K., and Rohrer, B. (2006). Multiple, parallel cellular suicide mechanisms participate in photoreceptor cell death. Exp Eye Res *83*, 380-389.
38. Luzzati, F., De Marchis, S., Fasolo, A., and Peretto, P. (2006). Neurogenesis in the caudate nucleus of the adult rabbit. J Neurosci *26*, 609-621.
39. Martin, R.E., Elliott, M.H., Brush, R.S., and Anderson, R.E. (2005). Detailed characterization of the lipid composition of detergent-resistant membranes from photoreceptor rod outer segment membranes. Invest Ophthalmol Vis Sci *46*, 1147-1154.
40. Mehalow, A.K., Kameya, S., Smith, R.S., Hawes, N.L., Denegre, J.M., Young, J.A., Bechtold, L., Haider, N.B., Tepass, U., Heckenlively, J.R.*, et al.* (2003). CRB1 is essential for external limiting membrane integrity and photoreceptor morphogenesis in the mammalian retina. Hum Mol Genet *12*, 2179-2189.

41. Menu dit Huart, L., Lorentz, O., Goureau, O., Leveillard, T., and Sahel, J.A. (2004). DNA repair in the degenerating mouse retina. Mol Cell Neurosci *26*, 441-449.
42. Montgomery, J.E., Parsons, M.J., and Hyde, D.R. (2010). A novel model of retinal ablation demonstrates that the extent of rod cell death regulates the origin of the regenerated zebrafish rod photoreceptors. The Journal of comparative neurology *518*, 800-814.
43. Mowat, F.M., Petersen-Jones, S.M., Williamson, H., Williams, D.L., Luthert, P.J., Ali, R.R., and Bainbridge, J.W. (2008). Topographical characterization of cone photoreceptors and the area centralis of the canine retina. Mol Vis *14*, 2518-2527.
44. Nixon, S.J., Carter, A., Wegner, J., Ferguson, C., Floetenmeyer, M., Riches, J., Key, B., Westerfield, M., and Parton, R.G. (2007). Caveolin-1 is required for lateral line neuromast and notochord development. J Cell Sci *120*, 2151-2161.
45. Pike, L.J. (2003). Lipid rafts: bringing order to chaos. J Lipid Res *44*, 655-667.
46. Portera-Cailliau, C., Sung, C.H., Nathans, J., and Adler, R. (1994). Apoptotic photoreceptor cell death in mouse models of retinitis pigmentosa. Proc Natl Acad Sci U S A *91*, 974-978.
47. Richard, M., Roepman, R., Aartsen, W.M., van Rossum, A.G., den Hollander, A.I., Knust, E., Wijnholds, J., and Cremers, F.P. (2006). Towards understanding CRUMBS function in retinal dystrophies. Hum Mol Genet *15 Spec No 2*, R235-243.
48. Rohrer, B., Lohr, H.R., Humphries, P., Redmond, T.M., Seeliger, M.W., and Crouch, R.K. (2005). Cone opsin mislocalization in Rpe65-/- mice: a defect that can be corrected by 11-cis retinal. Invest Ophthalmol Vis Sci *46*, 3876-3882.
49. Schlegel, A., Volonte, D., Engelman, J.A., Galbiati, F., Mehta, P., Zhang, X.L., Scherer, P.E., and Lisanti, M.P. (1998). Crowded little caves: structure and function of caveolae. Cell Signal *10*, 457-463.
50. Senin, II, Hoppner-Heitmann, D., Polkovnikova, O.O., Churumova, V.A., Tikhomirova, N.K., Philippov, P.P., and Koch, K.W. (2004). Recoverin and rhodopsin kinase activity in detergent-resistant membrane rafts from rod outer segments. J Biol Chem *279*, 48647-48653.

51. Seno, K., Kishimoto, M., Abe, M., Higuchi, Y., Mieda, M., Owada, Y., Yoshiyama, W., Liu, H., and Hayashi, F. (2001). Light- and guanosine 5'-3-O-(thio)triphosphate-sensitive localization of a G protein and its effector on detergent-resistant membrane rafts in rod photoreceptor outer segments. J Biol Chem *276*, 20813-20816.
52. Shin, D.H., Kim, J.S., Kwon, B.S., Lee, K.S., Kim, J.W., Kim, M.H., Cho, S.S., and Lee, W.J. (2003). Caveolin-3 expression during early chicken development. Brain Res Dev Brain Res *141*, 83-89.
53. Stegert, M.R., Tamaskovic, R., Bichsel, S.J., Hergovich, A., and Hemmings, B.A. (2004). Regulation of NDR2 protein kinase by multi-site phosphorylation and the S100B calcium-binding protein. J Biol Chem *279*, 23806-23812.
54. Stern, C.M., and Mermelstein, P.G. (2010). Caveolin regulation of neuronal intracellular signaling. Cell Mol Life Sci *67*, 3785-3795.
55. Stork, O., Zhdanov, A., Kudersky, A., Yoshikawa, T., Obata, K., and Pape, H.-C. (2004). Neuronal functions of the novel serine/threonine kinase Ndr2. The Journal of Biological Chemistry *279*, 45773-45781.
56. Sun, T., Xiao, H.S., Zhou, P.B., Lu, Y.J., Bao, L., and Zhang, X. (2006). Differential expression of synaptoporin and synaptophysin in primary sensory neurons and up-regulation of synaptoporin after peripheral nerve injury. Neuroscience *141*, 1233-1245.
57. Swaney, J.S., Patel, H.H., Yokoyama, U., Head, B.P., Roth, D.M., and Insel, P.A. (2006). Focal adhesions in (myo)fibroblasts scaffold adenylyl cyclase with phosphorylated caveolin. J Biol Chem *281*, 17173-17179.
58. Ueda, H. (2002). Caveolin-1 localisation in Müller cells of the retina. Acta Histochem Cytochem, 423-428.
59. Vecino, E., Velasco, A., Caminos, E., and Aijon, J. (1997). Distribution of S100 immunoreactivity in the retina and optic nerve head of the teleost Tinca tinca L. Microsc Res Tech *36*, 17-25.
60. Young, R.W. (1969). A difference between rods and cones in the renewal of outer segment protein. Invest Ophthalmol *8*, 222-231.

61. Zeiss, C.J., and Johnson, E.A. (2004). Proliferation of microglia, but not photoreceptors, in the outer nuclear layer of the rd-1 mouse. Invest Ophthalmol Vis Sci *45*, 971-976.

DOI:10.14753/SE.2014.1845

XI. List of publications

Publications related to the theme of the PhD Thesis:

1. Berta, A.I., Kiss, A.L., Kemeny-Beke, A., Lukats, A., Szabo, A., and Szel, A. (2007a). Different caveolin isoforms in the retina of melanoma malignum affected human eye. Mol Vis *13*, 881-886. IF:2,329
2. Berta, A.I., Kiss, A.L., Lukats, A., Szabo, A., and Szel, A. (2007b). Distribution of caveolin isoforms in the lemur retina. J Vet Sci *8*, 295-297.
3. Berta, A.I., Boesze-Battaglia, K., Genini, S., Goldstein, O., O'Brien, P.J., Szel, A., Acland, G.M., Beltran, W.A., and Aguirre, G.D. (2011a). Photoreceptor Cell Death, Proliferation and Formation of Hybrid Rod/S-Cone Photoreceptors in the Degenerating STK38L Mutant Retina. PLoS One *6*, e24074. IF:4,092
4. Berta, A.I., Boesze-Battaglia, K., Magyar, A., Szel, A., and Kiss, A.L. (2011b). Localization of caveolin-1 and c-src in mature and differentiating photoreceptors: raft proteins co-distribute with rhodopsin during development. J Mol Histol *2011*, 22. IF: 1,484

Publications not related to the theme of the PhD Thesis:

None.

DOI:10.14753/SE.2014.1845

XII. Acknowledgements

I would like thank all my colleagues and friends in the Institute of Human Morphology, especially the members of the Laboratory of Cell- and Molecular Biology; and the co-workers of the Eye Research Lab, School of Veterinary Medicine at the University of Pennsylvania in Philadelphia.

In both labs I received a lot of technical support from Katalin Lőcsey, Margit Kutasi, Svetlana Savina, Jessica Rowling and Lydia Melnyk.

Special thanks to my teachers: Ágoston Szél, Anna L. Kiss, Gustavo Aguirre, Kathleen Boesze-Battaglia, Attila Magyar and Pál Röhlich.